JAKELINE ROSA DE OLIVEIRA

ADSORPTION AND VOLATILIZATION OF MERCURY IN TROPICAL SOILS

LAVRAS- MG
2021

JAKELINE ROSA DE OLIVEIRA

ADSORPTION AND VOLATILIZATION OF MERCURY IN TROPICAL SOILS

Thesis presented to the Federal University of Lavras, as part of the requirements of the graduate program in Soil Science, area of concentration in Environmental Resources and Land Use, to earn the title of Doctor.

Prof. Dr. João José Granate de Sá e Melo Marques

Advisor

Prof. Dr. Teogenes Senna de Oliveira

Co-advisor

LAVRAS-MG

2021

Ficha catalográfica elaborada pelo Sistema de Geração de Ficha Catalográfica da Biblioteca Universitária da UFLA, com dados informados pelo(a) próprio(a) autor(a).

Oliveira, Jakeline Rosa de.
Adsorption and volatilization of mercury intropical soils / Jakeline Rosa de Oliveira. - 2021.
103 p.

Orientador(a): João José Granate de Sá e Melo Marques.
Coorientador(a): Teogenes Senna de Oliveira.
Tese (doutorado) - Universidade Federal de Lavras, 2021.
Bibliografia.

1. Mercury. 2. Soil. 3. Adsorption. I. Marques, João José Granate de Sá e Melo. II. Oliveira, Teogenes Senna de. III. Título.

JAKELINE ROSA DE OLIVEIRA

ADSORPTION AND VOLATILIZATION OF MERCURY IN TROPICAL SOILS

Thesis presented to the Federal University of Lavras, as part of the requirements of the graduate program in Soil Science, area of concentration in Environmental Resources and Land Use, to earn the title of Doctor.

APPROVED in 19 February 2021.

Dr. Tiago Osório Ferreira	ESALQ/USP
Dr. José João Lelis Leal de Souza	UFV
Dr. Mário César Guerreiro	UFLA
Dr. Geila Santos Carvalho	UFLA

Prof. Dr. João José Granate de Sá e Melo Marques

Advisor

Prof. Dr. Teogenes Senna de Oliveira

Co-advisor

LAVRAS-MG

2021

Ao meu amado filho, Pedro Oliveira Costa

Dedico

AGRADECIMENTOS

Em primeiro lugar agradeço a Deus, por sempre me iluminar e conceder oportunidades, como essa grande conquista.

Agradeço à minha mãe Maria do Rosário, meu filho Pedro Oliveira e aos meus irmãos Adão Henrique e Jéssica Oliveira, família que sempre me incentivou e me apoiou.

À Universidade Federal de Lavras (UFLA), especialmente ao Departamento de Ciência do Solo (DCS), pela oportunidade de cursar o doutorado e realização deste trabalho. Ao Conselho Nacional de Desenvolvimento Científico e Tecnológico (CNPq) pela concessão da bolsa de doutorado. À Coordenação de Aperfeiçoamento de Pessoal de Nível Superior (CAPES) e à Fundação de Apoio à Pesquisa de Minas Gerais (FAPEMIG) pelo subsídio financeiro.

Ao meu orientador professor João José Granate de Sá e Melo Marques, pela orientação, apoio, paciência e ensinamentos. Obrigada por tornar esse período de doutoramento mais leve.

Ao meu co-orientador Teogenes Senna de Oliveira pela colaboração na execução do projeto.

A todo corpo docente do DCS-UFLA por todos os valiosos ensinamentos. Aos funcionários do DCS - Mari, Lívia, Aline e Geila pela amizade, paciência, presteza e contribuição na realização das análises.

À Universidade Federal de Viçosa (UFV), em especial ao Departamento de Solos, por me acolherem carinhosamente, durante o período de análises. Aos funcionários do DPS-UFV, Paloma, Ramon, Janilson e José Maurício que me auxiliaram na realização das análises. Aos professores do Departamento de Física, Renê Chagas e Sukarno Olavo, pela auxílio nas análises de caracterização.

Às amigas da salinha da Geoquímica: Francielle Lima e Isabela Vasques pela amizade, companheirismo, apoio, parceria e pelos conselhos.

Às amigas Monna Lysa e Anaclaudia pela amizade incondicional, pelas risadas e pela ajuda na condução dos experimentos. À amiga Marina Justi por compartilhar comigo um lar, alegrias, tristezas e pelos conselhos. Aos demais amigos da pós-graduação em especial a Hellen Marota, Marlon Castro, Rayane Oliveira, Patrícia Barros, Francis Henrique, Nathalie Sena, Mariana Gonçalves, Cesar Ferreira, Márcio Felipe pelo carinho e amizade.

Agradeço imensamente ao meu companheiro e amigo Marcel Thomas pela colaboração na análise e discussões dos resultados, pelo apoio incondicional, incentivos, pelos bons momentos e por fazer parte da minha vida. Obrigada por me acalmar quando me desesperava e por me incentivar sempre.

Agradeço a todos que, direta e indiretamente, contribuíram para a conclusão desta importante jornada.

RESUMO GERAL

O mercúrio (Hg) possui um ciclo biogeoquímico complexo, sendo o resultado de vários processos físicos, químicos e bioquímicos. E esses processos ditam as espécies químicas de Hg dominantes e também a sua distribuição nos compartimentos que compõem o ambiente (ar, água, solo, biota, sedimento), produzindo padrões de distribuição complexos, alguns ainda não conhecidos, principalmente em ambientes tropicais. Neste contexto, objetivou-se avaliar a adsorção e volatilização de Hg em solos tropicais. A tese foi dividida em dois capítulos: Capítulo 1- avaliou-se a capacidade de adsorção de Hg. O experimento de adsorção foi conduzido em delineamento inteiramente casualizado em esquema fatorial 5 × 8, com cinco solos com textura e teor de matéria orgânica contrastantes e oito concentrações de Hg (0, 0,05, 0,1, 0,2, 0,4, 0,8, 1,2 e 2,4 mg L^{-1}). Um material zeólita também foi adicionado no estudo de sorção para fins de comparação; Capítulo 2- neste capítulo avaliou-se a volatilização de Hg de quatro solos tropicais em condição seco e úmido e a capacidade de adsorção de Hg de quatro materiais adsorventes: hopcalite; zeólita-NaP; dois biochars (W e P). Como principais resultados temos que os solos arenosos e de textura média, com baixos teores de matéria orgânica, apresentaram menor capacidade de adsorção de Hg quando comparados aos solos de textura argilosa, muito argilosa e um solo orgânico. A análise por meio de espectrometria de infravermelho mostrou que os grupos funcionais oxigenados (Al-O, Si-O, Fe-O) dos argilominerais e óxidos presentes no solo são responsáveis pela alta capacidade de adsorção de Hg. A zeólita clinoptilolita possui capacidade de adsorver Hg e apresenta potencial para remediação de solos contaminados com Hg. O conteúdo de Hg volatilizado em solo seco foi 3,7, 3,4, 1,6 e 3,8 mg kg^{-1} d^{-1} de Hg e em solo úmido foi 5,5, 4,6, 2,5 e 4,2 mg kg^{-1} d^{-1} de Hg em Nitossolo Vermelho, Latossolo Vermelho, Organossolo e Cambissolo Háplico, respectivamente. A hopcalite foi o material com maior capacidade de adsorção de Hg com 97, 53, 93 e 7% do valor de Hg volatilizado pelo Nitossolo Vermelho, Latossolo Vermelho, Organossolo e Cambissolo Háplico, em solo seco, respectivamente. O zeólita NaP adsorveu 1,0, 0,3, 0,2, 0,4 mg kg^{-1} de Hg, esses valores representam uma adsorção de 27, 8, 14 e 9% do valor total volatilizado por Nitossolo Vermelho, Latossolo Vermelho, Organossolo e Cambissolo Háplico, respectivamente, na condição de solo seco. Os biochars W e P apresentaram baixa capacidade de adsorção de Hg (0,5 a 9%), quando comparados a hopcalite e zeólita NaP. Solos com baixos teores de matéria orgânica possuem menor capacidade de adsorver Hg e maior capacidade de volatilizar Hg.

Palavras-chave: Zeólita. Biochar. Resíduos. FTIR. Especiação química. Óxidos.

GENERAL ABSTRACT

Mercury (Hg) has a biogeochemical cycle complex, as a result of several physical, chemical and biochemical processes. These processes dictate the dominant chemical species of Hg and also their distribution in the compartments that compose the environment (air, water, soil, biota, sediments), producing complex patterns of distribution, some yet unknown, particularly in tropical environments. In this context, the objective was to evaluate the adsorption and volatilization of Hg in tropical soils. The thesis was divided into two chapters: Chapter 1- Hg adsorption capacity was evaluated. The adsorption experiment was conducted in a completely randomized design in a 5 × 8 factorial scheme, with five soils with contrasting texture and organic matter content and eight Hg concentrations (0, 0.05, 0.1, 0.2, 0, 4, 0.8, 1.2 and 2.4 mg L-1). A zeolite material was also added to the sorption study for comparison purposes. Chapter 2- this chapter evaluated the volatilization of Hg from four tropical soils in dry and humid conditions and the Hg adsorption capacity of four adsorbent materials: hopcalite; zeolite-NaP; two biochars (W and P). As main results we have that the soils sand and sandy clay loam texture, with low contents of organic matter, presented less capacity of adsorption of Hg when compared to the soils of clay loam, clay and an organic soil. The analysis by means of infrared spectrometry showed that the oxygenated functional groups (Al-O, Si-O, Fe-O) of the clay minerals and oxides present in the soil are responsible for the high Hg adsorption capacity. Clinoptilolite zeolite has the ability to adsorb Hg and has the potential to remedy soils contaminated with Hg. The volatilized Hg content under dry soil condition was 3.7, 3.4, 1.6, and 3.8 mg kg^{-1} d^{-1} of Hg and under moist soil condition was 5.5, 4.6, 2.5, and 4.2 mg kg^{-1} d^{-1} of Hg in Typic Rhodustult, Humic Rhodic Acrustox, Typic Ustifolist and Oxic Dystrudept, respectively. Hopcalite was the material with the highest Hg adsorption capacity with 97, 53, 93 and 7% of the Hg value volatilized by Typic Rhodustult, Humic Rhodic, Typic Ustifolist and Oxic Dystrudept, in dry soil condition, respectively. Zeolite NaP adsorbed 1.0, 0.3, 0.2, 0.4 mg kg^{-1} of Hg, these values represent an adsorption of 27, 8, 14 and 9% of the total volatilized value by Typic Rhodustult, Humic Rhodic, Typic Ustifolist and Oxic Dystrudept, respectively, in the dry soil condition. Biochars W and P showed low Hg removal capacity (0.5 to 9%), when compared to hopcalite and zeolite NaP. Soils with low levels of organic matter have less capacity to adsorb Hg and greater capacity to volatilize Hg.

Keywords: Zeolite. Biochar. Waste. FTIR. Chemical speciation. Oxides.

SUMMARY

FIRST PART

1 GENERAL INTRODUCTION

Mercury (Hg) is a highly toxic and mobile element in the environment, and represents a risk to global public health, being listed as one of the ten main chemical concern products (WHO, 2017). In soils, Hg can be originated from natural sources (geological, volcano eruptions, forest fires) (OBRIST et al., 2018; ERMOLIN et al., 2018) generally in low concentrations or from anthropogenic sources (chlorine and alkali industries, mining, smelting, coal burning, plastics, pesticides, gold and silver extraction, batteries, painting, amalgams, and sewage sludge) (ECKLEY et al., 2020; OBRIST et al., 2018; O´CONNOR et al., 2019).

Mercury has a complex biogeochemical cycle, as a result of several physical, chemical, and biochemical processes (GUSTIN et al., 2020). These processes dictate the dominant chemical species of Hg and also their distribution in the compartments that compose the environment (air, water, soil, biota, sediments), producing complex patterns of distribution, some yet unknown, particularly in tropical environments (YIN et al., 2013).

In soils, the Hg species are found as inorganic and/or organic. In the inorganic form, Hg can be found in three different oxidation states: elemental Hg (Hg^0), which is mainly found in the vapor form, the mercurous ion (Hg_2^{2+}), unstable in natural systems, and the mercuric ion (Hg^{2+}). In the organic form, Hg^{2+} can bind covalently to an organic radical, being methylmercury (CH_3Hg^+) and dimethylmercury ($(CH_3)_2Hg$) the most common forms (O´CONNOR et al., 2019). Owing to its chemical variability, Hg undergoes a wide set of physical (leaching, erosion, and volatilization) and biochemical transformations (methylation, photochemistry, and biological reduction), depending on soil properties such as mineralogy, pH, temperature, amount and type of organic matter, and microorganisms (GUSTIN et al., 2020).

In tropical soils, the main sorbents of Hg are organic matter (O.M), clay, and oxides (CARVALHO et al., 2019; JISKRA et al., 2014; SOARES et al., 2015). Overall, the soil inorganic components, such as oxides or clay minerals, are not able to adsorb as much Hg as the organic matter, since they present lower specific surface area compared to O.M. However, they can both be important binding sites to Hg, since tropical soils have low organic matter content. Carvalho et al. (2019) studied the background content of Hg in tropical soils, and observed a high correlation between clay and Fe oxides with Hg. As for Soares et al. (2015), in a study of Hg adsorption in soils, they attributed greater retention capacity of Hg to the hydroxyl functional groups and –SH of the organic matter in the soil surface layer with high O.M content.

Soil pH is also a determinant property to controlling Hg adsorption, since it affects the surface charge characteristics in soil particles and the Hg speciation in solution (JISKRA et al., 2014). The increase in pH is known to disperse the humic substances (SPARKS, 2003; JIANG et al., 2015), which likely increases the exposition of reactive sites to the Hg species, and also enhances the complexation of Hg by the functional carboxyl groups of organic matter (DONG et al., 2013).

The effects of pH were observed by Park et al., 2018, studying the Hg adsorption in flooded soils in the Mississippi River. They observed that with an increase in the pH of the solution from 2 to 10, the amount of Hg adsorbed by the soil increased linearly from 9.8 to 51.5 mg g^{-1}. The authors attributed this higher adsorption to the Hg species formed at pH 3 and 10: $HgCl^{+}$, $HgCl_2$, HgClOH and $Hg(OH)_2$. The authors also observed that $Hg(OH)_2$ became dominant at pH 7 and 100% under pH 8.5. Adsorption of neutral mononuclear species, such as Hg $(OH)_2$, by clay surfaces can occur through several mechanisms that are difficult to distinguish from each other. The soluble character of mercury hydroxide ($HgOH_2$) leads to special Hg sorption properties in soil clay minerals mainly through covalent bonds with internal sphere complexes (LANFOT et al., 2013; SONON and THOMPSON, 2005).

Besides the species retained in the soil, Hg can also exist as volatile species, such as Hg^0 and dimethyl-Hg, which have the potential to be released to the atmosphere if present in the soil. Globally, the average emissions of Hg are estimated in approximately 1 ng m^{-2} h^{-1} in non-enriched areas (AGNAN et al., 2016; ECKLEY et al., 2020; GWOREL et al., 2020), and 100.000 ng m^{-2} h^{-1} in highly contaminated sites (AGNAN et al., 2016). In contaminated sites, such as active gold mining areas, the annual emissions vary between 10 to 105 kg $year^{-1}$, and 51 kg $year^{-1}$ in abandoned Hg mining areas (AGNAN et al., 2016; PIRRONE et al., 2010).

In the atmosphere, Hg is widely dispersed and transported through long distances before being newly deposited in the soil or another environmental spheres, thus having several implications in the global distribution of Hg (ZHENG et al., 2012), being the re-emissions higher than the primary Hg emissions (SMITH-DOWNEY et al., 2010; LAMBORG et al., 2002; GWOREL et al., 2020; O'CORNNEL et al., 2019). Within climate regions, the highest amounts of Hg are emitted or re-emitted from soils in the tropical regions (45%), followed by the temperate zones (41%), with the lowest emissions in the polar regions (8%), and the emissions from volcanos and geothermal areas correspond to 5% (GWOREK et al., 2020).

Therefore, technologies to interrupt the transfer of Hg between the soil and the atmosphere are of great relevance, particularly in tropical environments that have environmental factors (soil temperature, solar radiation, humidity, soil cover) that favor this

process of Hg volatilization in soils (CARPI and LINDBERG, 1997; GUSTIN and STAMENKOVIC, 2005; YU et al., 2018). In this context, this thesis study brings a singular importance in the comprehension of the Hg adsorption and volatilization processes in tropical soils.

2 HYPOTHESIS AND THESIS OBJECTIVES

The main objective of this thesis research was to evaluate the adsorption capacity and Hg volatilization in tropical soils and to identify the mechanisms and factors that influence these processes. Thus, objectives were based on the following hypotheses:

- Tropical soils, with low organic matter content, have low adsorption capacity and high volatilization capacity of Hg;
- Soil water content influences the formation of volatile Hg species in the soil solution, thus soil moisture increased the volatilization of Hg;
- Materials developed from industrial waste adsorb elemental Hg volatilized contaminated soil.

3 THESIS WRITING PLAN

The hypotheses of this thesis research were dealt with in two chapters.

In chapter 1, the adsorption capacity of Hg in five tropical soils and a natural zeolite was evaluated and the adsorption process characterized by infrared spectroscopy.

In chapter 2, the volatilization of Hg in three contaminated soils and incubated in the laboratory was evaluated and a soil contaminated by artisanal gold mining activity, in dry and moist soil conditions. In addition, to evaluate the volatilized Hg adsorption capacity of these soils, four adsorbent materials were synthesized from industrial waste.

REFERENCES

AGNAN, Y. *et al.* New Constraints on Terrestrial Surface-Atmosphere Fluxes of Gaseous Elemental Mercury Using a Global Database. **Environmental Science and Technology**, v. 50, n. 2, p. 507–524, 2016.

CARPI, A.; LINDBERG, S. E. Sunlight-Mediated emission of elemental mercury from soil amended with municipal sewage sludge. **Environmental Science and Technology**, v. 31, n. 7, p. 2085–2091, 1997.

CARVALHO, G. S. *et al.* Selenium and mercury in Brazilian Cerrado soils and their relationships with physical and chemical soil characteristics. **Chemosphere**, v. 218, p. 412–415, 2019.

DONG, X. *et al.* Mechanistic investigation of mercury sorption by Brazilian pepper biochars of different pyrolytic temperatures based on x-ray photoelectron spectroscopy and flow calorimetry. **Environmental Science and Technology**, v. 47, n. 21, p. 12156–12164, 2013.

ECKLEY, C. S. *et al.* The assessment and remediation of mercury contaminated sites: A review of current approaches. **Science of the Total Environment,** v. 707, p. 136031, 2020. Disponível em: <https://doi.org/10.1016/j.scitotenv.2019.136031>.

ERMOLIN, M. S. *et al.* Nanoparticles of volcanic ash as a carrier for toxic elements on the global scale. **Chemosphere**, v. 200, p. 16–22, 2018. Disponível em: <https://doi.org/10.1016/j.chemosphere.2018.02.089>.

GUSTIN, M. S. *et al.* Mercury biogeochemical cycling: A synthesis of recent scientific advances. **Science of the Total Environment,** v. 737, 2020.

GUSTIN, M. S.; STAMENKOVIC, J. Effect of watering and soil moisture on mercury emissions from soils. **Biogeochemistry**, v. 76, n. 2, p. 215–232, 2005.

GWOREK, B.; DMUCHOWSKI, W.; BACZEWSKA-DĄBROWSKA, A. H. Mercury in the terrestrial environment: a review. **Environmental Sciences Europe**, v. 32, n. 1, 2020. Disponível em: <https://doi.org/10.1186/s12302-020-00401-x>.

JIANG, T. *et al.* Modeling of the structure-specific kinetics of abiotic, dark reduction of Hg(II) complexed by O/N and S functional groups in humic acids while accounting for time-dependent structural rearrangement. **Geochimica et Cosmochimica Acta**, v. 154, p. 151–167, 2015. Disponível em: <http://dx.doi.org/10.1016/j.gca.2015.01.011>.

JISKRA, M. *et al.* Kinetics of Hg(II) exchange between organic ligands, goethite, and natural organic matter studied with an enriched stable isotope approach. **Environmental Science and Technology**, v. 48, n. 22, p. 13207–13217, 2014.

LAFONT, D. *et al*. Sorption and desorption of mercury(II) in saline and alkaline soils of Bahía Blanca, Argentina. **Environmental Earth Science** 70, 1379–1387, 2013. https://doi.org/10.1007/s12665-013-2221-6

O'CONNOR, D. *et al.* Mercury speciation, transformation, and transportation in soils, atmospheric flux, and implications for risk management: A critical review. **Environmental International**, v. 126, n. March, p. 747–761, 2019. Disponível em: <https://doi.org/10.1016/j.envint.2019.03.019>.

OBRIST, D. *et al.* A review of global environmental mercury processes in response to human and natural perturbations: Changes of emissions, climate, and land use. **Ambio**, v. 47, n. 2, p. 116–140, 2018. Disponível em: <https://doi.org/10.1007/s13280-017-1004-9>.

PARK, J. H. *et al.* Mercury adsorption in the Mississippi River deltaic plain freshwater marsh soil of Louisiana Gulf coastal wetlands. **Chemosphere,** v. 195, p. 455–462, 2018. Disponível em: <https://doi.org/10.1016/j.chemosphere.2017.12.104>.

PIRRONE N. *et al*. Global mercury emissions to the atmosphere from anthropogenic and natural sources. **Atmosphere Chemistry Physcal**. v. 10, p. 5951–5964, 2010.

REIS, A. T. *et al.* Development and validation of a simple thermo-desorption technique for mercury speciation in soils and sediments. **Talanta**, v. 99, p. 363–368, 2012. Disponível em: <http://dx.doi.org/10.1016/j.talanta.2012.05.065>.

SMITH-DOWNEY, N. V.; SUNDERLAND, E. M.; JACOB, D. J. Anthropogenic impacts on global storage and emissions of mercury from terrestrial soils: Insights from a new global model. **Journal of Geophysical Research: Biogeosciences**, v. 115, n. 3, p. 1–11, 2010.

SOARES, L. C. *et al.* Accumulation and oxidation of elemental mercury in tropical soils. **Chemosphere**, v. 134, p. 181–191, 2015. Disponível em: <http://dx.doi.org/10.1016/j.chemosphere.2015.04.020>.

SONON, L. S, THOMPSON, M. L. Sorption of a noniônico polyoxyethylene lauryl ether surfactant por 2: 1 layer silicates. **Clays Clay Miner** 53: 45-54, 2005.

SPARKS, D. L. **Environmental soil chemistry**. Boca Raton: Academic Press; 2003.

YIN, R. *et al.* Mercury isotope variations between bioavailable mercury fractions and total mercury in mercury contaminated soil in Wanshan Mercury Mine, SW China. **Chemical Geology**, v. 336, p. 80–86, 2013. Disponível em: <http://dx.doi.org/10.1016/j.chemgeo.2012.04.017>.

YU, Q. *et al.* Gaseous elemental mercury (GEM) fluxes over canopy of two typical subtropical forests in south China. **Atmospheric Chemistry and Physics**, v. 18, n. 1, p. 495–509, 2018.

ZHENG, Y. *et al.* Review of technologies for mercury removal from flue gas from cement production processes. **Progress in Energy and Combustion Science**, v. 38, n. 5, p. 599–629, 2012. Disponível em: <http://dx.doi.org/10.1016/j.pecs.2012.05.001>.

SECOND PART – ARTICLES

ARTICLE 1

Journal: Archives of Agronomy and Soil Science

DOI: 10.1080/03650340.2020.1845318

Mercury adsorption in tropical soils and zeolite: characterization by Fourier-transform infrared spectroscopy

J.R.Oliveira[a]; I.C.F. Vasquesb; F.R.D. Lima[a]; G.S. Carvalho[a]; M.T.P. Job[b]; T.S. Oliveira[b]; J.J. Marques[a]*

[a] Department of Soil Science, Federal University of Lavras, Lavras, MG, CEP 37200-000, Brazil

[b] Department of Soil Science, Federal University of Viçosa, Viçosa, MG, CEP 36570-000, Brazil

Abstract

The aim of this study was to evaluate the capacity for Hg adsorption, understand the mechanisms of Hg sorption in tropical soils, and study the potential for Hg sorption by a natural zeolite for possible application in remediation of soils contaminated with Hg. The soil samples used in this study were collected from the 0 to 20 cm layer in areas of native vegetation in the state of Minas Gerais, Brazil. The experiment was conducted in a completely randomized design in a 5 × 8 factorial arrangement, with five soils of contrasting characteristics and eight Hg concentrations (0, 0.05, 0.1, 0.2, 0.4, 0.8, 1.2, and 2.4 mg L^{-1}). A zeolite material was also added in the sorption study for purposes of comparison. Samples of the five soils under study and the zeolite before and after Hg adsorption were characterized by Fourier-transform infrared spectroscopy (FTIR). The species $HgOH_2$, HgClOH, and $HgCl_2$ predominates in the contaminating solutions. Analysis through FTIR showed that the oxygenated functional groups

(Al-O, Si-O, Fe-O) of the clay minerals and oxides present in the soil are responsible for the high Hg adsorption capacity. The zeolite clinoptilolite has potential for remediation of soils contaminated with Hg.

Keywords: soil contamination, Hg speciation, FTIR spectroscopy, adsorption isotherm, oxides.

Introduction

Mercury is recognized as a global pollutant because it can remain in the atmosphere for more than a year, reaching ecosystems that are distant from the source of pollution (Sądej et al. 2020; Rolka et al. 2018). In soils, abnormal concentrations of this element are generally caused by mining operations (Berdonces et al. 2017; Windmoller et al. 2015) and by industrial activities, such as chlor-alkali factores (Rodrigues et al. 2010; Balzino et al. 2015).

After entering in contact with the soil, the mobility of Hg through the soil profile affects its bioavailability through the processes of reduction, oxidation, leaching, and volatilization, which generate scenarios of potential risk to human health through bioaccumulation in the food chain (Sądej et al. 2020; Rolka et al. 2018). Nevertheless, the bioavailability of mercury in the soil is determined by its chemical speciation (Hg^0, Hg^{2+}, HgOH, CH_3Hg^+) and by the physical and chemical properties of the soil.

The dynamics of Hg in tropical soils, including its adsorption and bioavailability, is governed by the texture of the soil and its geochemical composition (Carvalho et al. 2019). This is different from what occurs in temperate and boreal soils, where Hg retention and accumulation are mainly controlled by the organic matter contents (Osterwalder et al. 2017; Skyllberg et al. 2003; Kyllönen et al. 2012). Due to these particularities, the tropical environment deserves a different approach when studying Hg adsorption.

Considering the important role of adsorption processes during Hg retention in soils, finding materials capable of increasing this capacity of adsorption/immobilization in an efficient manner is of utmost importance, especially in regard to remediation of soils

contaminated with Hg. Among the materials currently evaluated, natural zeolites stand out. The zeolite clinoptilolites, which are natural zeolites, have high capacity for adsorption of heavy metals (Belova 2019), derived from their unique chemical and physical characteristics, such as high cation exchange, porosity, specific surface area, internal structure, and crystallinity (Belova 2019).

Many studies have shown that the zeolites can behave as good adsorbents for Hg, but many of them focus on water treatment (Tauanov et al. 2020). Problems related to soil contamination with Hg in tropical soils are widely reported (Araújo et al. 2019; Vasques et al. 2020), and using zeolites in this case means a promising alternative. The comparison of a well-known adsorptive product (i.e. zeolite) with different tropical soils clarifies the adsorption potential of 1: 1 clay minerals and oxides, typically found in these environments.

This lack of studies with Hg adsorption in tropical soils leaves a gap concerning the mechanism of Hg retentions in different soils. Fourier - transform infrared spectroscopy (FTIR) has been used to better characterize Hg adsorption mechanisms in soils (Ding et al. 2017; Xue et al. 2013), but in general, the focus is on soils from temperate climates. With FTIR, it is possible to identify the vibrations of functional groups and the soil molecular structures that can help explain the process involved in Hg adsorption and desorption (Xue et al. 2013). Therefore, the use of FTIR together with the characterization of Hg adsorption process in tropical soils is yet something newly studied.

Thus, knowing how Hg binds to soil colloids is of great importance for understanding soil contamination and for development of strategies so that Hg does not disperse in the environment and, consequently, enter the food chain. The aims of this study were (1) to evaluate Hg adsorption capacity in five typical soils of Brazil with contrasting properties and identify the adsorption mechanisms using FTIR and (2) to evaluate the adsorption capacity of natural zeolite clinoptilolite for application in remediation of Hg contaminated soils. Therefore, this

study is a first step on unveiling Hg retention mechanisms in tropical soils, allowing further studies that want to collaborate on the topic.

Materials and Methods

Characterization the soil samples and of the zeolite

The soil samples used in this study were collected at a depth of 0 to 20 cm from areas of native vegetation in the south of Minas Gerais, Brazil. The soils were classified according to the Soil Survey Staff (2014) as follows: Ustic Quartzipsamment (sand - Sa), Typic Haplustox (sandy clay loam - SaClLo), Typic Rhodustult (clay loam - ClLo), Humic Rhodic Acrustox (clay - Cl), and Typic Ustifolist (organic soil - OS). The chemical and particle size properties of the soils studied and of the zeolite are shown in Table 1 (Teixeira et al. 2017). From our knowledge, no study has covered such wide soil properties in a study of Hg adsorption in tropical environments. The oxide concentrations were determined by Total Reflection X - Ray Fluorescence Spectroscopy (TXRF S2 Picofox™ High Efficiency), according to Towett et al. (2013) with modifications. The Hg concentration in the soil samples before the adsorption trial was determined by the USEPA 3051a method (USEPA 2007).

Table 1. Particle size and chemical properties of the investigated soils collected from the 0 - 20 cm layer and of zeolite

Soil type	pH	CEC	Clay	Silt	Sand	O.M	Hg
	KCl	$cmol_c\ kg^{-1}$	----------$g\ kg^{-1}$----------			$g\ kg^{-1}$	$\mu g\ kg^{-1}$
Sand (Sa)	4.0	4.8	70	10	920	9	3.6
Sandy Clay Loam (SaClLo)	4.1	2.7	220	50	730	12	13.4
Clay Loam (ClLo)	5.8	7.8	380	180	440	20	76.6
Clay (Cl)	5.5	4.5	540	260	200	20	34.7
Organic Soil (OS)	4.2	19	300	430	270	212	141.1
Zeolite (Ze)	7.4	1.6	-	-	-	-	-
	Al_2O_3	SIO_2	P_2O_5	K_2O	CaO	TiO	Fe_2O_3
	----------%----------						
Sand (Sa)	10.0	89.7	0.3	0.9	0.1	0.4	0.5
Sandy Clay Loam (SaClLo)	14.8	39.7	0.0	0.2	0.0	0.5	3.3
Clay Loam (ClLo)	9.9	22.1	0.1	0.2	0.3	1.7	12.6
Clay (Cl)	12.3	10.2	0.0	0.1	0.0	1.6	22.6
Organic Soil (OS)	14.1	12.6	0.2	0.1	0.0	1.6	3.9

Zeolite (Ze)	12.0	68.0	0.0	1.4	2.3	0.4	1.1

CEC: cation exchange capacity at pH 7; O.M: Organic matter by oxidation with Na - dichromate and sulfuric acid; Hg: concentration of Hg by the 3051A method (USEPA, 2007) and determined by FI - HG - AAS (Segade and Tyson 2003).

For mineralogical characterization, the soil and zeolite samples were analyzed by X - Ray diffraction in the X'Pert PRO device with Cu radiation (CuKα) in the 4 - 70° 2θ range at intervals of 0.01 ° 2θ at 1 step s^{-1}, with the voltage of 40 kV and current of 30 mA.

Hg adsorption

The experiment of Hg adsorption was conducted on the soil and zeolite clinoptilolite samples using a solid: solution ratio of 1: 10. Samples of 2.0 g of solid were weighed and placed in 50 mL centrifuge tubes. To each tube, 20 mL of Hg contaminant solution was added at concentrations of 0, 0.05, 0.1, 0.2, 0.4, 0.8, 1.2, and 2.4 mg L^{-1}, using $HgCl_2$ as a source. The mercury chloride solutions were prepared in a background solution of 0.1 M $NaNO_3$ (Zhang et al. 2012), with five replications. The pH values of the Hg ($HgCl_2$ + $NaNO_3$) contaminant solutions ranged from 5.5 to 6.5. The Hg concentrations used to contaminate the soil were based on reference values according to Brazilian legislation for Hg concentrations in soils of 0.05 mg of Hg per kg of dry soil as a quality reference value (valor de referência de qualidade - VRQ) and 12 mg of Hg per kg of dry soil as an agricultural investigation value (valor de investigação agrícola - VI) (COPAM, 2011). Therefore, it could also be possible to investigate the suitability of these values concerning the available adsorption sites in tropical soils.

After addition of the Hg solutions, the samples were left to react for 72 h, with successive periods of 12 h of shaking and 12 h of rest. During the adsorption trial, the pH of the solution was monitored in the initial and final phase of the trial, and its values were used for the chemical simulation model of the inorganic Hg species, described in section Speciation of Hg.

Shaking was performed at 120 rpm in a horizontal shaker at ambient temperature. After 72 h, the samples were centrifuged at 3,500 rpm for 20 min to obtain a clear supernatant, in which the Hg concentration was determined.

Determination of Hg concentration

Analytical determination of Hg in the supernatant solutions of the adsorption trial was conducted using Flow Injection Hydride Generation Atomic Absorption Spectrometry (FI - HG - AAS) with a quartz cell (Perkin Elmer AAnalyst 800) and electrodeless discharge lamps for Hg (Segade and Tyson 2003).

The detection limit was calculated according to the American Public Health Association (2012) using seven blank samples in each lot for analysis, and the value was less than 0.52 µg kg^{-1} in all the samples.

Fourier - Transform Infrared Spectroscopy - FTIR

Samples of the five soils studied and of the zeolite clinoptilolite, with and without Hg, were characterized by Fourier-transform infrared spectroscopy (FTIR). The dry samples (at 35 ºC) were ground in an agate mill and sieved in a 0.15 mm screen. The FTIR analysis was conducted in a Perkin Elmer Spectrum 1000 device equipped with a total attenuated reflectance accessory in which the powder from each sample was inserted in a diamond crystal support. The FTIR spectra from 32 scans were registered in the wavenumber range of 4000 - 400 cm^{-1}, with resolution of 2 cm^{-1}.

Data analysis

The Hg content adsorbed (mg kg^{-1}) in the samples was calculated according to Equation 1:

$$y = \frac{C_i - C_e * V}{Ms} \quad (1)$$

Where:

y - the amount of Hg adsorbed (mg kg^{-1});

C_i - the initial concentration of Hg added (mg L^{-1});

C_e - the equilibrium concentration after 72 h (mg L^{-1});

V - the final volume (mL);

M_s - the weight of soil or zeolite dried in a laboratory oven (kg).

Isotherms were chosen according to various studies regarding Hg adsorption (Ding et al. 2017; Xue et al. 2013). The adsorption data were analyzed using the following equations:

Freundlich equation (Dada et al. 2012):

$$Q_e = K_f * C_e^{1/n} \quad (2)$$

Where:

Q_e - the amount of metal adsorbed per gram of the adsorbent at equilibrium (mg g^{-1});

K_f - Freundlich isotherm constant (mg g^{-1});

C_e - the equilibrium concentration of adsorbate (mg L^{-1});

n - adsorption intensity.

Langmuir (Dada et al. 2012):

$$q_e = \frac{Q_0 - K_L C_e}{1 + K_L * C_e} \quad (3)$$

Where:

qe - the amount of Hg adsorbed (mg kg^{-1});

Q_0 - maximum monolayer coverage capacity (mg g^{-1})

K_L - Langmuir isotherm constant (L mg^{-1});

C_e - the equilibrium concentration of adsorbate (mg L^{-1}).

Speciation of Hg

Determining the species of Hg is an important step in evaluating its mobility and, consequently, its potential for toxicity in the soil. To evaluate the speciation of Hg in the contaminating solution ($HgCl_2$ and $NaNO_3$) and in the supernatant solution from adsorption, the chemical equilibrium program Visual Minteq (Gustafsson 2005) was used.

The cations inserted for speciation were calcium, magnesium, potassium, and sodium, that have been they were determined by Inductively Coupled Plasma Optical Emission Spectrometry (ICP - OES) of Perkin Elmer™. The wavelengths and pulse heights for the elements analyzed were 317.9 nm and 9.0 mm for Ca, 279.2 nm and 9.0 mm for Mg, 308.2 nm and 9.0 mm for Al, and 766.4 nm and 9.0 mm for K, respectively. The Hg concentration was determined using Flow Injection Hydride Generation Atomic Absorption Spectrometry (FI - HG - AAS) with a quartz cell (Perkin Elmer AAnalyst 800) and electrodeless discharge lamps for Hg (Segade and Tyson 2003).

The anions used were phosphate, chloride, nitrate, and sulfate, and they were analyzed by ion chromatography using the Thermo Scientific™ Dionex™ ICS - 1100 (Dionex ICS - 1100), with high exchange capacity IonPac™ AS19 IC analytical columns, 4 x 250 mm, and ASRS300 suppressor of 4 mm with suppression capacity up to 200 mL/ min using the eluent buffer Na_2CO_3/ $NaHCO_3$ in a gradient.

The results of Hg speciation presented in this study were based on the pH measured in the contaminant solution and in the contaminant solution in contact with the soils and the zeolite during the adsorption trial. Simulation of speciation was carried out in a range of ± 1 pH unit above and below the measured value of the pH.

For the speciation of Hg in the presence of organic content, the NICA - Donnan model was created by combining the NICA isotherm with a Donnan model to assess complexation between humic substances and metals (Kinniburgh et al. 1999). The content of dissolved

organic carbon (DOC) inserted in the NICA - Donnan model was estimated from the O.M. (Table 1) as being 7% of the measured total organic carbon (Araújo et al. 2014; Gmach et al. 2018).

Results and discussion

Mineralogical characteristics of the soils and of the zeolite clinoptilolite

The main minerals identified in the five soils studied by X - ray diffraction (XRD) analysis were kaolinite, quartz, gibbsite, hematite, and goethite (Figure 1). The predominance of 1: 1 clay and oxides indicates that the soils are highly weathered, which is a well - known characteristic for tropical soils, such as Brazilian soils (Fontes and Carvalho 2005). In zeolite, the main mineral found was clinoptilolite.

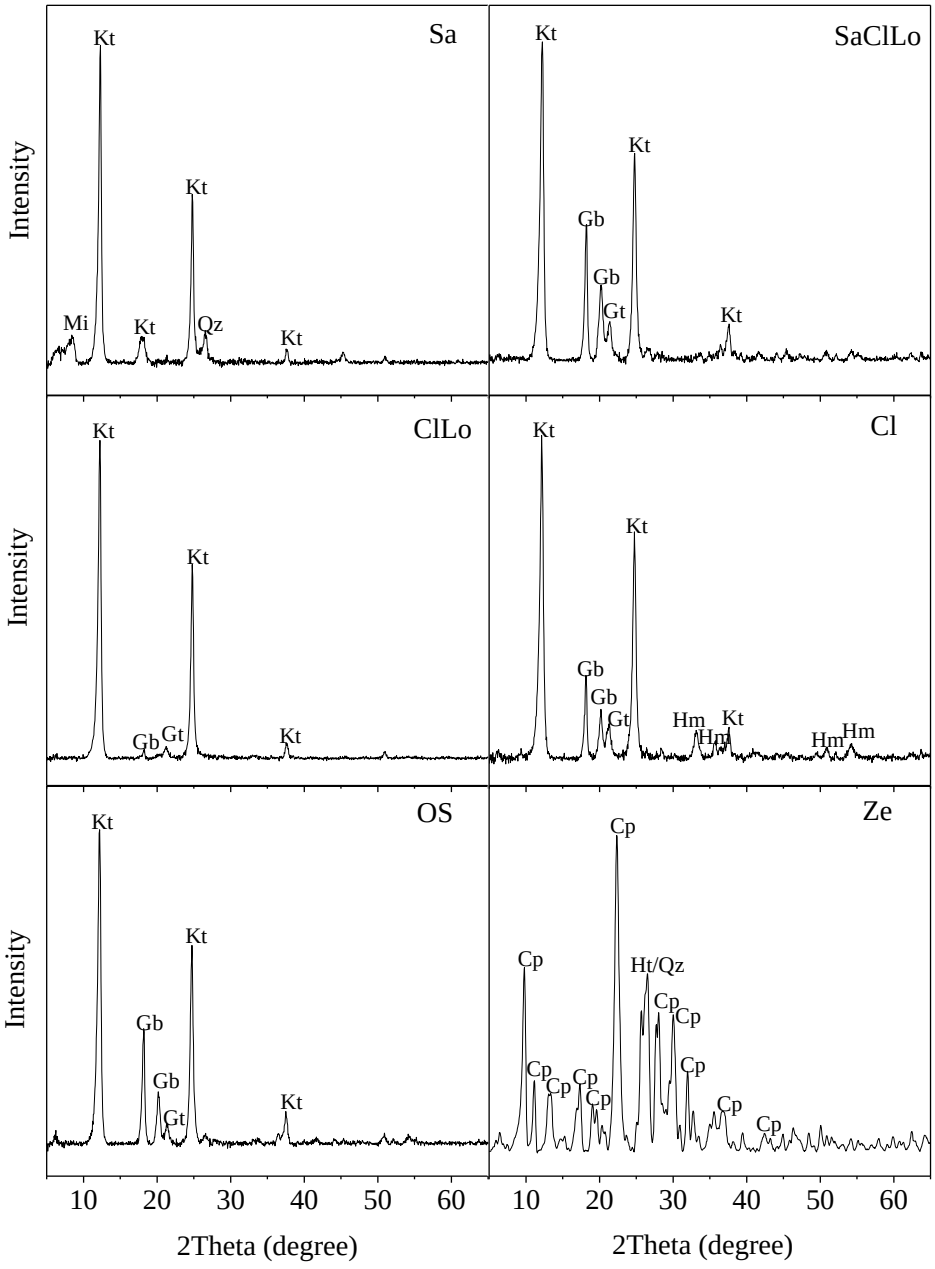

Figure 1. X-ray diffractograms of soils and zeolite. Minerals are identified above the peaks as follows: Kt = kaolinite; Gt = goethite; Gb = gibbsite; Hm = hematite; Qz = quartz, Mi = mica; Cp = clinoptilolite; and Ht = heulandite.

Hg adsorption

The mean percentage of Hg adsorbed reached more than 98% of the Hg originally in the contaminating solution. The high capacity of Hg adsorption by soils was also reported by other

researchers (Ding et al. 2017; Xue et al. 2013). This high capacity of Hg adsorption can be explained by the large number of adsorption locations in the mineral matrix of tropical soils (Coufalík et al. 2012).

Characteristics of adsorption isotherms

The experimental data of the amount of Hg adsorbed for each soil and for zeolite were fitted to the isothermic models of Freundlich and Langmuir (Figure 2). The Sa, SaClLo, and the Ze exhibited linear isotherms for the Langmuir and Freundlich models (Figure 2), which are characteristic isotherms for sorption at low concentrations (Cabrera et al. 2005), such as in the present study (0.05 - 2.4 mg L^{-1} of Hg).

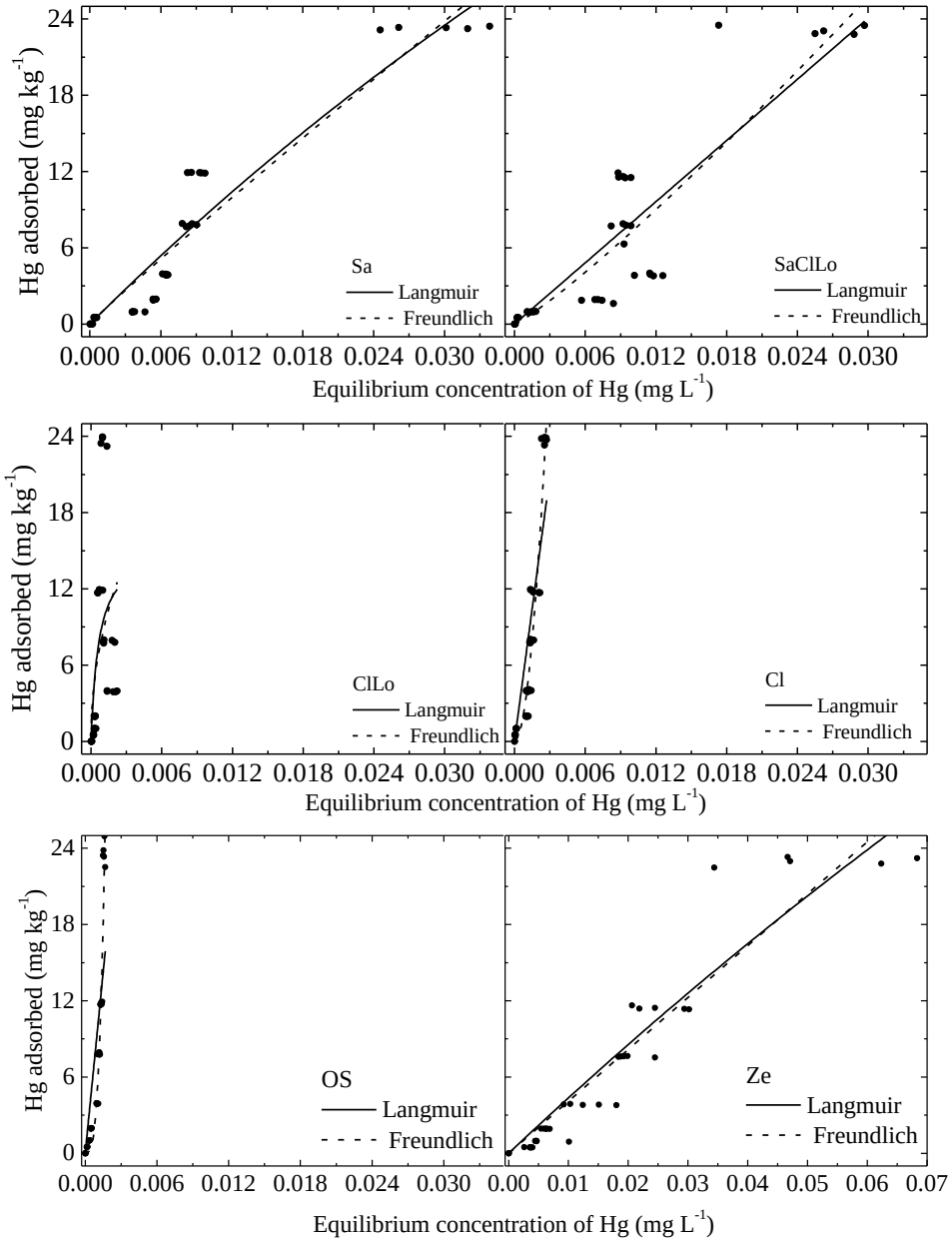

Figure 2. Adsorption isotherms for Hg according to the Langmuir and Freundlich model for the five Brazilian soils (0 - 20 cm) used in this study and for the zeolite.

The ClLo, Cl, and OS exhibited high adsorption affinity with Hg, forming type H isotherms for Langmuir and Freundlich (Giles et al. 1960). The type H isotherm is a special case of the type L isotherm, in which the solute shows high affinity for the soil matrix (Sposito

2008). The systems described by the type H isotherms likely have adsorption through covalent bonds, with formation of inner sphere complexes (specific adsorption) (Ding et al. 2017).

In the Sa, SaClLo, ClLo, and Cl, the O.M contents are low (Table 1). Thus, the high affinity of Hg adsorption in these soils is probably due to their mineral content, which in these soils is mainly composed of kaolinite and oxides (Figure 1) (Coufalík et al. 2012).

In contrast, in OS, the high Hg adsorption capacity (Figure 2) may be explained by the affinity of Hg to oxygenated functional groups of organic matter, such as hydroxyl, carboxylic, aromatic, and sulfur ligands (Miretzki et al. 2005b). Mercury is particularly prone to establish covalent bonds in adsorption locations with the reduced form of sulfur (Ding et al. 2017).

In the Ze, some precipitation of Hg may have occurred during the sorption processes due to the high pH of 7.4. According to the simulation of chemical speciation made, with this pH (7.4) and with the cation compositions found in our solutions, the formation of solid species of Hg ($HgOH_2$, $HgCl_2$, and HgO) is thermodynamically possible.

These species probably precipitated on the surface of the zeolite (Faulconer and Mazyck 2017). In systems in which pH is greater than the point of zero charge (PZC) of its constituents, as in zeolite, which has a PZC of ~ 6.0 (Castañeda-Juárez et al. 2019), the surface is negatively charged, such that the Hg cations have an electrostatic attraction to the surface. Thus, even though all the Hg species precipitated, they may have undergone reabsorption, which may explain the Hg adsorption (Figure 2), even with high pH values. Although the specific surface area and CEC are an important factor in metal ion adsorption processes, in porous materials like zeolite, the internal surface area is much more critical than the external (Ören and Kaya 2006). This also assists in explaining the Hg adsorption in the zeolite, even with a low value of CEC (1.6 $cmol_c\ kg^{-1}$).

The relevant parameters for evaluating Hg adsorption in the five soils and in zeolite were obtained from the Langmuir and Freundlich equations and are listed in Table 2. Two main

constants were obtained from the Langmuir equation (Table 2). The Q_0 parameter is generally used to estimate the maximum values of adsorption, since adsorption in a monolayer on a homogeneous surface is assumed (Ding et al. 2017). The Q_0 value was 139.05 mg kg^{-1} for Cl, 126.40 mg kg^{-1} for OS, 54.21 mg kg^{-1} for SaClLo, 0.23 mg kg^{-1} for the Ze, 0.15 mg kg^{-1} for Sa, and 0.02 mg kg^{-1} for ClLo.

Table 2. Adsorption isotherm constants and coefficients of determination (R^2) derived from the Langmuir and Freundlich equations of Hg adsorption in the studied soils and zeolite

Isotherm		Soil					
		Sand (Sa)	Sandy Clay Loam (SaClLo)	Clay Loam (ClLo)	Clay (Cl)	Organic Soil (OS)	Zeolite (Ze)
Langmuir equation	Q_0	0.15	54.21	0.02	139.05	126.40	0.23
	K_L	6.2	0.01	1528.5	0.05	0.07	1.95
	R^2	0.91**	0.80**	0.28^{NS}	0.80**	0.70**	0.91**
Freundlich equation	K_F	677.81	1421.3	235.23	2.32	5.15	407.91
	n	1.00	0.98	2.08	0.52	0.29	1.00
	R^2	0.90**	0.81**	0.21^{NS}	0.92**	0.93**	0.91**

^{NS} not significant, **significant at the 0.001 level. R^2 - coefficient of determination; Q_0 - the maximum sorption value (mg kg^{-1} soil); K_F - Freundlich constant (mg kg^{-1}); K_L - Langmuir constant related to the binding energy of the metal in the ground (mg L^{-1}); and n- soil affinity parameter for solute (dimensionless).

Nevertheless, saturation of the adsorption locations was not observed in the concentration range used in this experiment (0.05, 0.1, 0.2, 0.4, 0.8, 1.2, and 2.4 mg L^{-1} Hg) for all the soils and the zeolite. Therefore, the Langmuir fittings generate Q_0 values that do not represent the maximum adsorption capacity of the soils and zeolite.

The contamination range that was applied that tried to simulate the VRQ and the agricultural investigation value was then totally absorbed and not all adsorption sites were fully occupied. This means that even when Hg concentrations are up to the investigation value (our maximum concentration), there is a small possibility that Hg would be spread in the

environment, showing the suitability of this criteria when evaluating contaminated tropical soils. Soil properties were the main responsible for avoiding Hg moving in soil profile, but it does not mean that the Hg concentration at the investigation value does not cause risks, since Hg contents in soil above 0.36 mg kg^{-1} were enough to promote toxic effects on soil microbiota (Lima et al. 2019).

The K_L parameter represents the binding energy of Hg adsorption. The greater the value of K_L, the stronger the degree of spontaneous reaction (Ding et al. 2017). The adsorption intensity for Hg (II) occurred in the following order (Table 2): ClLo > Sa > Ze > OS > Cl > SaClLo. The highest K_L value for Sa soil may be due to the presence of primary minerals in its composition (Figure 1). According to Pablo et al. (2011) the Hg shows high bonding energy with minerals 2: 1 and the adsorption process occurs by inner-sphere complexes (covalent bonds) in the silanol and aluminum surface. Zeolite revealed to be an excellent option to adsorb Hg and it was already highlighted by other authors (Tauanov et al. 2020), but the clay and organic matter contents of the Cl and OS has surpassed its efficiency, showing the relevant role of tropical soils and their properties on Hg adsorption.

In the Freundlich equation, K_F represents adsorption capacity (Ding et al. 2017; Xue et al. 2013). The K_F values ranged from 2.32 to 1421.3 (Table 2). The *n* constant in the Freundlich model indicates the adsorption intensity or affinity between the adsorbate and adsorbent (Dada et al. 2012). The greater the value of 1/ n, the more quickly the adsorption process by the soil occurs (Xue et al. 2013). The values of 1/ n for the soils were in decreasing order as follows: OS > Cl > SAClLo > Ze > Sa > ClLo. The low Hg adsorption capacity in Clay Loam (ClLo) may have occurred due to the background concentration of Hg and to its chemical characteristics. Among the studied soils, this was the one that had the highest initial concentration of Hg (76 µg kg^{-1}) and the highest concentration of Ca and Mg. Therefore, during the adsorption test, potential sorption sites were heavily occupied with other cations, mainly Ca

and Mg as this soil has a base saturation index (BSI) of 80%. That resulted in low adsorption capacity for the added Hg.

These results indicate that the adsorption capacity of the heavy soil and organic soil is greater, and that the adsorption process in these soils probably occurs more spontaneously compared to the other types of soil and to zeolite.

Fourier - Transform Infrared Spectroscopy - FTIR

Analysis by FTIR was performed with the aim of investigating the Hg adsorption mechanisms in tropical soils and in zeolite. The FTIR spectra of the soils and of zeolite before and after contamination with Hg are shown in Figure 3. The soils exhibited peaks in the region of 400 - 4000 cm^{-1}, with maximum absorption at 3600, 3428, 2000, 1631, 1019, 740, 600, 530, and 420 cm^{-1} (Figure 3).

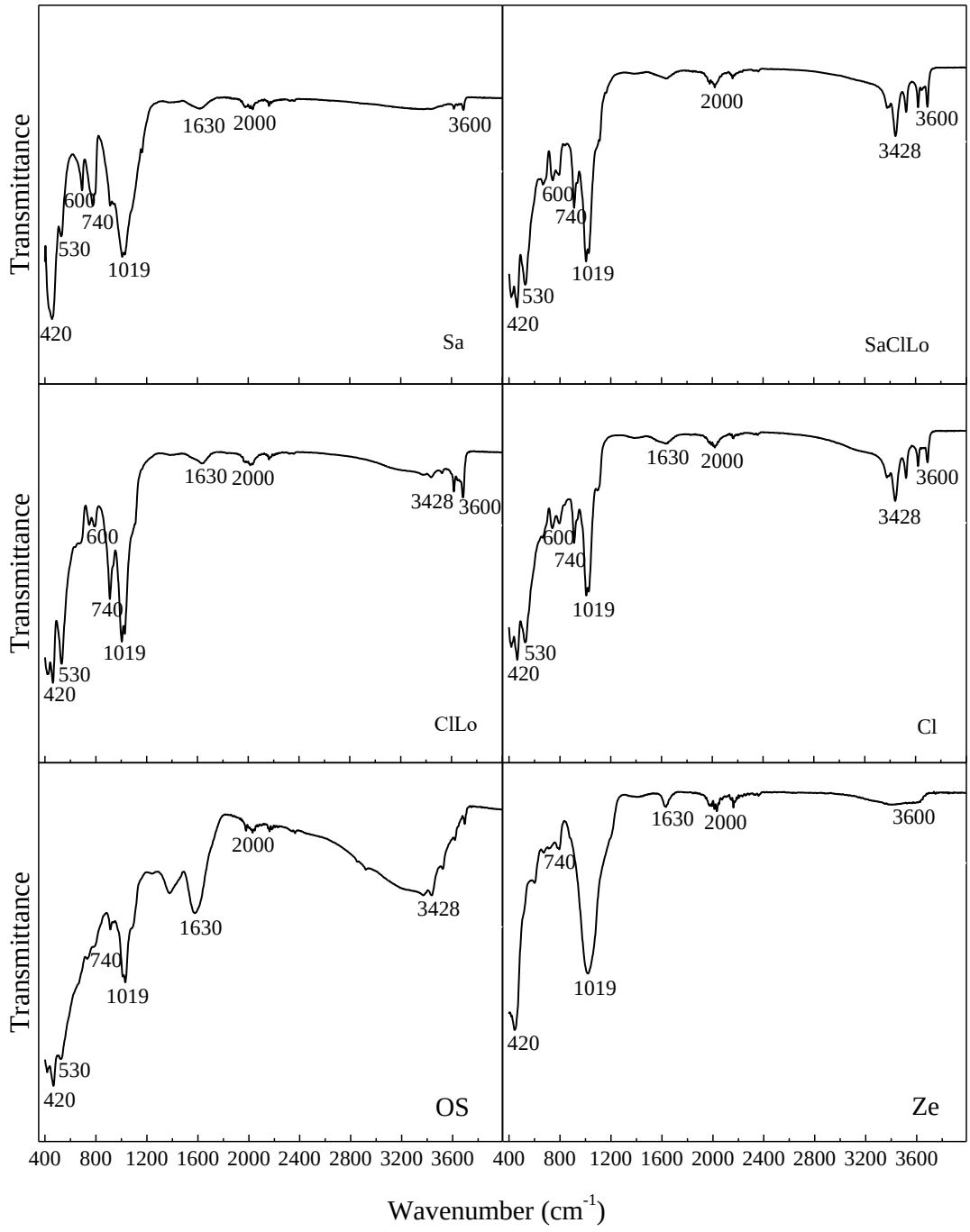

Figure 3. Fourier-transform infrared (FTIR) spectra of five soil samples and a zeolite, without Hg contamination.

Based on the main peaks that appear in the FTIR, the absorption bands of the soils can be clustered, according to their composition, into three regions: 4000 - 2000, 2000 - 1400, and

1200 - 400 cm^{-1} (Ma et al. 2017), corresponding to the region of bonds of oxygen - hydrogen, organic matter, and inorganic matrix of the soil (Krivoshein et al. 2020), respectively.

The relative absorbances of the main peaks found in the soils and in the zeolite without Hg and with Hg were quantified and compared to understand the mechanism of interaction of Hg with the functional groups (Table 3).

Table 3. The functional groups and mean relative absorbance (%) of the FTIR spectra of the soil samples and soil-Hg

Soil or soil-Hg	Relative absorbance at (cm^{-1})								
complex	3600	3428	2000	1630	1019	740	600	530	420
Sa	1.84	1.85	1.66	1.80	18.36	9.20	6.68	16.11	18.55
Sa - Hg	1.60	1.53	1.55	1.42	17.74	8.85	5.84	14.60	17.25
SaClLo	4.76	4.55	1.38	1.56	27.30	11.64	16.55	32.27	35.08
SaClLo - Hg	4.26	4.05	1.95	1.40	23.53	10.38	14.71	28.40	30.74
ClLo	5.73	3.63	1.93	2.38	29.90	10.49	15.43	35.24	37.73
ClLo - Hg	5.52	3.33	2.18	2.23	26.77	9.63	13.92	30.95	33.63
Cl	3.92	7.04	1.48	1.64	18.42	11.22	15.96	28.29	29.57
Cl - Hg	4.14	7.32	1.57	1.84	17.32	11.00	14.99	25.88	27.94
OS	3.19	7.08	1.43	7.17	14.13	12.54	16.32	21.35	22.57
OS - Hg	2.08	3.73	2.40	3.96	9.46	7.34	9.83	13.33	14.56
Ze	0.94	1.08	1.25	1.31	16.95	4.39	7.68	9.40	21.35
Ze - Hg	1.12	1.27	1.00	1.44	16.67	4.50	7.70	9.20	21.54

All the peaks of the soil in the 3600 cm^{-1} region decreased after contamination by Hg, due to strong interaction between the OH functional groups and the metal ions, revealing that the Hg can be adsorbed in clay minerals, quartz, and oxides (Figure 1), with hydrogen bonds formed by OH (Elkhatib et al. 2017). The stretching regions of 3697, 3651, and 3621 cm^{-1} are related to the vibration of the internal groups (Al - OH, Si - OH) between the kaolinite tetrahedral sheet and octahedral sheet (Sarkar et al. 2000).

A different behavior was observed only in the Cl. There was an increase in the peak intensity at 3600 cm^{-1} (Table 3), which may be due to its mineralogical composition (Figure 1) and high concentration of Fe oxides (Table 1). According to Kim et al. (2004), there is an angular deformation on the surface of Fe oxides during Hg sorption due to the establishment of covalent bonds. These deformations can change the intensity of the infrared energy absorption bands.

At 3428 cm^{-1}, where absorbance is attributed to the water molecule (Elkhatib et al. 2017), there was reduction in the relative absorbances upon comparing spectra of Hg contaminated and non-contaminated soils. These changes occur due to the ease with which Hg reacts with water, forming $HgOH_2$ and $HgOH^+$ (Soldán et al. 2002). The peaks of the 2200 to 2000 cm^{-1} bands are mainly attributed to stretching of the Si - O of the quartz present in the soil.

In the present study, the soils had wider variations in the absorbance bands at 450 - 1630 cm^{-1} (Table 3). This is the region in which vibrations of the functional groups of most of the clay minerals and oxides present in the soils occur (Krivoshein et al. 2020), such as aluminum oxides (Al - O and Al - OH), identified by vibrations of their reactive groups between 400 - 1100 cm^{-1} (Elkhatib et al. 2017). Vibrations also occur in the regions attributed to Fe oxides, such as hematite, which exhibits FTIR peaks at 530 and 420 cm^{-1}, corresponding to the Fe - O vibrations present in its structure (Schwertmann and Cornell 1991), and goethite, with peaks in the 670 to 450 cm^{-1} region, attributed to the asymmetric stretchings of Fe - O and Fe - OH (Blanch et al. 2008). The affinity between Hg and oxides in tropical soils was reported by Soares et al. (2015). Carvalho et al. (2019) also found a high positive correlation ($r > 0.80$) between the natural content of Hg and the oxide content in the soil, especially Fe oxides.

Thus, it can be affirmed that in tropical soils, Hg is more adsorbed in the functional groups of inorganic materials, such as clays and oxides (Ding et al. 2017). In clay minerals, these covalent bonds are formed between Hg and the silanol (≡ SiOH) and aluminol (≡ AlOH)

surfaces (Sarkar et al. 2000; Sha'Ato and Ajayi 2011). This mechanism explains why some soils, even with low CEC, such as ours, can adsorb a high amount of Hg.

The organic soil exhibited the greatest band differences after adsorption of Hg, with reduction of ~ 50% in relative absorbances (Table 3) of the soil inorganic and organic materials. The bands in the 1630 cm^{-1} region indicate the presence of C = C carbon bound to the aromatic structures and to C = O stretching of the carboxyl ion. When Hg interacts with the oxygen atoms of the carboxyl groups, the C = O bond increases, reducing the absorbances in the soil - Hg complex (Violante et al. 2007).

Complexation between organic acids and Hg can reduce production of methylated mercury, reducing the availability of inorganic Hg dissolved for the methylation performed by bacteria (Tomiyasu et al. 2017). The importance of organic matter in Hg adsorption was reported by Xue et al. (2013), with more than 98% (10 mg kg^{-1}) of Hg adsorbed in soils with O.M content > 50 g kg^{-1}. Xia et al. (1999) also indicated that the bond of Hg to humic acid surfaces was dominated by interactions with organic thiol functional groups in combination with carboxyl and phenol functional groups.

For the zeolite material, the relative absorbance values showed little variation in the presence of Hg (Table 3), probably because the Hg precipitated on the surface of the zeolite due to pH 7.4.

Speciation of Hg

The chemical speciation program Visual Minteq (Gustafsson 2005) was used to determine the inorganic species of Hg in the contaminating solution and in the supernatants after the adsorption experiments (Figure 4A and B). Minteq is an excellent option to determine Hg species in solution when other equipments are not available and it is a tool widely employed by other researches that also studied Hg and its dynamics in soils (Xu et al. 2014), mine wastes

(Navarro et al. 2009) and rivers (Sierra et al. 2017). However, it was not used yet to predict Hg species in a wide range of soil properties in tropical environments such as in our study, and it showed to be efficient also to this use.

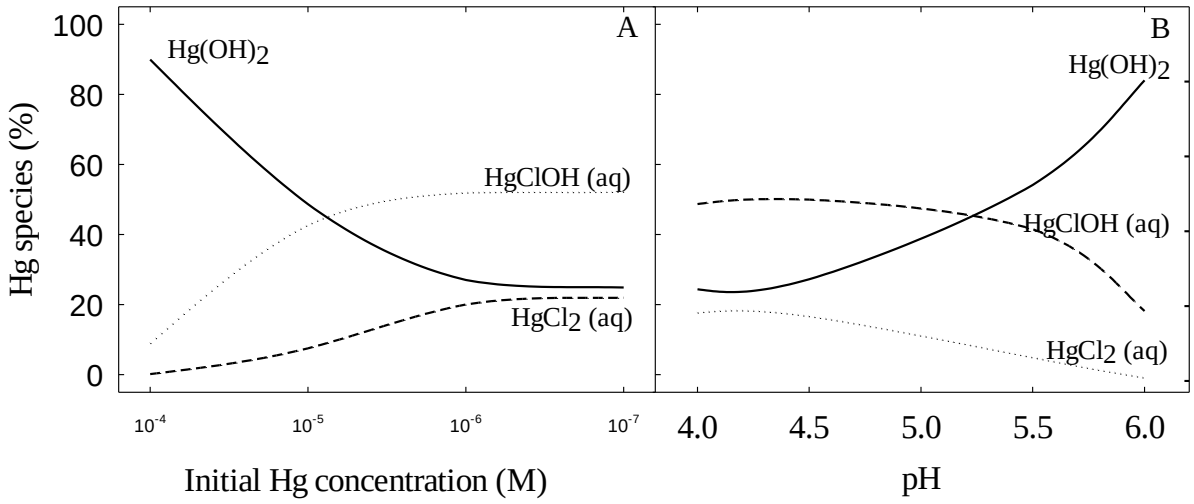

Figure 4. (A) Speciation of inorganic mercury in the contaminating solution in relation to initial concentrations of Hg, $Cl^- = 10^{-5}$ M, pH = 6. (B) Speciation of inorganic Hg in relation to the pH obtained in the adsorption trial of the soils and of zeolite, 10^{-5} M Cl^- and 10^{-5} M Hg.

The results show that the inorganic species dominant in the contaminant solution with pH 6 and 10^{-5} M Cl, which is the condition of the present study, were $HgOH_2$, HgClOH, and $HgCl_2$. When the initial concentration of Hg was greater than 10^{-4} M, 90% was of $HgOH_2$. As the solution became less concentrated, the percentage of $HgOH_2$ declined and the percentage of HgClOH increased. This higher formation of neutral chemical species may explain the greater adsorption of Hg in the soils, since from an energetic perspective, adsorption increases as the number of OH groups bound to Hg increases, due to its ability to create hydrogen bonds with the soil surfaces (Castro et al. 2011).

Although the Hg was supplied as $HgCl_2$, simulation indicated that this form was never the most prevalent under the conditions of the experiment (Figure 4). The absence of the

chemical species Hg^{2+} can also be noted in the solutions. When the ion Hg^{2+} was present in the solutions, it was lower than 1% in relation to the other species of Hg. This is a characteristic that differentiates Hg from other toxic metals, because it dissociates at a lower pH (Barrow and Cox 1992). The pK_1 value of Hg is 3.4 therefore, most of its chemical species in the solution studied were not in the form of Hg^{2+}, since the pH of all the soils and zeolites were higher than pH 4 (Table 1).

The increase in pH, as described in Figure 4, leads to a reduction in competitive binding of protons and to an increase in surface potential, which consequently increases electrostatic and specific binding between the Hg and the soil and zeolite surface. In addition, increases in pH can result in the formation of Hg hydroxide species ($HgOH_2$). Sorption of Hg on the solid surface is frequently reported in relation to predominance of hydrolyzed species of Hg (Miretzky et al. 2005a; Miretzky et al. 2005b).

The simulation of the chemical Hg species in the soil solution was made considering the DOC with the NICA - Donnan model and it shows both Hg in inorganic species and Hg complexed by organic species (Figure 5). According to the NICA - Donnan model, the bonds between metals and dissolved organic matter occur forming complexes with carboxylic functional groups (FA1) or phenolic functional groups (FA2) (Kinniburgh et al. 1999).

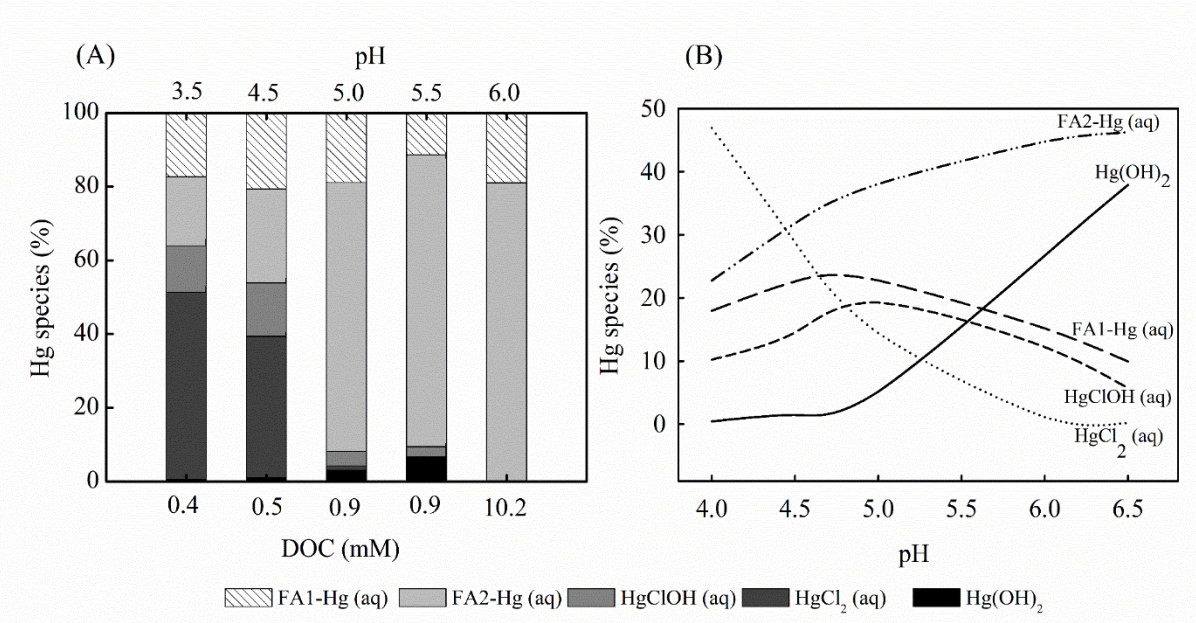

Figure 5. (A) Speciation of inorganic and organic Hg in relation to the dissolved organic carbon (DOC) and pH obtained in the adsorption trial of the soils, 10^{-5} M Cl^- and 10^{-5} M Hg. (B) Speciation of inorganic and organic Hg in relation to the pH obtained in the adsorption trial of the soils, 10^{-4} M DOC, 10^{-5} M Cl^- and 10^{-5} M Hg.

In soils with low DOC concentrations (0.4 and 0.5 mM) and low pH (3.5 and 4.5), the dominant species were inorganic, $HgCl_2$, HgClOH, and $HgOH_2$. On the other hand, in soils with 0.9 mM of DOC, the dominant species were FA1 - Hg and FA2 - Hg, with the inorganic species comprising less than 10% of the Hg in solution. For the soil with 10.2 mM of DOC, 100% of the Hg in solution was estimated to be oganically complexed, with 80% FA2 - Hg and 20% FA1 - Hg. Based on the simulation, Hg has formed complexes mainly with functional phenolic groups (FA2 - Hg), a result that agrees with our FTIR analysis (Figure 3 and Table 3).

Farmers frequently perform liming on soils to increase base saturation to 60% and soil pH to around 6, thus obtaining satisfactory crop development which leads to changes in Hg retention in these soils. Considering a concentration of 10^{-5} M Hg in the solution, which was the maximum concentration of Hg added in this study (Figure 4A and Figure 5B), applying

lime to increase soil pH to 6 would increase the percentage of Hg as $Hg(OH)_2$ and also as FA2 - Hg. On the other hand, $HgCl_2$ in the soil solution would be reduced from 20% (in the 'inorganic' simulation, Figure 4B) and 50% (in the 'organic' simulation, Figure 5B) to virtually 0%. That means that most of the Hg would remain in the form of $Hg(OH)_2$ and FA2 - Hg. Thermodynamic calculations of surface complexation models suggest that hydroxy metal species, like MOH^+ and $M(OH)_2$, are equally or even more adsorbed than free aqueous species (Castro et al. 2011).

The species of Hg complexed by dissolved organic matter, FA2 - Hg, dominant in soil solution with pH 6, reduces the adsorption of Hg on the surface of soil colloids (Ravichandran 2004). Several authors verified that Hg complexation by dissolved organic matter in aqueous solutions is the main factor reducing Hg adsorption in alkaline pHs (Liu et al. 2018; Ravichandran 2004; Schwartz et al. 2019).

Species formed by chloride complexes ($HgC1_2$ and $HgCl^-$) are not strongly adsorbed by the soil (Miretzky et al. 2005a; Park et al. 2018), thus remaining in the soil solution and exhibiting mobility through the soil profile. Considering that tropical soils generally have low pHs (Fontes and Alleoni 2006) and require pH adjustment for adequate crop growth, liming tends to increase Hg retention in soils that may be contaminated, reducing Hg mobilization to the environment.

Thus, soil management practices should take the predominant form of Hg into consideration, because this speciation of Hg indicates the response and mobility of Hg as an essential part of its risk analysis (Shetaya et al. 2019). Some countries are already taking Hg speciation and soil conditions into consideration to evaluate soil environmental quality. In 2018, China introduced reference values for the total Hg and methyl-Hg concentrations under specific soil pH values, due to differences in the bioavailability of Hg under different pH conditions (O'Connor et al. 2018).

Conclusions

Tropical soils have high capacity for Hg adsorption. From the Hg concentrations used in this study, it was not possible to observe maximum adsorption capacity by the Langmuir model, meaning that not all adsorption sites were fully occupied by Hg. Soil properties, particularly the ones of soil tropical, are responsible for strong Hg bindings during adsorption process.

The oxygenated inorganic functional groups of Si - O, Al - O, and Fe - O of the 1: 1 minerals, and Al and Fe oxides are mainly responsible for Hg adsorption in tropical soils with low organic matter contents.

Zeolite clinoptilolite has high Hg adsorption capacity and may be a promising alternative for remediation of Hg contaminated soils.

Acknowledgments

The authors would like to thank the following Brazilian institutions: the National Council for Scientific and Technological Development (CNPq), the Minas Gerais State Research Foundation (Fapemig), and the Coordination for the Improvement of Higher Education Personnel (CAPES) for financial support.

References

American Public Health Association. 2012. A Standard Methods for the Examination of Water and Wastewater APHA, Washington.

Araújo LG, Figueiredo CC, Borges IB, Ramos MLG, Rocha OC. Guerra AF. 2014. Organic matter fractions in soil under coffee with split applications of phosphorus and water regimes. Rev Bras Eng Agríc.Ambient. 18(3):1017–1022.

Araújo PRM, Biondi CM, do Nascimento CWA, da Silva FBV, Alvarez AM. 2019. Bioavailability and sequential extraction of mercury in soils and organisms of a mangrove

contaminated by a chlor-alkali plant. Ecotoxicol Environ Saf. 183:109469. https://doi.org/10.1016/j.ecoenv.2019.109469

Balzino M, Seccatore J, Marin T, De Tomi G, Veiga MM. 2015. Gold losses and mercury recovery in artisanal gold mining on the Madeira River, Brazil. J Clean Prod. 102:370-377. http://dx.doi.org/10.1016/j.jclepro.2015.05.012.

Barrow JN, Cox VC. 1992. The effects of pH and chloride concentration on mercury sorption. II. By a soil. J Soil Sci. 43:305-312. https://doi.org/10.1111/j.1365-2389.1992.tb00138.x

Belova TP. 2019. Adsorption of heavy metal ions (Cu^{2+}, Ni^{2+}, Co^{2+} and Fe^{2+}) from aqueous solutions by natural zeolite. Heliyon. 5(9):e02320. https://doi.org/10.1016/j.heliyon.2019.e02320

Blanch AJ, Quinton JS, Lenehan CE, Pring A. 2008. The crystal chemistry of Albearing goethites: an infrared spectroscopic study. Mineral Mag. 72:1043–1056.

Berdonces L, Higueras MA, Fernández-Pascual PL, Borreguero M, Carmona, M. 2017. The role of native lichens in the biomonitoring of gaseous mercury at contaminated sites. J Environ Manage. 186(3)207–213. https://doi.org/10.1016/j.jenvman.2016.04.047

Cabrera C, Gabaldón C, Marzal P. 2005. Sorption characteristics of heavy metal ions by a natural zeolite. J Chem Technol Biotechnol. 80(4):477–481. https://doi.org/10.1002/jctb.1189

Carvalho GS, Oliveira JR, Curi N, Schulze DG, Marques JJ. 2019. Selenium and mercury in Brazilian Cerrado soils and their relationships with physical and chemical soil characteristics. Chemosphere. 218:412–415. https://doi.org/10.1016/j.chemosphere.2018.11.099

Castañeda-Juárez M, Martínez-Miranda V, Almazán-Sánchez PT, Linares-Hernández I, Santoyo-Tepole F, Vázquez-Mejía G. 2019. Synthesis of TiO_2 catalysts doped with Cu, Fe, and Fe/Cu supported on clinoptilolite zeolite by an electrochemical-thermal method for the

degradation of diclofenac by heterogeneous photocatalysis. J Photochem Photobiol A Chem. 380:111834. https://doi.org/10.1016/j.jphotochem.2019.04.045

Castro L, Dommergue A, Renard A, Ferrari C, Ramirez-Solis A, Maron L. 2011. Theoretical study of the solvation of $HgCl_2$, HgClOH, $Hg(OH)_2$ and $HgCl_3^-$: A density functional theory cluster approach. Phys Chem Chem Phys. 13(37):16772–16779. https://doi.org/10.1039/c1cp22154j.

Conselho Estadual de Política Ambiental (COPAM), 2011. Deliberação Normativa 166, de 29 junho 2011.[accessed 2019 dec 10]. http://www.siam.mg.gov.br/sla/download.pdf.

Coufalík P, Krásenský P, Dosbaba M, Komárek J. 2012. Sequential extraction and thermal desorption of mercury from contaminated soil and tailings from Mongolia. Cent Eur J Chem. 10(5):1565–1573. https://doi.org/10.2478/s11532-012-0074-6.

Dada AO, Olalekan AP, Olatunya AM, Dada O. 2012. Langmuir, Freundlich, Temkin and Dubinin-Radushkevich isotherms studies of equilibrium sorption of Zn^{2+} unto phosphoric acid modified rice husk. IOSR J Applied Chemistry. 3(8):38-45. https://doi.org/10.9790/5736-0313845.

Ding X, Wang R, Li Y, Gan Y, Liu S, Dai J. 2017. Insights into the mercury(II) adsorption and binding mechanism onto several typical soils in China. Environ Sci Pollut Res. 24(30):23607–23619. https://doi.org/10.1007/s11356-017-9835-2.

Elkhatib E, Moharem M, Mahdy A, Mesalem M. 2017. Sorption, release and forms of mercury in contaminated soils stabilized with water treatment residual nanoparticles. L Degrad Dev. 28(2):752–761. https://doi.org/10.1002/ldr.2559

Faulconer EK, Mazyck DW. 2017. Influence of activated carbon surface oxygen functionality on elemental mercury adsorption from aqueous solution. J Environ Chem Eng. 5(3):2879–2885.

http://dx.doi.org/10.1016/j.jece.2017.05.036

Fontes MPF, Alleoni LRF. 2006. Electrochemical attributes and availability of nutrients, toxic elements, and heavy metals in tropical soils. Sci Agric. 63(6):589–608. https://doi.org/10.1590/s0103-90162006000600014.

Fontes MPF, Carvalho IA. 2005. Color attributes and mineralogical characteristics, evaluated by radiometry of highly weathered tropical soils. Soil Science Society of America Journal 69: 1162-1172.

Giles CH, MacEwan TH, Nakhwa SN, Smith D. 1960. Studies in adsorption. Part XI. A system of classication of solution adsorption isotherms, and its use in diagnosis of adsorption mechanisms and in measurement of specific surface areas of solids. J Chem Soc. 3973-3993.

Gmach MR, Cherubin MR, Kaiser K, Cerri EP. 2018. Process that influence dissolved organic matter in the soil: A review. Scientia Agricola.77(3):1-10. https://doi.org/10.1590/1678-992x-2018-0164

Gustafsson JP. Visual MINTEQ (version 2.32). Department of Land and Water Resources Engineering. The Royal Institute of Technology, Stockholm, Sweden, 2005. http://www.lwr.kth.se/english/OurSoftWare/Vminteq/.

Kim CS, Rytuba JJ, Brown Jr GE. 2004. EXAFS study of mercury(II) sorption to Fe and Al-(hydr)oxides: I. Effects of pH. J Colloid Interf Sci. 271:1-15. https://doi.org/ 10.1016/S0021-9797(03)00330-8.

Kinniburgh DG, Riemsdijk WH, Koopal LK, Borkovec M, Benedetti MF, Avena MJ. 1999. Ion binding to natural organic matter: competition, heterogeneity, stoichiometry and thermodynamic consistency. Coll Surf A: Phys-icochem Engineer Aspects. 151:147-166. https://doi.org/10.1016/S0927-7757(98)00637-2.

Krivoshein PK, Volkov DS, Rogova OB, Proskurnin MA. 2020. FTIR photoacoustic spectroscopy for identification and assessment of soil components: Chernozems and their size fractions. Photoacoustics. 18(6):100162. https://doi.org/10.1016/j.pacs.2020.100162

Kyllönen K, Hakola H, Hellén H, Korhonen M, Verta M. 2012. Atmospheric mercury fluxes in a southern boreal forest and wetland. Water Air Soil Pollut. 223(3):1171–1182. https://doi.org/10.1007/s11270-011-0935-1

Lima FRD, Martins GC, Silva AO, Vasques ICF, Engelhardt MM, Cândido GS, Pereira P, Reis RHCL, Carvalho GS,Windmoller CC, Moreira FMS, Guilherme LRG, Marques JJ. 2019. Critical mercury concentration in tropical soils: Impact on plants and soil biological attributes. Sci Total Environ. 666:472-479. https://doi:10.1016/j.scitotenv.2019.02.216

Liu P, Ptacek CJ, Blowes DW, 2018. Mercury complexation with dissolved organic matter released from thirty-six types of biochar. Bull Environ Contamin Toxic.103:175-180. https://doi.org/10.1007/s00128-018-2397-2.

Ma F, Zeng Y, Du C, Shen Y, Ma H, Xu S, Zhou J. 2017. Soil variability description using Fourier transform mid-infrared photoacoustic spectroscopy coupling with RGB method. Catena. 152:190–197. http://dx.doi.org/10.1016/j.catena.2017.01.005

Miretzky P, Bisinoti MC, Jardim WF. 2005a. Sorption of mercury (II) in Amazon soils from column studies. Chemosphere. 60(11):1583-1589. https://doi.org/10.1016/j.chemosphere.2005.02.050

Miretzky P, Bisinoti MC, Jardim WF, Rocha JC. 2005b. Factors affecting Hg (II) adsorption in soils from the Rio Negro basin (Amazon). Quim Nova. 28(3):438–443. https://doi.org/10.1590/S0100-40422005000300014

Navarro A, Cardellach E, Corbella M. 2009. Mercury mobility in mine waste from Hg-mining

areas in Almería, Andalusia (Se Spain). J Geochem Explor. 101:236-246. https://doi:10.1016/j.gexplo.2008.08.004

O'Connor D, Hou D, Ye J, Zhang Y, Ok YS, Song Y, Coulon F, Peng T, Tian L. 2018. Lead-based paint remains a major public health concern: A critical review of global production, trade, use, exposure, health risk, and implications. Environ Int. 121:85-101. https://doi.org/10.1016/j.envint.2018.08.052

Ören AH, Kaya A. 2006. Factors affecting adsorption characteristics of Zn^{2+} on two natural zeolites. J Hazard Mater. 131(1-3):59-65. https://doi.org/10.1016/j.jhazmat.2005.09.027

Osterwalder S, Bishop K, Alewell C, Fritsche J, Laudon H, Åkerblom S, Nilsson MB. 2017. Mercury evasion from a boreal peatlaLimand shortens the timeline for recovery from legacy pollution. Sci Rep. 7(1):1–9. https://doi.org/10.1038/s41598-017-16141-7.

Pablo L, Chávez ML, Abatal M. 2011. Adsorption of heavy metals in acid to alkaline environments by montmorillonite and Ca-montmorillonite. C Engin J. 171:1276-1286. https://doi.org/10.1016/j.cej.2011.05.055.

Park JH, Wang JJ, Xiao R, Pensky SM, Kongchum M, DeLaune RD, Seo DC. 2018. Mercury adsorption in the Mississippi River deltaic plain freshwater marsh soil of Louisiana Gulf coastal wetlands. Chemosphere. 195:455–462. https://doi.org/10.1016/j.chemosphere.2017.12.104

Ravichandran M. 2004. Interactions between mercury and dissolved organic matter- a review. Chemosphere. 55:319–331. doi:10.1016/j.chemosphere.2003.11.011.

Rodrigues SM, Henriques B, Coimbra J, Ferreira da Silva E, Pereira ME, Duarte AC. 2010. Water-soluble fraction of mercury, arsenic and other potentially toxic elements in highly contaminated sediments and soils. Chemosphere. 78(11):1301–1312. http://dx.doi.org/10.1016/j.chemosphere.2010.01.012

Rolka E, Szostek R, Grzybowski L, Ciećko Z. 2018. The uptake and translocation of mercury in plants of white cabbage (Brassica oleracea var. capitate f. alba) grown in soil contaminated with this element. Fresen Environ Bulletin. 27:3896-3905.

Sadej W, Żołnowski AC, Ciećko Z, Grzybowski L, Szostek R. 2020. Evaluation of the impact of soil contamination with mercury and application of soil amendments on the yield and chemical composition of Avena sativa L., J Environ Sci Health, Part A. 55(1)82-96. http://dx.doi.org/10.1080/10934529.2019.1667671.

Sarkar D, Essington ME, Misra KC. 2000. Adsorption of Mercury(II) by Kaolinite. Soil Sci Soc Am J. 64(6):1968–1975. https://doi.org/10.2136/sssaj2000.6461968x

Schwartz GE, Sanders JP, McBurney AM, Brown SS, Ghosh U, Gilmour CC. 2019. Impact of dissolved organic matter on mercury and methylmercury sorption to activated carbon in soils: implications for remediation. Environ Science: Proc Impacts.21:485-496. https://doi.org/10.1039/c8em00469b.

Segade SR, Tyson JF. 2003. Determination of inorganic mercury and total mercury in biological and environmental samples by flow injection-cold vapor-atomic absorption spectrometry using sodium borohydride as the sole reducing agent. Spectrochimica Acta Part B-Atomic Spectroscopy. 1031. Retrieved from https://scholarworks.umass.edu/chem_faculty_pubs/1031.

Sha'Ato R, Ajayi SO. 2011. Specific and exchange adsorption of mercury (II) on Ca-saturated kaolinitic soils in Central Nigeria. Int J Environ Waste Manag. 8(1–2):78–91. https://doi.org/10.1504/IJEWM.2011.040966

Schwertmann U, Cornell RM. 1991. Iron Oxides in the Laboratory: Preparation and Characterization. Wiley-VCH, Weinheim.

Shetaya WH, Huang JH, Osterwalder S, Mestrot A, Bigalke M, Alewell C. 2019. Sorption

kinetics of isotopically labelled divalent mercury ($^{196}Hg^{2+}$) in soil. Chemosphere. 221:193–202. https://doi.org/10.1016/j.chemosphere.2019.01.034

Sierra J, Roig N, Giménez Papiol G, Pérez-Gallego E, Schuhmacher M. 2017. Prediction of the bioavailability of potentially toxic elements in freshwaters. Comparison between speciation models and passive samplers. Sci Total Environ. 605-606:211–218. http://doi:10.1016/j.scitotenv.2017.06.136

Skyllberg U, Qian J, Frech W, Xia K, Bleam WF. 2003. Distribution of mercury, methyl mercury and organic sulphur species in soil, soil solution and stream of a boreal forest catchment. Biogeochemistry. 64(1):53–76. https://doi.org/10.1023/A:1024904502633

Soares LC, Egreja Filho FB, Linhares LA, Windmoller CC, Yoshida MI. 2015. Accumulation and oxidation of elemental mercury in tropical soils. Chemosphere. 134:181–191. https://doi.org/10.1016/j.chemosphere.2015.04.020

Soil Survey Staff. 2014. Keys to Soil Taxonomy, 12th ed. USDA-Natural Resources Conservation Service, Washington, DC.

Soldán P, Lee EPF, Wright TG. 2002. Microsolvation of Hg and Hg^{2+}: Energetics of $Hg{\cdot}H_2O$, $Hg^{2+}{\cdot}H_2O$ and $HgOH^+$. J Phys Chem A. 106(37):8619–8626. https://doi.org/10.1021/jp0263119

Sposito G. 2008. The Chemistry of Soils, 2nd ed. New York, NY:Oxford UniversityPress.

Tauanov Z, Lee J, Inglezakis VJ. 2020. Mercury reduction and chemisorption on the surface of synthetic zeolite silver nanocomposites: Equilibrium studies and mechanisms. J Mol Liq. 305:112825. http://doi:10.1016/j.molliq.2020.112825

Teixeira PC, Donagemma GK, Fontana A, Teixeira WG. 2017. Manual de métodos de análise de solo [Manual of soil analysis methods]. Brasilia (DF): EMBRAPA. Portuguese.

Tomiyasu T, Kodamatani H, Imura R, Matsuyama A, Miyamoto J, Akagi H, Kocman D, Kotnik J, Fajon V, Horvat M. 2017. The dynamics of mercury near Idrija mercury mine, Slovenia: Horizontal and vertical distributions of total, methyl, and ethyl mercury concentrations in soils. Chemosphere. 184:244–252. https://doi.org/10.1016/j.chemosphere.2017.05.123

Towett EK, Shepherd KD, Cadisch G. 2013. Quantification of total element concentrations in soils using total X-ray fluorescence spectroscopy (TXRF). Sci Total Environ. 463-464:374-388. https://doi.org/10.1016/j.scitotenv.2013.05.068

USEPA. 2007. Method 3051A for use of Microwave assisted acid digestion of sediments, sludges, soils, and oils. U.S. Environmental Protection Agency, Cincinnati, OH.

Vasques ICF, Lima FRD, Oliveira JR, Morais EG, Pereira P, Guilherme LRG, Marques JJ. 2020. Comparison of bioaccessibility methods in spiked and field Hg contaminated soils. Chemosphere. 254:126904. https://doi.org/10.1016/j.chemosphere.2020.126904

Violante A, Huang PM, Gadd GM. 2007. Biophysico-chemical processes of heavy metals and metalloids in soil environments. Wiley. doi:10.1002/9780470175484.

Windmöller CC, Durão WA, de Oliveira A, do Valle CM. 2015. The redox processes in Hg-contaminated soils from Descoberto (Minas Gerais, Brazil): Implications for the mercury cycle. Ecotoxicol Environ Saf. 112:201–211. http://dx.doi.org/10.1016/j.ecoenv.2014.11.009

Xia K, Skyllberg UL, Bleam WF, Bloom PR, Nater EA, Helmke PA. 1999. X-ray absorption spectroscopic evidence for the complexation of Hg(II) by reduced sulfur in soil humic substances. Environ Sci Technol. 33(2):257–261. https://doi.org/10.1021/es980433q

Xu J, Kleja DB, Biester H, Lagerkvist A, Kumpiene J. 2014. Influence of particle size distribution, organic carbon, pH and chlorides on washing of mercury contaminated soil. Chemosphere. 109:99-105. doi:10.1016/j.chemosphere.2014.02.058

Xue T, Wang RQ, Zhang MM, Dai JL. 2013. Adsorption and Desorption of Mercury(II) in Three Forest Soils in Shandong Province, China.sade Pedosphere. 23(2):265-272. http://dx.doi.org/10.1016/S1002-0160(13)60015-6

Zhang M, Liu J, Tian C, Wang R, Dai J. 2012. Effect of pH, Temperature, and the Role of Ionic Strength on the Adsorption of Mercury(II) by Typical Chinese Soils. Commun Soil Sci Plant Anal. 43(11):1599-1613.

Supplementary Material

Mercury adsorption in tropical soils and zeolite: characterization by Fourier-transform infrared spectroscopy

J.R.Oliveira[a]; I.C.F. Vasquesb; F.R.D. Lima[a]; G.S. Carvalho[a]; M.T.P. Job[b]; T.S. Oliveira[b]; J.J. Marques[a]*

[a] Department of Soil Science, Federal University of Lavras, Lavras, MG, CEP 37200-000, Brazil

[b] Department of Soil Science, Federal University of Viçosa, Viçosa, MG, CEP 36570-000, Brazil

Table S1. Particle size and chemical properties of the investigated soils collected from the 0-20 cm layer

Soil	K[1]	P[1]	Ca[2]	Mg[2]	Al[2]	H+Al[3]	SB[4]	T	BSI	ASI
	--mg kg^{-1}--		----------$cmol_c$ kg^{-1}----------					$cmol_c$ kg^{-1}	----%-----	
Sand (Sa)	48	19.2	0.3	0.1	0.7	4.3	0.5	4.8	10	59
Sandy Clay Loam (SaClLo)	42	0.5	0.4	0.1	0.3	2.1	0.6	2.7	23	32
Clay Loam (ClLo)	22	0.4	5.8	0.4	0	1.5	6.3	7.8	80	0
Clay (Cl)	42	0.4	1	1.1	0	2.3	2.2	4.5	49	1
Organic Soil (OS)	12	2.8	0.1	0.1	2.1	18.7	0.3	19	1	89

(1) P- K: extractant Mehlich, (2) Ca- Mg-Al: extractant KCl 1 mol L^{-1}; (3) H+Al: extractant SMP; SB: sum of bases, T: cation exchange capacity at pH 7, OM: Organic matter by oxidation with Na-dichromate and sulfuric acid, BSI: base saturation index, ASI: aluminum saturation index.

ARTICLE 2

Article prepared according to guidelines of the journal Science of the Total Environment
(Current status: Under review)

Volatilization of elemental Hg from soils: synthesis and characterization of adsorbent materials from industrial waste

J.R.Oliveira[a]; I.C.F. Vasques[b]; F.R.D. Lima[a]; M.T.P. Job[b]; G.S. Carvalho[a]; T.S. Oliveira[b]; J.J. Marques[a*]

[a] Department of Soil Science, Federal University of Lavras, Lavras, MG, CEP 37200-000, Brazil

[b] Departament of Soil Science, Federal University of Viçosa, Viçosa, MG, CEP 36570-000, Brazil

Contact: João José Marques; Federal University of Lavras, 1001, Dr Sylvio Menecucci Avenue, Minas Gerais, Brazil. Postal Code: 37200-000; E-mail: jmarques@ufla.br

Abstract

Four materials were synthesized to evaluate the adsorption capacity of Hg volatilized from soils: zeolite-NaP; two biochars (W and P) and hopcalite. Hg volatilization was also evaluated in four typical Brazilian soils in dry and moist conditions. A Hg trap system was built to measure soil Hg volatilization and adsorption by the synthetic materials under laboratory conditions. Typic Rhodustult, Humic Rhodic Acrustox, and Typic Ustifolist were incubated with 12 mg kg^{-1} of Hg, using $HgCl_2$ at 25 ºC for 48 h. Oxic Dystrudept was already contaminated in a former mining area and had a high Hg content (6.9 mg kg^{-1}). The volatilized Hg content under dry soil condition was 3.7, 3.4, 1.6, and 3.8 mg kg^{-1} d^{-1} of Hg and under moist soil condition was 5.5, 4.6, 2.5, and 4.2 mg kg^{-1} d^{-1} of Hg in Typic Rhodustult, Humic Rhodic

Acrustox, Typic Ustifolist and Oxic Dystrudept, respectively. Hopcalite was the material with the highest Hg adsorption capacity with 97, 53, 93 and 7% of the Hg value volatilized by Typic Rhodustult, Humic Rhodic, Typic Ustifolist and Oxic Dystrudept, in dry soil condition, respectively. Zeolite NaP adsorbed 1.0, 0.3, 0.2, 0.4 mg kg^{-1} of Hg, these values represent an adsorption of 27, 8, 14 and 9% of the total volatilized value by Typic Rhodustult, Humic Rhodic, Typic Ustifolist and Oxic Dystrudept, respectively, in the dry soil condition. Biochars W and P showed low Hg removal capacity (0.5 to 9%), when compared to hopcalite and zeolite NaP.

Keywords: contamination, hopcalite, zeolite, biochar, emission, adsorption, mercury.

Graphical abstract

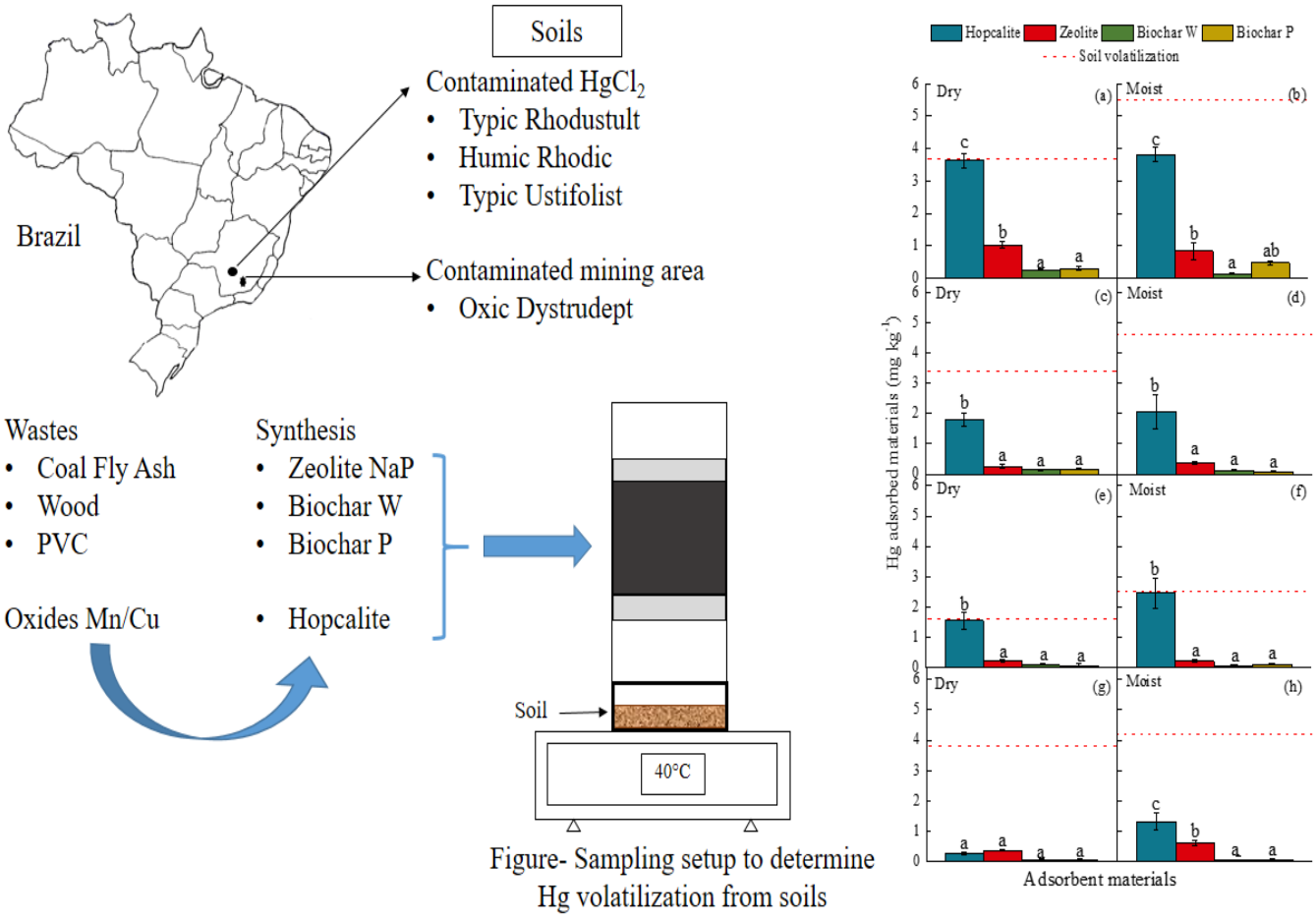

Figure- Sampling setup to determine Hg volatilization from soils

1. Introduction

The dynamics of Hg at the soil-atmosphere interface is an important component of the global and regional Hg biogeochemical cycle (Beckers and Rinklebe, 2017; Gustin and Jaffe, 2010; Pierce et al., 2015; Zheng et al., 2012). Global soil Hg emissions are around 500-1500 Mg yr^{-1}, which is approximately one third of the total global Hg anthropogenic emissions into the atmosphere (Agnan et al., 2016; UNEP 2013). When assessing Hg flow in 46 sites in the United States, Ericksen et al. (2006) estimated emissions of 52 Mg yr^{-1} in soils enriched with Hg and 43 Mg yr^{-1} in soils without anthropic contamination with Hg. Therefore, even at low concentrations, Hg can be emitted to atmosphere if there are favorable environmental conditions.

Mercury reactions in the environment are consequences of several factors, including its chemical speciation and the environmental conditions to which it is exposed. Environmental variables such as soil temperature (Rinklebe et al. 2010; Moore and Castro 2012), soil texture (Kocman and Horvat, 2010; Montoya et al., 2019), organic matter content (Kikuchi et al., 2013), and soil moisture (Kocman and Horvat, 2010; Sommar et al., 2016) can affect volatilization rates of soil Hg (Liu et al., 2014; Park et al., 2014). Once in the atmosphere, Hg can be dispersed and transported over long distances and later be deposited on the soil surface (Krabbenhof and Sunderland, 2013).

The method choice to measure Hg^0 emissions from soils depends on resource availability, as well as on specialized technical knowledge. Several studies have been published aiming the measurement of Hg volatilization rates at the interface soil-atmosphere (Converse et al., 2010; Margarelli and Fostier, 2005; Cizdziel et al., 2019; O'Connor et al., 2019). These studies use flow chambers or the micrometeorological technique. The use of flow chambers has the advantage of using simpler and less costly equipment (Osterwalder et al., 2018; Rinklebe et al., 2010), but it has as a use limitation concerning the great variation in the Hg^0 flow according

to operational conditions (chamber design and material, air pumping flow, moisture control) (Eckley et al., 2010; Wallschläger et al., 1999). The micrometeorological technique has the advantage of not disturbing the environment and consequently it leads to more representative quantification results, but requires the simultaneous measurement of several atmospheric parameters, thus its use is limited due to its complexity (Converse et al., 2010 Kim et al., 1995).

Most research using Hg^0 adsorbent materials is carried out to capture Hg from industrial emissions (Scala and Cimino, 2015; Xu et al., 2015; Yuan et al., 2012). Therefore, research efforts are needed to focus on developing acessible technologies in order to capture Hg emitted by soils, mainly in contaminated areas, and thus being able to interrupt this soil-atmosphere flow. Many materials are being evaluated for the oxidation, adsorption, and Hg catalysis. Most studied materials are metal oxides and waste materials such as zeolites and biochars (Mei et al., 2008; Cimino and Scala, 2015; Saleh, 2015; Xu et al., 2015; Saleh, 2016; Li et al., 2016; Xu et al., 2016, 2019; Zhao et al., 2017; Gao et al., 2018; Salama et al., 2018; Tauanov et al., 2018; Shan et al., 2019; Zendehdel et al., 2019; Zhang et al. 2019).

Coal combustion is a major source of anthropogenic Hg emissions in the atmosphere, representing ca. 60% of total emissions (Pacyna et al., 2010; UNEP, 2013). During this process of combustion, a residue called coal fly ash (CFA) is generated, which has a high content of silicon and aluminum and is highly reactive for being amorphous. Due to these characteristics, this waste is used as raw material for the synthesis of NaP zeolites (Aldahri et al., 2016; Cardoso et al., 2015a, 2015b; Ferrarini et al., 2016). NaP zeolites are widely used as catalyst carriers and adsorbents of potentialy toxic elements (Salama et al., 2018; Zendehdel et al., 2019; Zhang et al., 2019) due to the rich internal channel structure and the remarkable performance on metallic cations adsorption (Zhang et al., 2019; Tauanov et al., 2018).

Another alternative for Hg removal is biochar pyrolysed material from biomass, which forms low-cost carbon materials with properties similar to those of active carbon, with potential

application for the removal of Hg^0 (Gao et al., 2018; Li et al., 2016; Shan et al., 2019). Xu et al. (2016, 2019) studied a biochar produced by wood and polyvinylchloride (PVC) wastes and observed that the removal mechanism is chemosorption reactions at the active sites on the biochar surface functional groups.

Adsorbents based on metallic oxides have also been studied for the removal of Hg^0, as they are proven to have high adsorption and oxidation capacity, essential characteristics in the process of removing Hg^0 (Cimino and Scala, 2015; Mei et al., 2008; Saleh, 2015a; Saleh, 2016; Xu et al., 2015). For example, Zhao et al. (2017) studied a Mn/Cu bimetallic oxide sorbent to remove Hg^0 and concluded that this material has a high oxidation capacity for Hg^0.

Thus, this study aimed to explore two gaps of studies on Hg volatilization from soils: to synthesize adsorbent materials capable of capturing volatilized Hg from soils in low temperature conditions and to evaluate a simple and practical system to capture and measure volatile Hg from soils. In addition, based on the hypothesis that soil moisture is an important parameter in the flow of Hg from soil to atmosphere, the effects of soil moisture on Hg volatilization in four typical Brazilian soils was investigated.

2. Materials and Methods

2.1 Soil samples

Soil samples in this study were collected from 0 to 0.2 m, in natural areas with minimum anthropic influence in southern Minas Gerais, Brazil. The soils were classified according to the Soil Survey Staff (2014): Typic Rhodustult (23K 7,653,487 mN, 503,422 mE), Humic Rhodic Acrustox (23K 7,652,415 mN, 502,239 mE), and Typic Ustifolist (23K 7,652,415 mN, 503,917 mE). Also, a sample of Oxic Dystrudept (0-0.2 m) was collected in the Municipality of Descoberto, Minas Gerais, Brazil (23K 7,632,335 mN, 715,716 mE). This latter sample has

high Hg concentrations due to artisanal mining operations in the past (ca. 1850-1950) (Durão Junior et al., 2009; Tinôco et al., 2010) and was included to evaluate Hg losses from a long time contamination.

2.2 Soil properties determination

The samples were oven-dried at 30 °C, ground and sieved through 2 mm. The chemical and granulometric properties of the studied soils are shown in table 1. The standard methods of Teixeira et al. (2017) were used. The Hg content in the samples before incubation were determined by the USEPA 3051A method (USEPA, 2007).

Table 1- Granulometric and chemical properties of the Brazilian soils used in this study, collected at 0-0.2 m

Variable	Unit	Typic Rhodustult	Humic Rhodic Acrustox	Typic Ustifolist	Oxic Dystrudept
pH KCl		5.81	5.48	4.18	5.2
K[1]	mg kg^{-1}	21.95	42.23	11.8	36.82
P[1]		0.38	0.38	2.76	1.14
Ca[2]	$cmol_c$ kg^{-1}	5.82	0.97	0.12	2
Mg[2]		0.37	1.12	0.1	1.23
Al[2]		0.02	0.03	2.11	0.04
H+Al[3]		1.54	2.27	18.73	5.16
SB[4]		6.25	2.2	0.25	3.32
T[5]		7.79	4.47	18.98	3.36
OM[6]	g kg^{-1}	19.6	19.7	212.4	86.6
Clay	g kg^{-1}	380	540	300	320
Hg[7]	mg kg^{-1}	0.07	0.04	0.14	6.92

[(1)]extractant Mehlich-1; [(2)]extractant 1 mol L^{-1} KCl; [(3)]extractant SMP; [(4)] sum of bases; [(5)] cation exchange capacity at pH 7; [(6)] soil organic matter by oxidation with Na-dichromate and sulfuric acid; [(7)] digested by the method 3051A (USEPA, 2007) and determined by FI-HG-AAS (Penha et al., 2017).

For the mineralogical characterization, the clay fraction extracted from the soil samples was subjected to analysis by x-ray diffraction in a X'Pert PRO with CuKα radiation, varying from 4 to 70° 2θ, using a step of 0.01° 2θ, and a counting time per step of 1 s, at 40 kV and 30 mA.

2.3 Hopcalite Synthesis

Hopcalite was prepared by the co-precipitation method (Mele et al., 2012). The following chemical reagents were used: NH_4HCO_3, $KMnO_4$, $CuSO_4 \cdot 5H_2O$, H_2SO_4 (96 %, d = 1.83 g cm^{-3}) and $NaHCO_3$. All reagents were of analytical grade.

Initially 60 g of $KMnO_4$ were dissolved in 0.4 L of deionized water at 50 °C, constantly stirred for 10 minutes until complete dissolution. Then, 48 g of NH_4HCO_3 were added. The reaction begins to release heat until it reaches a temperature of 95 ºC, when MnO_2 precipitates. At the same time, the characteristic color of the K-permanganate disappears. The solution remained at room temperature for 3 h, and H_2SO_4 was added until pH = 3. In this suspension with MnO_2, 52 g of $CuSO_4 \cdot 5H_2O$ were added and stirred until dissolved. Then, 56 g of $NaHCO_3$ were added to precipitate Cu as $Cu(OH)_2CuCO_3$. The precipitate was washed with hot distilled water until no filtered SO_4^{2-} was observed by reaction with $BaCl_2$. The precipitate was dried at 70° C for 24 h. After drying, the samples of hopcalite were kept in a desiccator under vacuum to protect from being affected by air humidity.

2.4 Synthesis of zeolite NaP

The coal fly ash (CFA) used in the present study was collected in the electrostatic precipitator (EP), produced in the coal combustion at the Presidente Médici Thermal Power Plant (Candiota-RS, Brazil). After sampling, the fly ash samples were sieved through < 0.15 mm and oven dried at 105º C for 24 h. The total content of elements in the CFA was determined

by Total Reflection X-Ray Fluorescence Spectroscopy (TXRF), according by Towett et al. (2013) with modifications (Table S1-Supplementary data).

The zeolite NaP was synthesized by hydrothermal reaction using CFA with NaOH. For the synthesis, 15 g of CFA were placed in a borosilicate glass reactor with an internal volume of 500 mL, then 90 mL of 3 mol L^{-1} NaOH were added and kept for 24 h at 100° C in order to promote zeolithilization (Querol et al., 1997, 2001; Cardoso et al., 2015b).

After 24 h of hydrothermal activation, the reactor was removed from the greenhouse and, when at room temperature, the zeolite material was filtered (glass membrane, Millipore, 0.22 µm) and washed with deionized water until the residual NaOH was removed (filtrate pH < 10). Then the material was dried at 105º C for 12 h.

2.5 Biochar production

The biochars used in this study were provided by the Laboratory of Organic Matter and Waste of the Federal University of Viçosa, Brazil. The PVC and wood wastes (from constructions) used to make the biochars were ground and sieved through a 4 mm sieve, dried at 65 ºC for 48 h and characterized according Rodriguez et al. (2020) (Table S.2-Supplementary data).

Afterwards, the wastes were subjected to slow pyrolysis. The wastes were stored in metal tubes and hermetically sealed in a Linni Elektro Therm GMBH muffle, model KK260 SO 1060, equipped with a CC450 controller/thermal indicator. The heating rate was 10 °C min^{-1} until 500 °C and kept for one hour at there (Rodriguez et al., 2020).

2.6 Adsorbent characterization

2.6.1 X-Ray diffraction

The hopcalite, zeolite NaP, biochar W, and biochar P were characterized by x-ray diffraction in an X'Pert PRO apparatus with CoKα radiation in the range 4 - 70 °2θ using a step interval of 0.01 °2θ and a counting time per step of 1 s, with 40 kV tension and current of 30 mA.

2.6.2 SEM-EDS

To evaluate the morphological characteristics of the hopcalite, zeolite NaP, biochar W and biochar P materials, a scanning electron microscope (SEM), JEOL model JSM-6010LA, with a resolution of 4 nm at 20 kV. The spectrometric detector (EDS) was of the Silicon Drift type with a resolution of 133 eV. The materials were submitted to a gold covering (10 mA for 6 min) by using a coating system (Quorum Technologies LTD, shford, model Q150R). The micrograph magnification varied between 200 and 10.000 times.

2.6.3 FTIR spectrum

Hopcalite, zeolite NaP, biochar W, and P were characterized at infrared spectroscopy by Fourier transform (ATR- FTIR). The samples were dried at 35 ºC, ground in an agate mortar, and sieved in a 0.15 mm mesh. The analyses was performed in a Perkin Elmer Spectrum 1000 device with attenuated total reflectance, in which the powder of each sample was inserted into a diamond crystal port.The FTIR spectra of 32 scans were recorded in the wave number range 4000 - 400 cm^{-1} with a resolution of 2 cm^{-1} (Margenot et al., 2016).

2.6.4 Surface and textural characterization

The surface properties of hopcalite, zeolite NaP, biochar W and P (surface area, volume, size, pore distribution, and geometry) were determined by N_2 adsorption/desorption, using the BET method (Brunauer, Emmett and Teller, 1938) at -196 ºC in a Micromeritics equipment, model ASAP 2020. The samples were pre-treated before BET analysis with sample heating at a rate of 2 ºC min^{-1}, up to 300 ºC, for 6 hours, with a constant synthetic air flow of 130 mL min^{-1}. This treatment aimed to remove moisture on the solid surface and on the organic structure-directing agent. The N_2 adsorption isotherms were obtained in the range of P/Po, varying from 0.01 to 1.0. The total pore volume or cumulative volume (cm^3 g^{-1}) and the average pore diameter (nm) were determined at a relative pressure of 0.99. The pore size distribution was obtained by applying the BJH method (Barrett et al., 1951).

2.7 Elemental mercury volatilization

Volatility of soil Hg and adsorption was determined by a structure built with hopcalite, zeolite NaP, biochar P, and biochar W. The incubation of the soils Typic Rhodustult, Humic Rhodic Acrustox, and Typic Ustifolist was done with 12 mg kg^{-1} of Hg, using $HgCl_2$ and they were left to react at 25 ºC for 48 h. The Oxic Dystrudept already had a high Hg content (6.9 mg kg^{-1}) and was not contaminated (Table 1) in our experiment. To assess the influence of soil moisture on Hg volatility, tests were carried out with dry and humid soil samples (Kocman and Horvat, 2010), at 60 % of its field capacity to simulate a scenario of soil moisture after a typical spring-summer rain (20 mm) in the region where the soil samples were collected (INMET, 2019).

The system (Figure 1) was composed of: heating plate (1), soil sample incubated with Hg (2), glass borosilicate support structure (3), glass wool (4), and adsorbent materials (5). The soil samples incubated with Hg were placed in a glass container and connected to the support

structure containing the adsorbent materials. The system was placed on a hot plate with a constant temperature of 40 ºC (Kocman and Horvat, 2010) for 24 h, and kept inside a vertical flow hood with an air flow of 0.5 m s^{-1}.

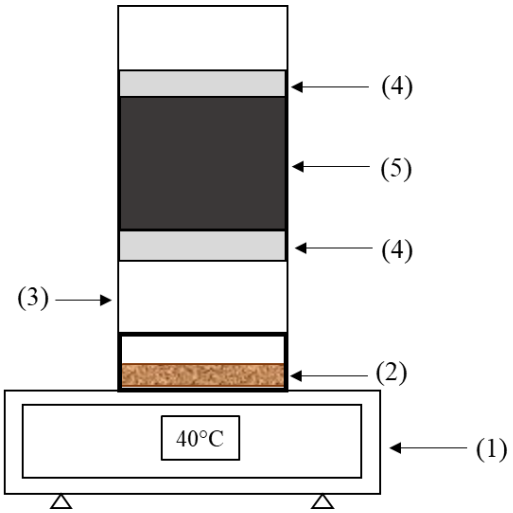

Figure 1. Sampling setup to determine Hg volatilization from soils: heating plate (1) soil sample with Hg (2), support structure (3), glass wool (4), adsorbent materials (5).

Blank samples, that is, samples composed only by the adsorbent materials without the presence of soil, were also run. They were kept in the same conditions as those with soil. After this period, the Hg content in soils and adsorbent materials was evaluated.

Considering that Hg losses could occur during the incubation time (48 h), the determination of the Hg content in the soils was carried out at the beginning of the volatilization test. Mercury volatilization data were obtained from the (i) Hg levels at the beginning of the test, (ii) background values of each soil, and (iii) Hg levels at the end of the test.

2.8 Mercury concentration determination

The Hg concentration in the soil and adsorbent materials was determined according to USEPA method 3051A (2007). One gram of soils, hopcalite, zeolite NaP, biochar W, and biochar P were digested with 10 mL of concentrated HNO_3 in Teflon® PTFE tubes. The vessels

were heated for 10 min. tiel reaching a pressure of 0.76 MPa and a temperature of 175 ºC and were then kept at such temperature and pressure for additional 10 min.

The analytical determination of Hg in soils, hopcalite, zeolite NaP, biochar W, and biochars P was done by Inductively Coupled Plasma Optical Emission Spectrometry (ICP-OES), in an equipment model Optima 7300DV, Perkin Elmer (Ghasemidehkordi et al., 2018).

2.9 Quality Control and Quality Assurance

To prepare the samples, a standard Au stock solution of 1000 mg L^{-1} was used for amalgamation of Hg and an aliquot of it with 1 mg L^{-1} of Au was added to all samples, calibration standards, and quality control standards. The calibration sample was prepared from a stock solution of 20 mg L^{-1} of Hg with the blank digestion solution matrix (conc. HNO_3) and 1 mg L^{-1} of Au. Quality control standards were prepared from a stock solution of 2 mg L^{-1} Hg, with a blank digestion solution and 1 mg L^{-1} Au (Han et al., 2006).

Ar each batch, two replicates of a certified sample with known Hg content (NIST SRM 2709a – "San Joaquin" soil) were added, as well as two blank samples for the calculation of the method detection limit (MDL). The MDL was calculated based on the standard deviation and the average Hg concentration of the blank samples, considering the Student's t-value for n = 7 and using the following equation (1) (APHA, 2012):

$$MDL = (\bar{x} + \mathrm{t} * \mathrm{s}) * \mathrm{d} \qquad (1)$$

where: $\bar{x}$ is the average content of the substance of interest in seven blank samples; t is the Student's-t value at 0.01 probability and n-1 degrees of freedom (for n = 7 and α = 0.01, t = 3.14); s is the standard deviation of the seven blank samples; and d is the dilution used in the sample. The MDL was calculated at 22 μg kg^{-1}.

All chemicals reagentes used were of analytical grade and all glassware was cleansed with 10 % HNO_3 to guarantee lack of contamination. The recovery rate of the certified sample

NIST SRM 2709a (“San Joaquin” soil) was 107 ± 16 %. Thus, the analytical procedure was considered satisfactory as acceptable recoveries are between 80 to 120 % (Hibbert, 1999).

2.10 Statistical Analysis

The data were analyzed according to a completely randomized design in a 4 × 4 × 2 factorial scheme with three replications, four soil types, four adsorbent materials, and two humidity levels. The data were submitted to variance analysis ($p < 0.05$) and the means were compared by Tukey test ($p < 0.05$). Independence, normality, linearity, and homoscedasticity were tested before analysis of variance (Su and Berenson, 2017).

3. Results and Discussion

3.1 Adsorbent characterization

3.1.1 X-ray diffraction analysis

The XRD pattern of the hopcalite showed an amorphous character and no diffraction related to the crystalline phases could be clearly identified (Figure 2). This diffraction pattern indicates the presence of mixed phases of Cu and Mn, common to Cu-and to Mn-oxides prepared by co-precipitation (Hutchings et al., 1998). These results are consistent with previous studies of amorphous hopcalite prepared by co-precipitation (Cole et al., 2010; Hutchings et al., 1998; Jones et al., 2009). According to these authors, interaction between Cu-oxides and Mn-oxides forms a highly disordered, low crystalline mixed oxide, which is the reason of the greater catalytic activity of hopcalite (Spassova et al, 1999).

After the hydrothermal phase and crystallization step, the main phase produced was identified as NaP zeolite ($Na_6Al_6Si_{10}O_{32}$ $12H_2O$). It is possible to observe the significant conversion of CFA into zeolite NaP and also the presence of quartz and mullite (Figure 2).

XRD spectral analysis of the biochar W and P produced at 500 °C showed a semi-crystalline phase (Figure 2). This can be attributed to the displacement and vacancy of structural atoms, mainly oxygen (Gerber et al., 2011), during pyrolysis favoring the amorphous phase. Several minerals identified were already present in the parent material of the biochars. The highest peaks were those of kainite (Ka), nephelite (Ne), and graphite (Gr). Other peaks are due to anydrite (Ad), silvite (Sv), and quartz (Qz).

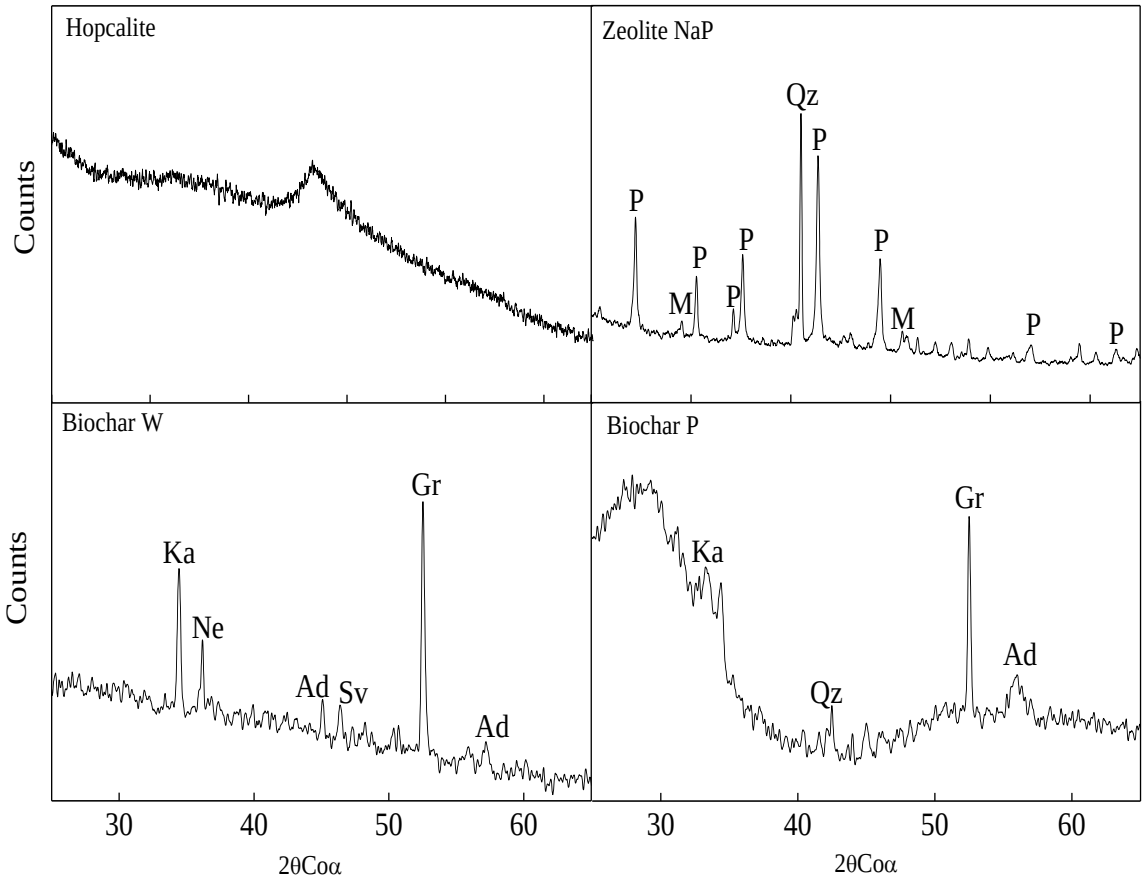

Figure 2. XRD spectra of hopcalite, zeolite NaP, biochar W and biochar P. P = zeolite NaP, M = mullite, Qz = quartz, Ka = kainite, Ne = nephelite, Ad = anydrite, Sv = sylvite, Gr = graphite.

3.1.2 SEM-EDS

The morphology of hopcalite is shown in Figures 3A and 3B. The hopcalite we synthesized was composed of aggregates of irregular spherical particles < 1 μm, with a rough surface. The morphology of the NaP zeolite synthesized in this study is shown in Figures 3C

and 3D. The shape of NaP zeolite was the same as reported in other studies (Cardoso et al., 2015a, b; Querol eta al., 2007). Typically, it is cauliflower-like, with well-defined edges and growth of anisotropic crystals, characteristic of the typical structure of the gismondine group (Breck, 1974; Sánchez-Hernández et al., 2016). This gismondin structure has smaller pore sizes than other zeolites, such as those with a Faujasite (FAU), Linde Type A (LTA), ZSM-5 (MFI), and Beta (BEA) structures, which makes the NaP zeolite useful for the separation of very small molecules as gas molecules (Tauanov et al., 2018; Zhang et al., 2019).

SEM micrographs revealed that the biochar W exhibits fibrous structures (Fernandez et al., 2012) (Figures 3E and F) probably due to the cellulosic structure of the parent material from which biochar was originated. These structures can be classified as fibrous and prismatic (Joseph et al., 2010), whereas the biochar P has a morphology characterized by small structures evenly spaced (Figure 3G and H).

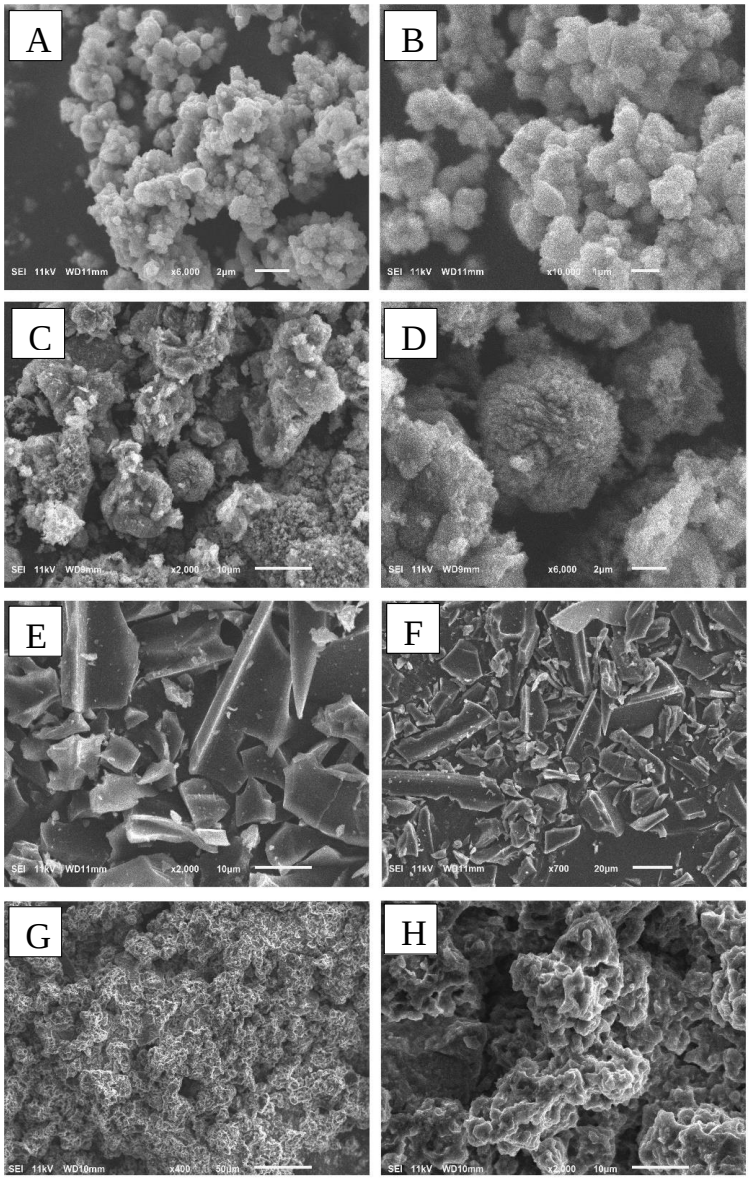

Element	Wt %	At %
O	21.8	49.4
Mn	65.8	43.4
Cu	12.3	7.0

Element	Wt %	At %
O	45.1	60.6
Na	19.7	16.7
Al	12.7	8.2
Si	22.5	14.5

Element	Wt %	At %
C	88.8	91.3
O	11.1	8.6

Element	Wt %	At %
C	20.8	32.9
O	36.6	45.1
Mg	9.0	5.9
Ca	33.4	15.9

Figure 3. SEM images: (A) and (B) hopcalite; (C) and (D) zeolite NaP synthesized 100 °C/24 hours; (E) and (F) biochar form wood (W); (G) and (H) biochar from PVC (P). Chemical composition by energy dispersive spectroscopy (EDS) for the adsorbent materials. Wt = weight percentage and At = atomic percentage.

The EDS analysis (Figure 3) showed that the hopcalite had no impurities on its catalytic surface (Cai et al., 2012). The weight proportion of Mn and Cu was 65 and 12 %. The atomic ratio of Cu/Mn in the hopcalite was approximately 0.16 and the weight ratio of Cu/Mn approximately 0.18. This Cu/Mn ratio contributes to the hopcalite morphology (Figures 3A and 3B), with small

and irregular particles. According to Jones et al. (2009) and Dey et al. (2017), MnO_2 acts as a spacer between the Cu crystals and reduces the size of the particles of hopcalite.

The presence of O, Si, Al, and Na (Figure 3) was verified on the zeolite surface. The Si/Al ratio of the zeolite was 1.78. The range 1.1 to 2.9 is considered the ideal ratio for the formation of the zeolite NaP from coal fly ash (CFA) (Cardoso et al., 2015b). Carbon is the major element in the biochar W with approximately 90% of the weight (Figure 3), but P, Mg, and Ca were also detected. These differences in the composition of the biochar are due to the composition of the material used (see supplementary data), which also causes differences in the morphology of the product obtained, as observed in Figure 3 E, F, G, and H.

3.1.3 Surface and textural characterization

Figure 4 shows the adsorption/desorption isotherms of N_2 at 77 K. The porosity of the zeolite NaP and the biochar P exhibit a type IV isotherm with high pressure desorption hysteresis (P/P0), which indicates a material with micropores (Sharma et al., 2012; Sharma et al., 2013). The hysteresis loops in these two materials are of the H2 and H3 type, associated with adsorbent materials that present a distribution of pore sizes and shapes not very well defined and in aggregates of plate-like particles that give rise to slit-shaped pores (Sing, 1985). This structure in NaP zeolite is formed by primary particles undergoing aggregation followed by crystallization and formation of empty spaces between adjacent crystalline particles (Sharma et al., 2013).

Hopcalite also exhibited an N_2 type IV adsorption/desorption isotherm but with a difference in hysteresis patterns as it presented an H1 loop, common in porous materials consisting of uniformly compacted spheres or clusters in a quite regular arrangement that gives rise to a mesoporous structure organized in a cylindrical shape (Sing, 1985, IUPAC). The

biochar W did not reveal a hysteresis defined during the adsorption/desorption of N_2, which can be associated with its morphology previously described.

The pore volume was calculated from the adsorption data using the BJH model (Barrett et al., 1951). All materials have a wide range of pore size distributions (1 - 35 nm). Hopcalite had greater pore volume with diameters < 5 nm. The zeolite had a pore volume three times greater in the diameter < 5 nm class, when compared to hopcalite. The biochar W and P showed low pore volumes.

The texture parameters of the materials were determined from the N_2 adsorption isotherms by the BET method (Figure 4). Zeolite was the material that had the largest surface area (53.4 m^2 g^{-1}), the largest pore volume (0.08 cm^3 g^{-1}), and the smallest pore size (0.9 nm). The biochars W and P had low specific surface area and pore volume but high pore diameter values.

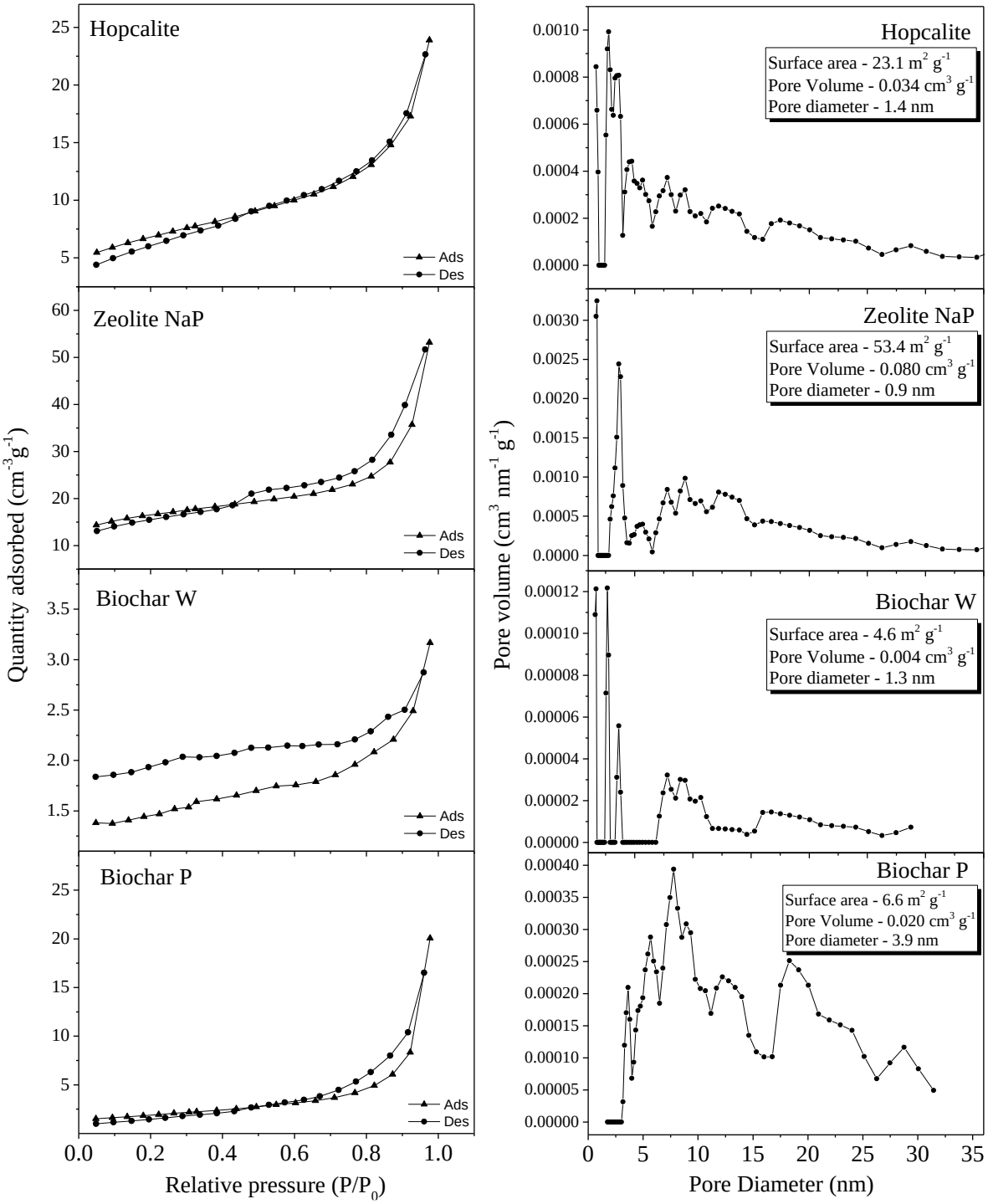

Figure 4- Adsorption/desorption isotherms with gas N2, pore size distribution curve, surface and texture parameters of the adsorbent synthesized materials: hopcalite, zeolite, biochar W, and biochar P.

3.1.4 FTIR spectrum

The formation of hopcalite was confirmed by the presence of three FTIR peaks (Figure 5), corresponding to the main functional groups of hopcalite on its surface, through the elongation of the MnO, CuO, and OH groups. The OH group is assigned to the 3480 cm^{-1} peak on the hopcalite surface, the MnO_2 group is assigned to the peak in the 1630 cm^{-1} band, and the CuO group to the 540 cm^{-1} (Dey et al., 2019; Dey et al., 2017). All functional groups identified in hopcalite contain oxygen. The adsorption strength on the hopcalite surface depends precisely on the oxygenated surface since Hg adsorption takes place mostly in the oxygenated functional groups (Dey et al., 2019; Ding et al., 2017).

The FTIR spectra of zeolite NaP match the infrared spectral data reported elsewhere for zeolite NaP (Albert et al., 1998; Breck, 1974; Huo et al., 2013) (Figure 5). Intense and sharp bands around 465 and 1007 cm^{-1} are related to the flexion and vibration mode of Si-O and Al-O bonds (Huo et al., 2013). The peak at 610 cm^{-1} indicates the double ring vibration that composes the structure of the zeolitic phase (Król et al., 2016; Quintero et al., 2012). In addition, the band around 750 cm^{-1} may be attributed to symmetrical stretching vibrations of the internal tetrahedron (Si, Al-O_4) in the zeolite structure (Courtney et al., 2015). The bands at 3480 and 1650 cm^{-1} are the characteristic peaks of water molecules (Król et al., 2016; Murphy et al., 2015).

Biochars W and P showed similar FTIR spectra (Figure 5). The differences between the biochars are: (i) the 2800 cm^{-1} spectral bands in the W biochar; and (ii) the 3400 cm^{-1} band in the P biochar. The 2800 cm^{-1} spectrum is attributed to the CH bond stretch band, representing the aliphatic group, typically methyl (CH_3) or methylene (CH_2) (Cantrell et al., 2012; Melo et al., 2013). These aliphatic groups are stable substances with low molecular weight of saturated and unsaturated fatty acids that are found in wood (Bodirlau and Teaca, 2007), which was the

parent material of this particular biochar W. An intense peak at 3400 cm^{-1} in biochar P is attributed to the vibration of the OH bond in the hydroxyl groups (Ding et al., 2017).

Other functional groups are also present in the biochar W and P (Figure 5). The group with triple bonded alkynes (C≡C) is shown from 2250 to 2100 cm^{-1} (Zhang et al., 2013). The peaks related to the chemical bindings in aromatic chains are from 1650 to 1500 cm^{-1}, represented by amide groups (N-H) (Zhang et al., 2013). The angular deformations in the C-H bonds of aromatic rings are in the range of 1290 to 1000 cm^{-1} and, from 900 to 650 cm^{-1}, the hydrogen groups (Barbosa, 2011; Li et al., 2015; Dong et al., 2016). The predominant functional groups in the biochar W and P are those containing C, due to the increased temperature during the pyrolysis process, and consequently loss of H, N, and O (Jesus et al., 2018; Rodriguez et al., 2020; Singh et al., 2012).

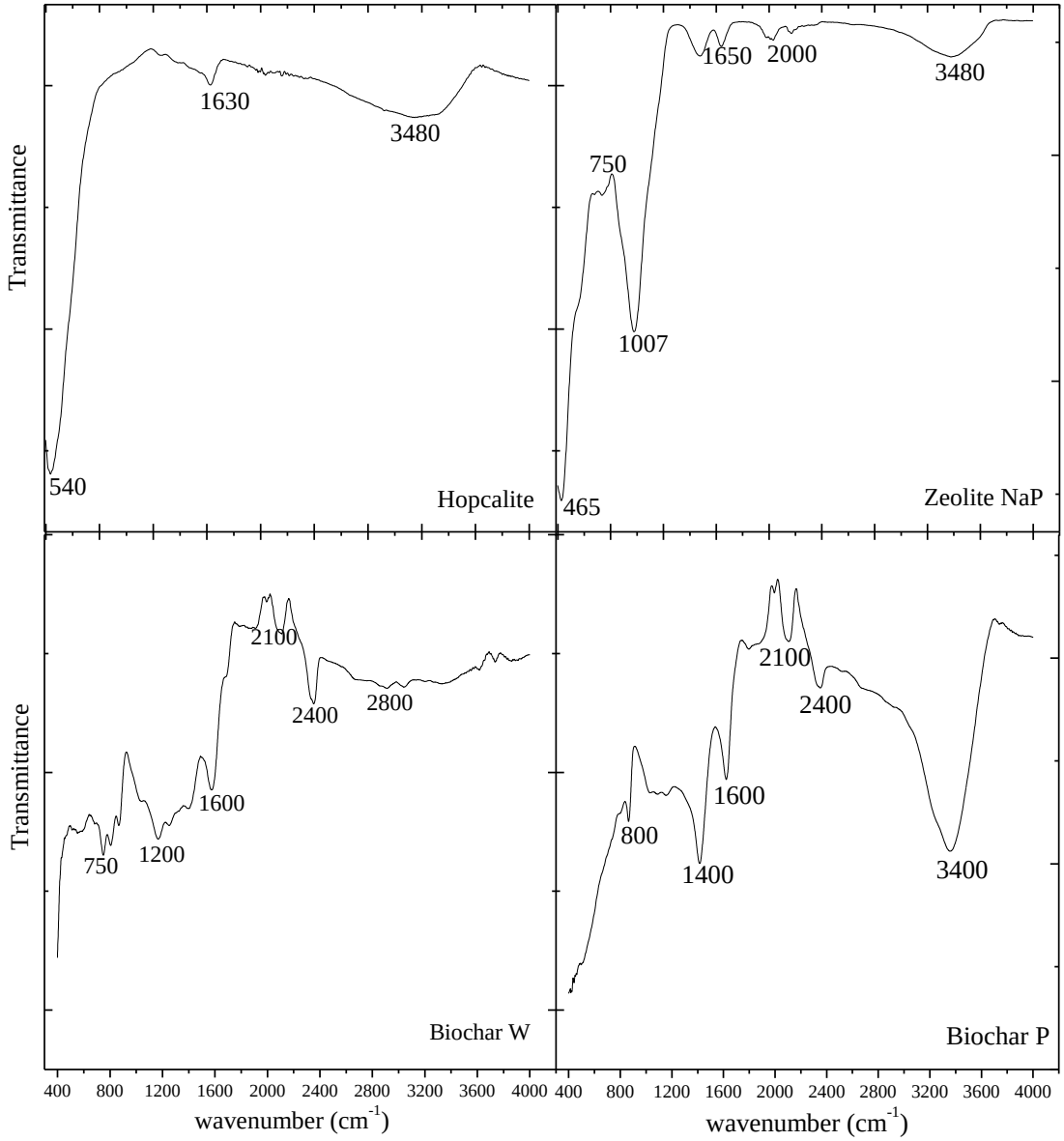

Figure 5- FTIR spectra of hopcalite, zeolite NaP, biochar W and biochar P.

3.2 Soil mineralogical characteristics

X-ray diffractograms (XRD) show that the Typic Rhodustult, Humic Rhodic Acrustox, and Typic Ustifolist used in this study have similar mineralogy, with the predominance of kaolinite, gibbisite, goethite, and hematite, these are typical minerals of highly weathered soils. However, since the Oxic Dystrudept is somewhat less weathered, it was also possible to identify the presence of 2:1 minerals such as smectite, vermiculite, and minerals of the mica and serpetinite group (Figure S.1- Supplementary Material).

3.2 Volatilization of Hg(0) from soils

3.2.1 Soils

The volatilized Hg content was 3.7, 3.4, 1.6, and 3.8 mg Hg kg^{-1} soil day^{-1} from Typic Rhodustult, Humic Rhodic Acrustox, Typic Ustifolist, and Oxic Dystrudept respectively, under dry conditions. Under moist conditions, volatilization was 5.5, 4.6, 2.5, and 4.2 mg kg^{-1} d^{-1} of Hg in Typic Rhodustult, Humic Rhodic Acrustox, Typic Ustifolist, and Oxic Dystrudept, respectively (Figure 7).

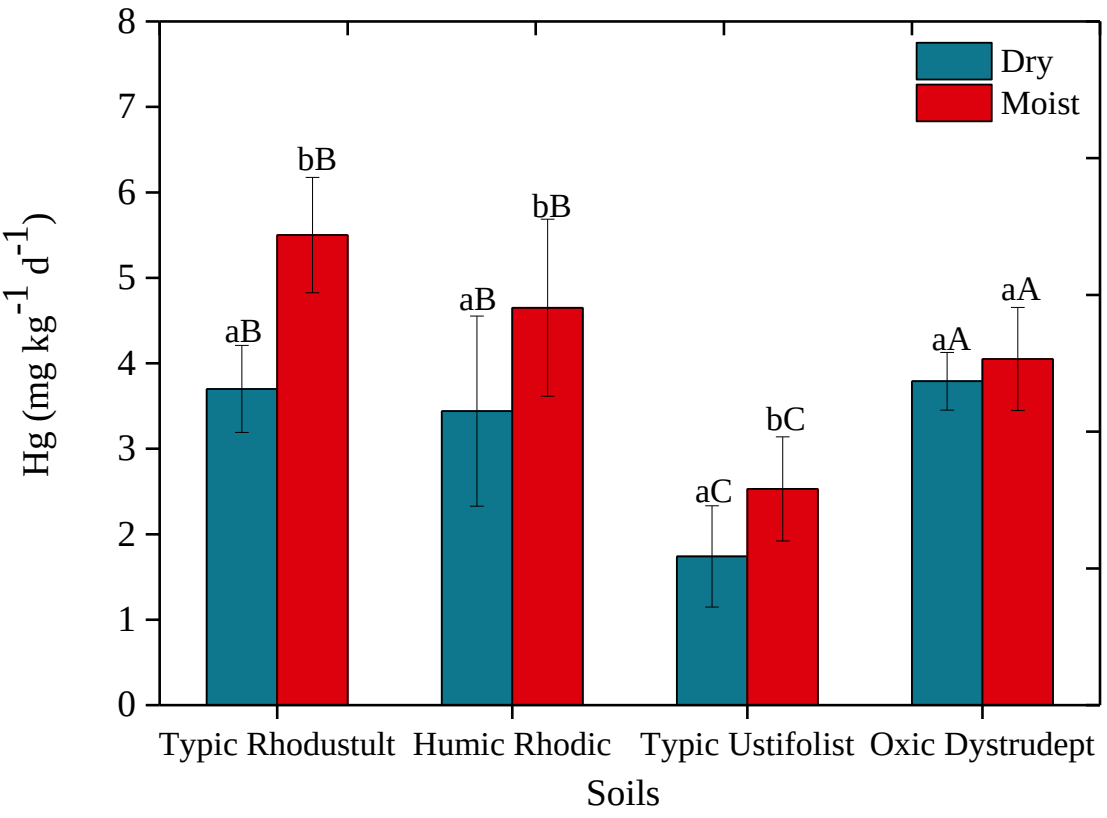

Figure 6. Lost Hg content from samples of Typic Rhodustult, Humic Rhodic Acrustox, Typic Ustifolist, and Oxic Dystrudept, from Brazil, kept at 40° C for 24 h, under dry and moist (60 % of field capacity) conditions. Lower case letters compare moisture conditions in each soil and upper case letters compare soils in each humidity condition, by Tukey test ($n = 3$ and $p < 0.05$).

Extrapolating our data over a time lapse of one year over an area of 1 hectare (bulk density = 0.9 g cm^{-3} and soil depth 0-20 cm), it is estimated that surface soil contaminated with 12 mg kg^{-1} of Hg can release up to 3.7 Mg ha^{-1} yr^{-1}, considering the Typic Rhodustult which

presented the highest Hg emission at the moist soil condition. At the same conditions, Hg emission estimated at the Typic Ustifolist would be 1.7 Mg ha^{-1} yr^{-1}. These results are superior to the field measurements made by García-Sánchez et al. (2006), using a flow chamber, which found an Hg emission rate of 0.2 Mg ha^{-1} yr^{-1} in an area contaminated by gold mining in Venezuela.

Hg^0 emission data from soils are still very uncertain due to the lack of direct measurements. According to Kocmam et al. (2013), Hg^0 emissions from soils contaminated by several anthropogenic sources (chlor-alkali industry, artisanal and small-scale gold mining, non-ferrous metal production) ranged from 14 to 34 Mg yr^{-1}. Using a dynamic flow chamber, Ericksen et al. (2006) conducted 1326 measurements of Hg^0 flow in agricultural, desert, pasture and forest ecosystems and obtained an estimation of Hg^0 flow rate between 34 and 69 Mg yr^{-1}. In general, soil properties are considered determinant factors for Hg emission together with Hg content and speciation, and Hg concentration in the atmosphere (Lin et al., 2010; Zhang e Lindberg, 1999; Xin e Gustin, 2007).

Typic Rhodustult and Humic Rhodic Acrustox, even being clayey, showed high Hg volatilization. Perhaps, the low OM content of these soils (Table 1) has allowed such volatilization in spite of the clay content. Soils with low OM contents have fewer Hg sorption sites and have increased Hg volatilization, for adsorbed Hg^{2+} is less likely to be reduced if compared to Hg^{2+} free in solution (Leterme et al., 2014; Schlüter 2000). In solution, Hg^{2+} can be reduced by abiotic and biotic causes. Generally, the abiotic reduction of Hg^{2+} is enhanced when the concentrations of Hg in soils are low (Nriagu et al., 1994; Schlüter 2000). That means that, at the high concentrations used in this study (12 mg kg^{-1} of Hg), biotic reduction was probably induced through the microbiological detoxification process (Dash et al., 2017; Devars et al., 2000; Naguib et al., 2018).

The biotic reduction process is mediated by bacteria resistant to Hg that have the merA gene, which reduces Hg^{2+} to Hg^0 that passively diffuses from inside the cells to the solution (Chen et al., 2018: Wang et al., 2020), and the merB gene, which produces enzymes capable of breaking the C-Hg bond and turning Hg^{2+} ions available for reduction (Barkay et al., 2003; Wang et al., 2020). Mahbub et al. (2016) observed 79 % of the initial Hg to be volatilized after 6 hours by a resistant bacterial isolate grown in medium with 3 mg L^{-1} of Hg.

The role of O.M. becomes more evident when comparing Typic Ustifolist, which revealed the lowest volatilization, to Typic Rhodustult and Humic Rhodic Acrustox (Figure 7). The lower loss of Hg may be due to their greater OM content (Table 1), as O.M. has been described by several authors as a major Hg sorbent in soils (Guédron et al., 2013; Gruba et al., 2014; Obrist et al., 2011; O'Driscoll et al., 2011). Also, the presence of O.M seems to increase the oxidation of Hg^0 to Hg^{2+} (Windmoller et al., 2015), which can also increase the adorption rates of Hg in soils, since Hg^{2+} is more adsorbed than Hg^0 (O'Connor et al., 2019), explaining why the soil with greater organic matter allows less volatilization. The sorption of Hg to organic matter is related to functional groups containing oxygen (C = O, carbonyl), sulfur (-SH, thiol), and nitrogen (-NH_2, amino and –CN, cyano), as Hg is a soft acid and tends to form strong bonds with these functional groups (Maia et al., 2019; Moharem et al., 2019; Wang et al., 2020). Thus, the content of organic material in soils can significantly affect the solubility, mobility and toxicity of soil Hg (Sysalova et al., 2017; Chai et al., 2012; Oliveira et al., 2020).

Due to the long time (several decades) since contamination, it was expected that the Oxic Dystrudept showed a lower Hg volatilization. Durão Junior et al. (2009), in a study on Hg speciation in this Descoberto area, found that most of the Hg at the site is in the form of Hg^{2+}, stabilized in the soil by sorption onto soil minerals (Fe, Mn, and Al oxides). Nevertheless, our data shows that ca. 58% (4 mg kg^{-1} d^{-1}) of the original Hg content may volatilize in only 24 h (Figure 7) under our experimental conditions, which included sieving and other drastic

disturbances. Thus, soils contaminated by Hg, even after long time, may volatilize high amounts of Hg, as long as environmental conditions are favorable. Long-term volatilization of Hg is a well-known concern in many places, including contaminated soils in a mercury mine in Spain emitting to the atmosphere 0.96 to 156 μg kg^{-1} d^{-1} of Hg (Kocman et al., 2004). As one might expect, the *in vitro* conditions under which we run our samples do not reflect field conditions. Under field conditions, Hg contaminated soil is expected to suffer higher variations in temperature and moisture, in addition to the stabilization effect of vegetation cover, all factors are known to affect significantly Hg emissions (Kockman et al., 2004; Fantozzi ert al., 2013).

With this high volatilization rate in soils of Decoberto, it would be expected that no Hg would be found. However, even greater contents of Hg were found in Descoberto in the past. One of the first studies in that site, 10 years ago, reported Hg concentrations in soils in the range of 0.0371-161 mg kg^{-1} (Durão Jr et al., 2009), suggesting intensive loss of Hg compared to current (2019) levels.. In addition, vegetation cover, soil compaction and structure can be responsible for differences between the so far unknown real Hg emissions in Descoberto and the emission we determined in laboratory. Soil structure disturbances can increase Hg^0 emissions after rupturing the thin oxidation layer on Hg-bearing particles (García-Sánchez et al., 2006).

Soil moisture is one of the main variables that affect soil Hg volatilization (Briggs and Gustin, 2013; Xin et al., 2007; Carpi and Lindberg, 1998; Gillis and Miller, 2000). Mercury volatilization in three (Typic Rhodustult, Humic Rhodic Acrustox, and Typic Ustifolist) out of four soils was increased by soil moisture (Figure 7), by 48, 26, and 34%, respectively. The increase in Hg volatilization with moisture can be due to the physical displacement of Hg^0 already present in the soil to above-air by water molecules. A chemical process is also likely to happen such as desorption of Hg^0 by water, creating an available pool of Hg^0. Soft acids such as Hg are more prone to establish bonds with N and S than O. Therefore, the oxygen-functional

groups from minerals can have more affinity for water. (Lindberg et al., 1999) (Gustin and Stamenkovic, 2005). Ci et al. (2016), after a rain simulation, observed an immediate (20 min.) increase in the flow of Hg^0 from the soil, and attributed this increase to the physical displacement of Hg by H_2O. Then, the movement of Hg in the soil profile towards the surface (i.e. emission to the atmosphere) is governed by the soil properties that influence its oxidation and adsorption (Carvalho et al., 2019; Ci et al., 2016; Montoya et al., 2019; Oliveira et al., 2020).

3.2.2 Adsorbents

The adsorbent materials studied showed differences in retaining Hg^0 volatilized from soils in dry and moist conditions (Figure 7). Below, each sorbent is discussed according to soil moisture, as this variable had a major influence on Hg volatilization in the evaluated soils (Figure 6).

Hopcalite was the material with the highest Hg adsorption capacity with 97, 53, 93, and 7 % of the Hg volatilized by Typic Rhodustult, Humic Rhodic, Typic Ustifolist, and Oxic Dystrudept, in dry soil condition. In moist conditions, hopcalite adsorbed 69, 44, 98, and 31% in Typic Rhodustult, Humic Rhodic, Typic Ustifolist and Oxic Dystrudept, respectively.

This result shows that hopcalite has high capacity to retain volatilized Hg. This is due to its amorphous character (Figure 2), to its porous structure formed by micropores (Figure 4), and to its surface composed of oxygenated functional groups MnO, CuO, and OH. These have strong interactions with Hg because they are capable of oxidizing Hg^0 to Hg^{2+} and adsorb it on its surface (Xu et al., 2015; Yang et al., 2011).

According to He et al. (2018), removal of Hg^0 by hopcalite begins with the physical adsorption process. Then the adsorbed Hg^0 is oxidized to Hg^{2+} by the transfer of electrons from Mn^{4+} and production of Mn^{3+}, which is reoxidized by CuO, returning to Mn^{4+}. The oxidized

Hg^{2+} then reacts with oxygen and forms HgO on the hopcalite surface. This ability of Mn- and Cu-hopcalite to react with Hg enhances the ability to capture Hg (Du et al., 2015; Wang et al., 2014).

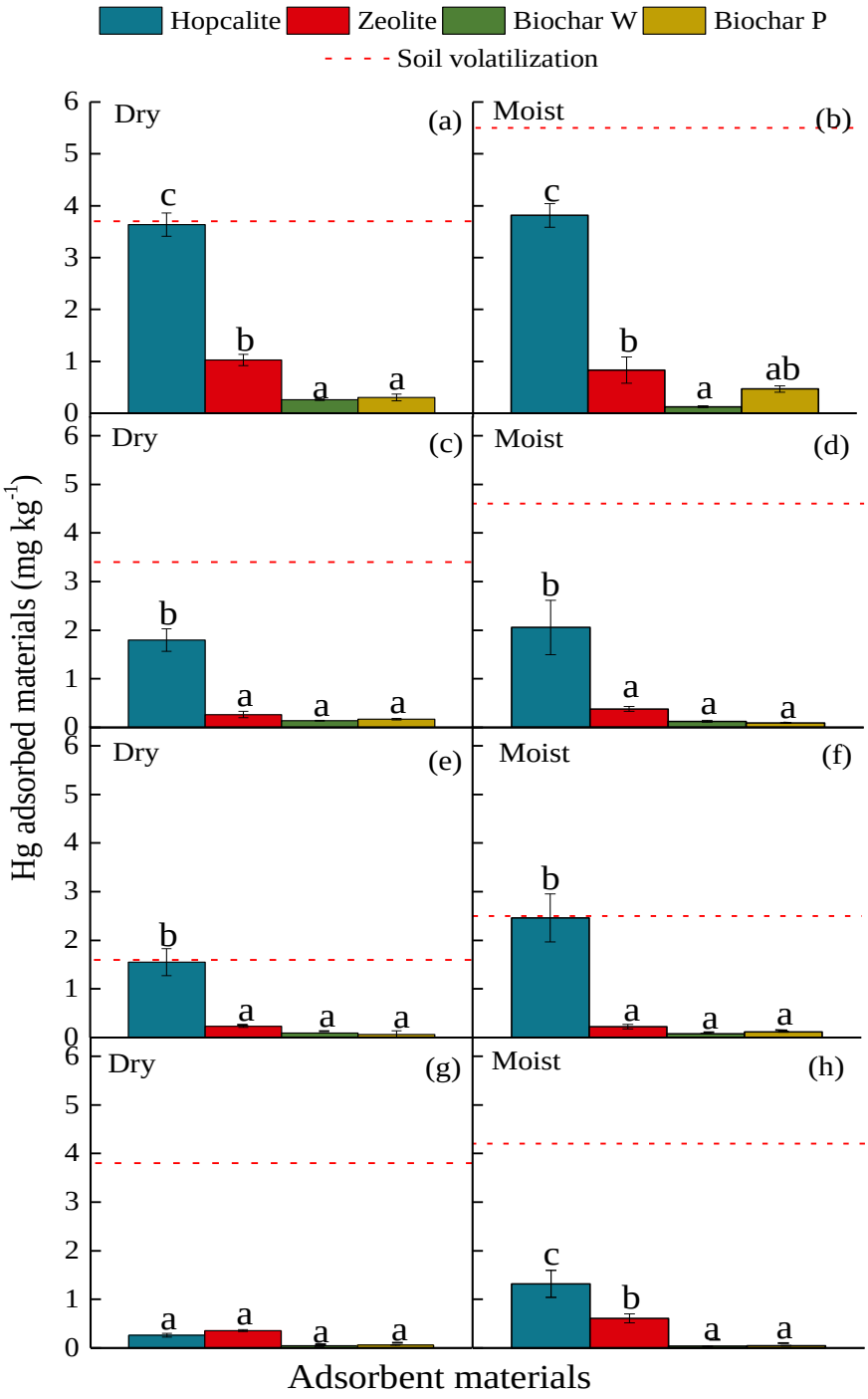

Figure 7. Hg content in adsorbent materials: hopcalite, zeolite NaP, biochar W and P obtained from the soil volatilization: Typic Rhodustult (a) and (b), Humic Rhodic Acrustox (c) and (d), Typic Ustifolist (e) and (f), and Oxic Dystrudept (g) and (h), maintained at 40 °C for 24 h, in

the conditions dry and moist (60% of the field capacity). Lowercase letters compare Hg content among the adsorbent materials, by Tukey test ($p < 0.05$). Dashed red line indicates the maximum volatilization of Hg during the test in each soil.

Zeolite NaP also showed potential for capturing Hg volatilized by soils, with adsorption of 1.0, 0.3, 0.2, 0.4 mg kg^{-1}, representing an adsorption of 27, 8, 14, and 9% of the total volatilized by Typic Rhodustult, Humic Rhodic, Typic Ustifolist, and Oxic Dystrudept, respectively, in the dry soil condition (Figure 7). The same Hg adsorption behavior was observed in the moist soil condition (Figure 7). The feasibility of zeolite NaP as Hg adsorbent is explained by its surface area and porosity, which were 53.4 m^2g^{-1} and 0.08 cm^3g^{-1}, respectively (Figure 4), in addition to its porous structure composed by mesopores (Figure 4) capable of retaining Hg^0 within its structure (Bohra et al., 2013; Sharma et al., 2013; Zhang et al., 2019). Thus, the NaP zeolite can either (i) adsorb Hg^0 directly into its pores or , ii) first oxidize Hg^0 and then adsorb Hg^{2+} by the anions on its surface.

However, even showing a greater surface area and porosity compared to hopcalite, zeolite NaP had lower Hg^0 adsorption potential (Figure 7), meaning adsorption of gaseous forms of Hg does not occur only through pure physical process; there is a chemical adsorption process involved as well. Studies show that when zeolites are activated with Ag, Au, Br, Fe and Mn their Hg^0 adsorption capacity are increased (Dong et al., 2009; Qi et al., 2015; Qu et al., 2009; Wei et al., 2015; Wdowin et al., 2014; Wiatros-Motyka et al., 2013).

Biochars W and P showed low Hg removal capacity (0.5 to 9 %) when compared to hopcalite and zeolite NaP (Figure 7). That was the result of its physical such and chemical characteristics, such as morphology (Figure 3) and IR absorbance (Figure 5). At low temperatures, like the one used in our study (40 °C), physisorption is favored, while at high temperatures chemisorption is favored (Li et al., 2015; Shen et al., 2017). In a study of Hg^0 removal by modified biochar, Shen et al (2017) observed that the highest efficiency of physical

and chemical adsorption was at ca. 120 °C. This helps us explain in part the low adsorption of Hg^0 by biochars W and P. Besides, the main functional groups found in the biochars W and P were aliphatics, alkynes, and amides (Figure 5), all groups with no oxygen. This may be the determining factor for low Hg adsorption, as oxygenated functional groups are responsible not only for the oxidation of Hg^0 (Ding et al., 2017; Tan et al., 2012) but also by its later adsorption by anionic species present on the surface (Huggins et al., 2003; Hutson et al., 2007; Shen et al., 2017).

The low values of Hg adsorption in all materials studied in Oxic Dystrudept may have occurred due to possible variations in volatile Hg chemical species as this soil is contaminated by Hg for a long period of time, unlike the other studied soils that were contaminated for this experiment using $HgCl_2$. This, the aged contamination, may have led to low values of Hg adsorption by the tested materials, which were synthesized to adsorb Hg^0. In addition to Hg^0, soils can volatilize dimethyl Hg [$(CH_3)_2Hg$] during methylation (Wallschlager et al., 1995; Wang et al., 2019). Methylation potential is directly linked to the time Hg remains in the soil, as the longer the time Hg remains in contact with the soil, the greater the potential for formation of methylHg and dimethylHg (Bisinoti and Jardim, 2004; Ma et al., 2018; Wallschlager et al., 1995; Wasserman et al., 2002; Weber et al., 1998). Thus, in areas contaminated by gold mining, Hg^0 can be oxidized for the formation of dimethylHg. This formation can occur in aerobic and anaerobic conditions (Bisinoti and Jardim, 2004; Ma et al., 2018).

4. Conclusions

The methods used in the synthesis of hopcalite and zeolite NaP are efficient as confirmed by XRD, SEM/EDS, FTIR, and BET analysis. Although its retention capacity is lower than hopcalite, considering that it is a material made from a waste and without any chemical modification, zeolite NaP seems promising for Hg retention at low temperature

conditions (40 °C). Both biochars W and P, pyrolysed at a temperature of 500 °C, show low Hg retention capacity. Soils with low levels of organic matter present high Hg^0 volatilization capacity regardless of their clay content and the increase in soil moisture favors the volatilization of Hg^0.

Acknowledgments

This study was funded by the Coordenação de Aperfeiçoamento de Pessoal de Nível Superior (CAPES), Conselho Nacional de Desenvolvimento Científico e Tecnológico (CNPq), and Fundação de Amparo à Pesquisa do Estado de Minas Gerais (Fapemig). The authors would like to thank the Federal Unversity of Viçosa for the analyzes carried out in the Soils Department. The authors would like to thank Renê Chagas da Silva, Sukarno Olavo Ferreira e Márcio José Gomes Alvarenga for their support in the analyzes of the characterization of the adsorbent materials.

References

Agnan, Y., Le Dantec, T., Moore, C.W., Edwards, G.C., Obrist, D., 2016. New Constraints on Terrestrial Surface-Atmosphere Fluxes of Gaseous Elemental Mercury Using a Global Database. Environ. Sci. Technol. 50, 507–524. https://doi.org/10.1021/acs.est.5b04013

Albert, B.R., Cheetham, A.K., Stuart, J.A., Adams, C.J., 1998. Investigations on P zeolites: Synthesis, characterisation, and structure of highly crystalline low-silica NaP. Microporous Mesoporous Mater. 21, 133–142. https://doi.org/10.1016/S1387-1811(97)00059-0

Aldahri, T., Behin, J., Kazemian, H., Rohani, S., 2016. Synthesis of zeolite Na-P from coal fly ash by thermo-sonochemical treatment. Fuel 182, 494–501.

https://doi.org/10.1016/j.fuel.2016.06.019

American Public Health Association. 2012. A Standard Methods for the Examination of Water and Wastewater APHA, Washington.

Barbosa, L.C.A., 2011. Espectroscopia no infravermelho na caracterização de compostos orgânicos, Editora UFV, Viçosa.

Barkay, T., Miller, S.M., Summers, A.O., 2003. Bacterial mercury resistance from atoms to ecosystems. FEMS Microbiol. Rev. 27, 355–384. https://doi.org/10.1016/S0168-6445(03)00046-9

Barrett, E.P., Joyner, L.G., Halenda, P.P., 1951. The Determination of Pore Volume and Area Distributions in Porous Substances. I. Computations from Nitrogen Isotherms. J. Am. Chem. Soc. 73, 373–380. https://doi.org/10.1021/ja01145a126

Beckers, F., Rinklebe, J., 2017. Cycling of mercury in the environment: Sources, fate, and human health implications: A review. Crit. Rev. Environ. Sci. Technol. 47, 693–794. https://doi.org/10.1080/10643389.2017.1326277

Bisinoti, M.C., Jardim, W.F., 2004. O comportamento do metilmercúrio (METILHg) no ambiente. Quim. Nova 27, 593–600. https://doi.org/10.1590/s0100-40422004000400014

Bodîrlău, R., Teacă, C.A., 2009. Fourier transform infrared spectroscopy and thermal analysis of lignocellulose fillers treated with organic anhydrides. Rom. Reports Phys. 54, 93–104.

Bohra, S., Kundu, D., Naskar, M.K., 2013. Synthesis of cashew nut-like zeolite NaP powders using agro-waste material as silica source. Mater. Lett. 106, 182–185. https://doi.org/10.1016/j.matlet.2013.04.080

Breck, D.W., 1964. Crystalline molecular sieves. J. Chem. Educ. 41, 678–689. https://doi.org/10.1021/ed041p678

Briggs, C., Gustin, M.S., 2013. Building upon the conceptual model for soil mercury flux: Evidence of a link between moisture evaporation and Hg evasion. Water. Air. Soil Pollut. 224. https://doi.org/10.1007/s11270-013-1744-5

Brunauer, S. Emmett, P.H., Taylor, E., 1938. Adsorption of gases in multimolecular layers. J. Americ Chem. Society. 60, 309-319.

Cai, L.N., Guo, Y., Lu, A.H., Branton, P., Li, W.C., 2012. The choice of precipitant and precursor in the co-precipitation synthesis of copper manganese oxide for maximizing carbon monoxide oxidation. J. Mol. Catal. A Chem. 360, 35–41. https://doi.org/10.1016/j.molcata.2012.04.003

Cantrell, K.B., Hunt, P.G., Uchimiya, M., Novak, J.M., Ro, K.S., 2012. Impact of pyrolysis temperature and manure source on physicochemical characteristics of biochar. Bioresour. Technol. 107, 419–428. https://doi.org/10.1016/j.biortech.2011.11.084

Cardoso, A.M., Horn, M.B., Ferret, L.S., Azevedo, C.M.N. 2015a. Integrated synthesis of zeolites 4A and Na–P1 using coal fly ash for application in the formulation of detergents and swine waste water treatment. J. Hazard. Mater., 287, 69-77. https://doi.org/10.1016/j.jhazmat.2015.01.042

Cardoso, A.M., Paprocki, A., Ferret, L.S., Azevedo, C.M.N., Pires, M., 2015b. Synthesis of zeolite Na-P1 under mild conditions using Brazilian coal fly ash and its application in wastewater treatment. Fuel 139, 59–67. https://doi.org/10.1016/j.fuel.2014.08.016

Carpi, A., Lindberg, S.E., 1998. Application of a Teflon® dynamic flux chamber for quantifying soil mercury flux: Tests and results over background soil. Atmos. Environ. 32, 873–882. https://doi.org/10.1016/S1352-2310(97)00133-7

Carvalho, G.S., Oliveira, J.R., Curi, N., Schulze, D.G., Marques, J.J., 2019. Selenium and

mercury in Brazilian Cerrado soils and their relationships with physical and chemical soil characteristics. Chemosphere 218, 412–415. https://doi.org/10.1016/j.chemosphere.2018.11.099

Chai, X., Liu, G., Zhao, X., Hao, Y., Zhao, Y., 2012. Complexion between mercury and humic substances from different landfill stabilization processes and its implication for the environment. J. Hazard. Mater. 209–210, 59–66. https://doi.org/10.1016/j.jhazmat.2011.12.077

Chen, S.C., Lin, W.H., Chien, C.C., Tsang, D.C.W., Kao, C.M., 2018. Development of a two-stage biotransformation system for mercury-contaminated soil remediation. Chemosphere 200, 266–273. https://doi.org/10.1016/j.chemosphere.2018.02.085

Ci, Z., Peng, F., Xue, X., Zhang, X., 2016. Air–surface exchange of gaseous mercury over permafrost soil: an investigation at a high-altitude (4700 m a.s.l.) and remote site in the central Qinghai-Tibet Plateau. Atmos. Chem. Phys. Discuss. 1–33. https://doi.org/10.5194/acp-2016-515

Cimino, S., Scala, F., 2016. Removal of Elemental Mercury by MnOx Catalysts Supported on TiO2 or Al2O3. Ind. Eng. Chem. Res. 55, 5133–5138. https://doi.org/10.1021/acs.iecr.5b04147

Cole, K.J., Carley, A.F., Crudace, M.J. 2010. Copper manganese oxide catalysts modified by gold deposition: the influence on activity for ambient temperature carbon monoxide oxidation. Catalysis Letters. 138, 143-147. https://doi.org/10.1007/s10562-010-0392-2

Converse, A.D., Riscassi, A.L., Scanlon, T.M., 2010. Seasonal variability in gaseous mercury fluxes measured in a high-elevation meadow. Atmos. Environ. 44, 2176–2185. https://doi.org/10.1016/j.atmosenv.2010.03.024

Courtney, T.D., Chang, C.C., Gorte, R.J., Lobo, R.F., Fan, W., Nikolakis, V., 2015. Effect of water treatment on Sn-BEA zeolite: Origin of 960 cm-1 FTIR peak. Microporous Mesoporous Mater. 210, 69–76. https://doi.org/10.1016/j.micromeso.2015.02.012

Dash, H.R., Sahu, M., Mallick, B., Das, S., 2017. Functional efficiency of MerA protein among diverse mercury resistant bacteria for efficient use in bioremediation of inorganic mercury. Biochimie 142, 207–215. https://doi.org/10.1016/j.biochi.2017.09.016

Devars, S., Avilés, C., Cervantes, C., Moreno-Sánchez, R., 2000. Mercury uptake and removal by euglena gracilis. Arch. Microbiol. 174, 175–180. https://doi.org/10.1007/s002030000193

Dey, S., Chandra Dhal, G., Mohan, D., Prasad, R., 2019. Synthesis of silver promoted CuMnOx catalyst for ambient temperature oxidation of carbon monoxide. J. Sci. Adv. Mater. Devices 4, 47–56. https://doi.org/10.1016/j.jsamd.2019.01.008

Dey, S., Dhal, G.C., Mohan, D., Prasad, R., 2017. Effect of preparation conditions on the catalytic activity of CuMnOx catalysts for CO oxidation. Bull. Chem. React. Eng. & Catal. 12, 437–451. https://doi.org/10.9767/bcrec.12.3.900.437-451

Ding, X., Wang, R., Li, Y., Gan, Y., Liu, S., Dai, J., 2017. Insights into the mercury(II) adsorption and binding mechanism onto several typical soils in China. Environ. Sci. Pollut. Res. 24, 23607–23619. https://doi.org/10.1007/s11356-017-9835-2

Dong, J., Xu, Z., Kuznicki, S.M., 2009. Mercury removal from flue gases by novel regenerable magnetic nanocomposite sorbents. Environ. Sci. Technol. 43, 3266–3271. https://doi.org/10.1021/es803306n

Dong, X., T. Guan, G. Li, Q. Lin, Zhao, X., 2016. Long-term effects of biochar amount on the content and composition of organic matter in soil aggregates under field conditions, J.

Soils Sediments. 16, 1481–1497, https://doi.org/10.1007/s11368-015-1338-5.

Du, W., Yin, L., Zhuo, Y., Xu, Q., Zhang, L., Chen, C., 2015. Performance of CuOx-neutral Al2O3 sorbents on mercury removal from simulated coal combustion flue gas. Fuel Process. Technol. 131, 403–408. https://doi.org/10.1016/j.fuproc.2014.11.039

Durão Júnior, W.A., Palmieri, H.E.L., Trindade, M.C., De Aquino Branco, O.E., Filho, C.A.C., Fleming, P.M., Da Silva, J.B.B., Windmöller, C.C., 2009. Speciation, distribution, and transport of mercury in contaminated soils from Descoberto, Minas Gerais, Brazil. J. Environ. Monit. 11, 1056–1063. https://doi.org/10.1039/b813997k

Eckley, C.S., Gustin, M., Lin, C.J., Li, X., Miller, M.B., 2010. The influence of dynamic chamber design and operating parameters on calculated surface-to-air mercury fluxes. Atmos. Environ. 44, 194–203. https://doi.org/10.1016/j.atmosenv.2009.10.013

Teixeira, P.C., Donagemma, G.K., Fontana, A., Teixeira, W.G., 2017. Manual de métodos de análise de solo. Brasilia (DF): EMBRAPA.

Ericksen, J.A., Gustin, M.S., Xin, M., Weisberg, P.J., Fernandez, G.C.J., 2006. Air-soil exchange of mercury from background soils in the United States. Sci. Total Environ. 366, 851–863. https://doi.org/10.1016/j.scitotenv.2005.08.019

Fantozzi, L., Ferrara, R., Dini, F., Tamburello, L., Pirrone, N., Sprovieri, F., 2013. Study on the reduction of atmospheric mercury emissions from mine waste enriched soils through native grass cover in the Mt. Amiata region of Italy. Environ. Res. 125, 69–74. https://doi.org/10.1016/j.envres.2013.02.004

Fernández, R.G., García, C.P., Lavín, A.G., Bueno De Las Heras, J.L., 2012. Study of main combustion characteristics for biomass fuels used in boilers. Fuel Process. Technol. 103, 16–26. https://doi.org/10.1016/j.fuproc.2011.12.032

Ferrarini, S.F., Cardoso, A.M., Paprocki, A., Pires, M., 2016. Integrated synthesis of zeolites using coal fly ash: Element distribution in the products, washing waters and effluent. J. Braz. Chem. Soc. 27, 2034–2045. https://doi.org/10.5935/0103-5053.20160093

Gao, L., Li, C., Zhang, J., Du, X., Li, S., Zeng, J., Yi, Y., Zeng, G., 2018. Simultaneous removal of NO and Hg0 from simulated flue gas over CoOx-CeO2 loaded biomass activated carbon derived from maize straw at low temperatures. Chem. Eng. J. 342, 339–349. https://doi.org/10.1016/j.cej.2018.02.100

García-Sánchez, A., Contreras, F., Adams, M., Santos, F., 2006. Atmospheric mercury emissions from polluted gold mining areas (Venezuela). Environ. Geochem. Health. 28, 529-540. https://doi.org/10.1007/s10653-006-9049-x

Gerber, I., Oubenali, M., Bacsa, R., Durand, J., Gonçalves, A., Pereira, M.F.R., Jolibois, F., Perrin, L., Poteau, R., Serp, P., 2011. Theoretical and experimental studies on the carbon-nanotube surface oxidation by nitric acid: Interplay between functionalization and vacancy enlargement. Chem. - A Eur. J. 17, 11467–11477. https://doi.org/10.1002/chem.201101438

Ghasemidehkordi, B., Malekirad, A.A., Nazem, H., Fazilati, M., Salavati, H., Shariatifar, N., Rezaei, M., Fakhri, Y., Mousavi Khaneghah, A., 2018. Concentration of lead and mercury in collected vegetables and herbs from Markazi province, Iran: a non-carcinogenic risk assessment. Food Chem. Toxicol. 113, 204–210. https://doi.org/10.1016/j.fct.2018.01.048

Gillis, A., Miller, D.R., 2000. Some potential errors in the measurement of mercury gas exchange at the soil surface using a dynamic flux chamber. Sci. Total Environ. 260, 181–189. https://doi.org/10.1016/S0048-9697(00)00562-3

Gruba, P., Błońska, E., Lasota, J., 2014. Predicting the concentration of total mercury in mineral horizons of forest soils varying in organic matter and mineral fine fraction content. Water.

Air. Soil Pollut. 225. https://doi.org/10.1007/s11270-014-1924-y

Guédron, S., Grangeon, S., Jouravel, G., Charlet, L., Sarret, G., 2013. Atmospheric mercury incorporation in soils of an area impacted by a chlor-alkali plant (Grenoble, France): Contribution of canopy uptake. Sci. Total Environ. 445–446, 356–364. https://doi.org/10.1016/j.scitotenv.2012.12.084

Gustin, M.S., Stamenkovic, J., 2005. Effect of watering and soil moisture on mercury emissions from soils. Biogeochemistry 76, 215–232. https://doi.org/10.1007/s10533-005-4566-8

Han, F.X., Patterson, W.D., Xia, Y., Sridhar, B.B.M., Su, F., 2006. Rapid determination of mercury in plant and soil samples using inductively coupled plasma atomic emission spectroscopy, a comparative study. Water. Air. Soil Pollut. 170, 161–171. https://doi.org/10.1007/s11270-006-3003-5

He, P., Zhang, Z. zhi, Peng, X. long, Wu, J., Chen, N. chao, 2018. Mercury capture by manganese modified copper oxide. J. Taiwan Inst. Chem. Eng. 85, 201–206. https://doi.org/10.1016/j.jtice.2018.01.045

Hibbert, D.B., 1999. Method validation of modern analytical techniques. Accredit. Qual. Assur. 4, 352–356. https://doi.org/10.1007/s007690050381

Huggins, F.E., Yap, N., Huffman, G.P., Senior, C.L., 2003. XAFS characterization of mercury captured from combustion gases on sorbents at low temperatures. Fuel Process. Technol. 82, 167–196. https://doi.org/10.1016/S0378-3820(03)00068-7

Huo, Z., Xu, X., Lv, Z., Song, J., He, M., Li, Z., Wang, Q., Yan, L., Li, Y., 2013. Thermal study of NaP zeolite with different morphologies. J. Therm. Anal. Calorim. 111, 365–369. https://doi.org/10.1007/s10973-012-2301-y

Hutchings, G.J., Mirzaei, A.A., Joyner, R.W., Siddiqui, M.R.H., Taylor, S.H., 1998. Effect of

preparation conditions on the catalytic performance of copper manganese oxide catalysts for CO oxidation. Appl. Catal. A Gen. 166, 143–152. https://doi.org/10.1016/S0926-860X(97)00248-2

Hutson, N.D., Attwood, B.C., Scheckel, K.G., 2007. XAS and XPS characterization of mercury binding on brominated activated carbon. Environ. Sci. Technol. 41, 1747–1752. https://doi.org/10.1021/es062121q

Instituto Nacional De Meteorologia (INMET). Available in: www.inmet.gov.br. Accessed on: 31 October. 2019.

Jesus, M.S., Napoli, A., Trugilho, P.F., Abreu Júnior, Á.A., Martinez, C.L.M., Freitas, T.P., 2018. Energy and mass balance in the pyrolysis process of eucalyptus wood. Cerne 24, 288–294. https://doi.org/10.1590/01047760201824032561

Jones, C., Cole, K.J., Taylor, S.H., Crudace, M.J., Hutchings, G.J., 2009. Copper manganese oxide catalysts for ambient temperature carbon monoxide oxidation: Effect of calcination on activity. J. Mol. Catal. A Chem. 305, 121–124. https://doi.org/10.1016/j.molcata.2008.10.027

Joseph, S.D., Camps-Arbestain, M., Lin, Y., Munroe, P., Chia, C.H., Hook, J., Van Zwieten, L., Kimber, S., Cowie, A., Singh, B.P., Lehmann, J., Foidl, N., Smernik, R.J., Amonette, J.E., 2010. An investigation into the reactions of biochar in soil. Aust. J. Soil Res. 48, 501–515. https://doi.org/10.1071/SR10009

Kikuchi, T., Ikemoto, H., Takahashi, K., Hasome, H., Ueda, H., 2013. Parameterizing soil emission and atmospheric oxidation-reduction in a model of the global biogeochemical cycle of mercury. Environ. Sci. Technol. 47, 12266–12274. https://doi.org/10.1021/es401105h

Kim, K., Steven, Lindberg, E., Meyers, T.P., 1995. Micrometeorological measurements of mercury vapor fluxes over background forest soils in eastern Tennessee. Atmospheric Environ. 29, 267-282. doi.org/10.1016/1352-2310(94)00198-T.

Kocman, D., Horvat, M., 2010. A laboratory based experimental study of mercury emission from contaminated soils in the River Idrijca catchment. Atmos. Chem. Phys. 10, 1417–1426. https://doi.org/10.5194/acp-10-1417-2010

Kocman, D., Horvat, M., Kotnik, J., 2004. Mercury fractionation in contaminated soils from the Idrija mercury mine region. J. Environ. Monit. 6, 696–703. https://doi.org/10.1039/b403625e

Kocman, D., Horvat, M., Pirrone, N., Cinnirella, S., 2013. Contribution of contaminated sites to the global mercury budget. Environ. Res. 125, 160–170. https://doi.org/10.1016/j.envres.2012.12.011

Krabbenhoft, D.P., Sunderland, E.M., 2013. Global change and mercury. Science. 341, 1457–1458. https://doi.org/10.1126/science.1242838

Król, M., Minkiewicz, J., Mozgawa, W., 2016. IR spectroscopy studies of zeolites in geopolymeric materials derived from kaolinite. J. Mol. Struct. 1126, 200–206. https://doi.org/10.1016/j.molstruc.2016.02.027

Leterme, B., Blanc, P., Jacques, D., 2014. A reactive transport model for mercury fate in soil—application to different anthropogenic pollution sources. Environ. Sci. Pollut. Res. 21, 12279–12293. https://doi.org/10.1007/s11356-014-3135-x

Li, G., Shen, B., Li, Y., Zhao, B., Wang, F., He, C., Wang, Y., Zhang, M., 2015. Removal of element mercury by medicine residue derived biochars in presence of various gas compositions. J. Hazard. Mater. 298, 162–169.

https://doi.org/10.1016/j.jhazmat.2015.05.031

Li, G., Wang, S., Wu, Q., Wang, F., Shen, B., 2016. Mercury sorption study of halides modified bio-chars derived from cotton straw. Chem. Eng. J. 302, 305–313. https://doi.org/10.1016/j.cej.2016.05.045

Lin, C.J., Gustin, M.S., Singhasuk, P., Eckley, C., Miller, M., 2010. Empirical models for estimating mercury flux from soils. Environ. Sci. Technol. 44, 8522–8528. https://doi.org/10.1021/es1021735

Lindberg, S.E., Zhang, H., Gustin, M., Vette, A., Marsik, F., Owens, J., Casimir, A., Ebinghaus, R., Edwards, G., Fitzgerald, C., Kemp, J., Kock, H.H., London, J., Majewski, M., Poissant, L., Pilote, M., Rasmussen, P., Schaedlich, F., Schneeberger, D., Sommar, J., Turner, R., Wallschläger, D., Xiao, Z., 1999. Increases in mercury emissions from desert soils in response to rainfall and irrigation. J. Geophys. Res. Atmos. 104, 21879–21888. https://doi.org/10.1029/1999JD900202

Liu, F., Cheng, H., Yang, K., Zhao, C., Liu, Y, Peng M, Li H., 2014. Characteristics and influencing factors of mercury exchang flux between soil and air in Guangzhou City. J. Geochem. Explor. 139:115– 121. https://doi.org/10.1016/j.gexplo.2013.09.005

Ma, M., Du, H., Wang, D., Sun, T., 2018. Mercury methylation in the soils and sediments of Three Gorges Reservoir Region. J. Soils Sediments 18, 1100–1109. https://doi.org/10.1007/s11368-017-1827-9

Magarelli, G., Fostier, H., 2005. Câmara de fluxo dinâmica : Aplicação na Bacia do Rio Negro Artigo. Quim. Nova 28, 968–974.

Mahbub, K.R., Krishnan, K., Megharaj, M., Naidu, R., 2016. Bioremediation potential of a highly mercury resistant bacterial strain Sphingobium SA2 isolated from contaminated

soil. Chemosphere 144, 330–337. https://doi.org/10.1016/j.chemosphere.2015.08.061

Maia, L.F.O., Hott, R.C., Ladeira, P.C.C., Batista, B.L., Andrade, T.G., Santos, M.S., Faria, M.C.S., Oliveira, L.C.A., Monteiro, D.S., Pereira, M.C., Rodrigues, J.L., 2019. Simple synthesis and characterization of L-Cystine functionalized Δ-FeOOH for highly efficient Hg(II) removal from contamined water and mining waste. Chemosphere 215, 422–431. https://doi.org/10.1016/j.chemosphere.2018.10.072

Margenot, A.J., Calderón, F.J., Parikh, S.J., 2016. Limitations and Potential of Spectral Subtractions in Fourier-Transform Infrared Spectroscopy of Soil Samples. Soil Sci. Soc. Am. J. 80, 10–26. https://doi.org/10.2136/sssaj2015.06.0228

Mei, Z., Shen, Z., Zhao, Q., Wang, W., Zhang, Y., 2008. Removal and recovery of gas-phase element mercury by metal oxide-loaded activated carbon. J. Hazard. Mater. 152, 721–729. https://doi.org/10.1016/j.jhazmat.2007.07.038

Mele, Ardita, Mele, I., Mele, Altin, 2012. Preparation-properties relation of Mn-Cu hopcalite catalyst. Am. J. Appl. Sci. 9, 265–270. https://doi.org/10.3844/ajassp.2012.265.270

Melo, L.C.A., Coscione, A.R., Abreu, C.A., Puga, A.P., Camargo, O.A., 2013. Influence of pyrolysis temperature on cadmium and zinc sorption capacity of sugar cane straw-derived biochar. BioResources 8, 4992–5004. https://doi.org/10.15376/biores.8.4.4992-5004

Moharem, M., Elkhatib, E., Mesalem, M., 2019. Remediation of chromium and mercury polluted calcareous soils using nanoparticles: Sorption –desorption kinetics, speciation and fractionation. Environ. Res. 170, 366–373. https://doi.org/10.1016/j.envres.2018.12.054

Montoya, A.J., Lena, J.C., Windmöller, C.C., 2019. Adsorption of gaseous elemental mercury on soils: Influence of chemical and/or mineralogical characteristics. Ecotoxicol. Environ.

Saf. 170, 98–106. https://doi.org/10.1016/j.ecoenv.2018.11.054

Moore, C.W., Castro, M.S., 2012. Investigation of factors affecting gaseous mercury concentrations in soils. Sci. Total Environ. 419, 136–143. https://doi.org/10.1016/j.scitotenv.2011.12.068

Murphy, B., Davis, M.E., Xu, B., 2015. The Effect of Adsorbed Molecule Gas-Phase Deprotonation Enthalpy on Ion Exchange in Sodium Exchanged Zeolites: An In Situ FTIR Investigation. Top. Catal. 58, 393–404. https://doi.org/10.1007/s11244-015-0383-z

Naguib, M.M., El-Gendy, A.O., Khairalla, A.S., 2018. Microbial Diversity of Mer Operon Genes and Their Potential Rules in Mercury Bioremediation and Resistance. Open Biotechnol. J. 12, 56–77. https://doi.org/10.2174/1874070701812010056

Nriagu, J.O., 1994. Mechanistic steps in the photoreduction of mercury in natural waters. Sci. Total Environ. 154, 1–8. https://doi.org/10.1016/0048-9697(94)90608-4

O'Connor, D., Hou, D., Ok, Y.S., Mulder, J., Duan, L., Wu, Q., Wang, S., Tack, F.M.G., Rinklebe, J., 2019. Mercury speciation, transformation, and transportation in soils, atmospheric flux, and implications for risk management: A critical review. Environ. Int. 126, 747–761. https://doi.org/10.1016/j.envint.2019.03.019

O'Driscoll, N.J., Canário, J., Crowell, N., Webster, T., 2011. Mercury speciation and distribution in coastal wetlands and tidal mudflats: Relationships with sulphur speciation and organic carbon. Water. Air. Soil Pollut. 220, 313–326. https://doi.org/10.1007/s11270-011-0756-2

Obrist, D., Johnson, D.W., Lindberg, S.E., Luo, Y., Hararuk, O., Bracho, R., Battles, J.J., Dail, D.B., Edmonds, R.L., Monson, R.K., Ollinger, S. V., Pallardy, S.G., Pregitzer, K.S., Todd, D.E., 2011. Mercury distribution across 14 U.S. Forests. Part I: Spatial patterns of

concentrations in biomass, litter, and soils. Environ. Sci. Technol. 45, 3974–3981. https://doi.org/10.1021/es104384m

Oliveira, J.R., Vasques, I.C.F. , Lima, F.R.D. , Carvalho, G.S. , Job, M.T.P. , Oliveira, T.S., Marques J.J., 2020. Mercury adsorption in tropical soils and zeolite: characterization by Fourier-transform infrared spectroscopy, Archives of Agronomy and Soil Science, DOI:10.1080/03650340.2020.1845318

Osterwalder, S., Sommar, J., Åkerblom, S., Jocher, G., Fritsche, J., Nilsson, M.B., Bishop, K., Alewell, C., 2018. Comparative study of elemental mercury flux measurement techniques over a Fennoscandian boreal peatland. Atmos. Environ. 172, 16–25. https://doi.org/10.1016/j.atmosenv.2017.10.025

Pacyna, E.G., Pacyna, J.M., Sundseth, K., Munthe, J., Kindbom, K., Wilson, S., Steenhuisen, F., Maxson, P., 2010. Global emission of mercury to the atmosphere from anthropogenic sources in 2005 and projections to 2020. Atmos. Environ. 44, 2487–2499. https://doi.org/10.1016/j.atmosenv.2009.06.009

Park, S.Y., Holsen, T.M., Kim, P.R., Han, Y.J., 2014. Laboratory investigation of factors affecting mercury emissions from soils. Environ. Earth Sci. 72, 2711–2721. https://doi.org/10.1007/s12665-014-3177-x

Penha, J.G., Carvalho, G.S., Abreu, L.B. de, Ribeiro, B.T., Costa, Enio Tarso de Souza Marques, J.J., 2017. Boletim Técnico - Procedimentos para quantificação de elementos-traço por espectrofotometria de absorção atômica em matrizes de interesse ambiental 1–21. https://doi.org/10.13140/RG.2.2.24948.55685

Qi, H., Xu, W., Wang, J., Tong, L., Zhu, T., 2015. Hg0 removal from flue gas over different zeolites modified by FeCl3. J. Environ. Sci. (China) 28, 110–117. https://doi.org/10.1016/j.jes.2014.05.050

Qu, Z., Yan, N., Liu, P., Chi, Y., Jia, J., 2009. Bromine chloride as an oxidant to improve elemental mercury removal from coal-fired flue gas. Environ. Sci. Technol. 43, 8610–8615. https://doi.org/10.1021/es901803s

Querol, X., Plana, F., Alastuey, A., López-Soler, A., 1997. Synthesis of Na-zeolites from fly ash. Fuel 76, 793–799. https://doi.org/10.1016/s0016-2361(96)00188-3

Querol, X., Umaña, J.C., Plana, F., Alastuey, A., Lopez-Soler, A., Medinaceli, A., Valero, A., Domingo, M.J., Garcia-Rojo, E., 2001. Synthesis of zeolites from fly ash at pilot plant scale. Examples of potential applications. Fuel 80, 857–865. https://doi.org/10.1016/S0016-2361(00)00156-3

Quintero, M., Perez, M., Meléndez, H., Rondon, J., Imbert, F., 2012. Síntesis y caracterización de la zeolita Beta. Avances Química. 224, 223-226.

Rinklebe, J., During, A., Overesch, M., Du Laing, G., Wennrich, R., Stärk, H.J., Mothes, S., 2010. Dynamics of mercury fluxes and their controlling factors in large Hg-polluted floodplain areas. Environ. Pollut. 158, 308–318. https://doi.org/10.1016/j.envpol.2009.07.001

Rinklebe, J., During, A., Overesch, M., Wennrich, R., Stärk, H.J., Mothes, S., Neue, H.U., 2009. Optimization of a simple field method to determine mercury volatilization from soils-Examples of 13 sites in floodplain ecosystems at the Elbe River (Germany). Ecol. Eng. 35, 319–328. https://doi.org/10.1016/j.ecoleng.2008.04.019

Rodriguez, J.A., Lustosa Filho, J.F., Melo, L.C.A., de Assis, I.R., de Oliveira, T.S., 2020. Influence of pyrolysis temperature and feedstock on the properties of biochars produced from agricultural and industrial wastes. J. Anal. Appl. Pyrolysis 149, 104839. https://doi.org/10.1016/j.jaap.2020.104839

Salama, T.M., Ali, I.O., Bakr, M.F., 2018. Functionalization of Synthesized NaP Zeolite with Silver Nanoparticles Capped with Alkyl Dimethyl Hydroxyethyl Ammonium for Sorption and Reduction of Chromate(VI) Oxoanions. J. Inorg. Organomet. Polym. 28, 334–351. https://doi.org/10.1007/s10904-017-0704-8

Sánchez-Hernández, R., López-Delgado, A., Padilla, I., Galindo, R., López-Andrés, S., 2016. One-step synthesis of NaP1, SOD and ANA from a hazardous aluminum solid waste. Microp. Mesop. Mater. 226, 267-277. https://doi.org/10.1016/j.micromeso.2016.01.037

Schlüter, K., 2000. Review: Evaporation of mercury from soils. An integration and synthesis of current knowledge. Environ. Geol. 39, 249–271. https://doi.org/10.1007/s002540050005

Shan, Y., Yang, W., Li, Y., Liu, Y., Pan, J., 2019. Preparation of microwave-activated magnetic bio-char adsorbent and study on removal of elemental mercury from flue gas. Sci. Total Environ. 697, 134049. https://doi.org/10.1016/j.scitotenv.2019.134049

Sharma, P., Yeo, J.G., Han, M.H., Cho, C.H., 2013. Knobby surfaced, mesoporous, single-phase GIS-NaP1 zeolite microsphere synthesis and characterization for H2 gas adsorption. J. Mater. Chem. A 1, 2602–2612. https://doi.org/10.1039/c2ta01311h

Sharma, P., Yeo, J.G., Kim, D.K., Cho, C.H., 2012. Organic additive free synthesis of mesoporous naoncrystalline NaA zeolite using high concentration inorganic precursors. J. Mater. Chem. 22, 2838–2843. https://doi.org/10.1039/c2jm14848j

Shen, B., Tian, L., Li, F., Zhang, X., Xu, H., Singh, S., 2017. Elemental mercury removal by the modified bio-char from waste tea. Fuel 187, 189–196. https://doi.org/10.1016/j.fuel.2016.09.059

Sing, K.S.W., Everett, D.H., Haul, R.A.W., Moscou, L., Pierotti, R.A., Rouquerol, J.,

Siemieniewska, T., 1985. Reporting Physisorption Data For Gas/Solid Systems With Special Reference To The Determination Of Surface Area And Porosity. Pure App. Chem. 57, 603-619.

Singh, S., Wu, C., Williams, P.T., 2012. Pyrolysis of waste materials using TGA-MS and TGA-FTIR as complementary characterisation techniques. J. Anal. Appl. Pyrolysis 94, 99–107. https://doi.org/10.1016/j.jaap.2011.11.011

Soil Survey Staff. 2014. Keys to Soil Taxonomy, 12th ed. USDA-Natural Resources Conservation Service, Washington, DC.

Sommar, J., Zhu, W., Shang, L., Lin, C.J., Feng, X., 2016. Seasonal variations in metallic mercury (Hg^0) vapor exchange over biannual wheat-corn rotation cropland in the North China Plain. Biogeosciences 13, 2029–2049. https://doi.org/10.5194/bg-13-2029-2016

Spassova, I., Khristova, M., Panayotov, D., Mehandjiev, D., 1999. Coprecipitated CuO–MnO Catalysts for Low-Temperature CO–NO x and CO–NO–O2 Reactions. J. Catal. 185, 43–57.

Su, H., Berenson, M.L., 2017. Comparing Tests of Homoscedasticity in Simple Linear Regression. JSM Math. Stat. 4, 1–10.

Sysalová, J., Kučera, J., Drtinová, B., Červenka, R., Zvěřina, O., Komárek, J., Kameník, J., 2017. Mercury species in formerly contaminated soils and released soil gases. Sci. Total Environ. 584–585, 1032–1039. https://doi.org/10.1016/j.scitotenv.2017.01.157

Tan, Z., Sun, L., Xiang, J., Zeng, H., Liu, Z., Hu, S., Qiu, J., 2012. Gas-phase elemental mercury removal by novel carbon-based sorbents. Carbon N. Y. 50, 362–371. https://doi.org/10.1016/j.carbon.2011.08.036

Tauanov, Z., Tsakiridis, P.E., Mikhalovsky, S. V., Inglezakis, V.J., 2018. Synthetic coal fly

ash-derived zeolites doped with silver nanoparticles for mercury (II) removal from water. J. Environ. Manage. 224, 164–171. https://doi.org/10.1016/j.jenvman.2018.07.049

Tinôco, A.A.P., Azevedo, I.C. d'Almeida D. de, Marques, E.A.G., Mounteer, A.H., Martins, C. de P., Nascentes, R., Reis, E.L., Natalino, R., 2010. Avaliação de contaminação por mercúrio em Descoberto, MG. Eng. Sanit. e Ambient. 15, 305–314. https://doi.org/10.1590/s1413-41522010000400003

Towett, E.K., Shepherd, K.D., Cadisch, G., 2013. Quantification of total element concentrations in soils using total X-ray fluorescence spectroscopy (TXRF). Sci. Total Environ. 463–464, 374–388. https://doi.org/10.1016/j.scitotenv.2013.05.068

UNEP, 2013. Global Mercury Assessment 2013: Sources, Emissions, Releases and Environmental Transport. UNEP Chemicals Branch, Geneva, Switzerland.

USEPA. 2007. Method 3051A for use of Microwave assisted acid digestion of sediments, sludges, soils, and oils. U.S. Environmental Protection Agency, Cincinnati, OH.

Wallschläger, D, Hintelmann, H., Evans, R.D., Wilken, R.D. 1995. Volatilization of dimethylmercury and elemental mercury from river elbe floodplain soils. Water, Air, and Soil Pollution, 80, 1325-1329.

Wallschläger, D., Turner, R.R., London, J., Ebinghaus, R., Kock, H.H., Sommar, J., Xiao, Z., 1999. Factors affecting the measurement of mercury emissions from soils with flux chambers. J. Geophys. Res. Atmos. 104, 21859–21871. https://doi.org/10.1029/1999JD900314

Wang, L., Hou, D., Cao, Y., Ok, Y.S., Tack, F.M.G., Rinklebe, J., O'Connor, D., 2020. Remediation of mercury contaminated soil, water, and air: A review of emerging materials and innovative technologies. Environ. Int. 134, 105281.

https://doi.org/10.1016/j.envint.2019.105281

Wang, P., Su, S., Xiang, J., You, H., Cao, F., Sun, L., Hu, S., Zhang, Y., 2014. Catalytic oxidation of Hg0 by MnOx-CeO2/γ-Al2O3 catalyst at low temperatures. Chemosphere 101, 49–54. https://doi.org/10.1016/j.chemosphere.2013.11.034

Wang, Z., Sun, T., Driscoll, C.T., Zhang, H., Zhang, X., 2019. Dimethylmercury in Floodwaters of Mercury Contaminated Rice Paddies. Environ. Sci. Technol. 53, 9453–9461. https://doi.org/10.1021/acs.est.8b07180

Wasserman, J.C., Amouroux, D., Wasserman, M.A.V., Donard, O.F.X., 2002. Mercury speciation in sediments of a tropical coastal environment. Environ. Technol. (United Kingdom) 23, 899–910. https://doi.org/10.1080/09593332308618357

Wdowin, M., Wiatros-Motyka, M.M., Panek, R., Stevens, L.A., Franus, W., Snape, C.E., 2014. Experimental study of mercury removal from exhaust gases. Fuel 128, 451–457. https://doi.org/10.1016/j.fuel.2014.03.041

Weber, J.H., Evans, R., Jones, S.H., Hines, M.E., 1998. Conversion of mercury(II) into mercury(0), monomethylmercury cation, and dimethylmercury in saltmarsh sediment slurries. Chemosphere 36, 1669–1687. https://doi.org/10.1016/S0045-6535(97)10042-X

Wei, Z., Luo, Y., Li, B., Cheng, Z., Wang, J., Ye, Q., 2015. Microwave assisted catalytic removal of elemental mercury from flue gas using Mn/zeolite catalyst. Atmos. Pollut. Res. 6, 45–51. https://doi.org/10.5094/APR.2015.006

Wiatros-Motyka, M.M., Sun, C.G., Stevens, L.A., Snape, C.E., 2013. High capacity co-precipitated manganese oxides sorbents for oxidative mercury capture. Fuel 109, 559–562. https://doi.org/10.1016/j.fuel.2013.03.019

Windmöller, C.C., Durão, W.A., de Oliveira, A., Do Valle, C.M., 2015. The redox processes

in Hg-contaminated soils from Descoberto (Minas Gerais, Brazil): implications for the mercury cycle. Ecotoxicol Environ Saf. 112:201–211.doi:10.1016/j.ecoenv.2014.11.009.

Xin, M., Gustin, M.S., 2007. Gaseous elemental mercury exchange with low mercury containing soils: Investigation of controlling factors. Appl. Geochemistry 22, 1451–1466. https://doi.org/10.1016/j.apgeochem.2007.02.006

Xu, H., Qu, Z., Zhao, S., Mei, J., Quan, F., Yan, N., 2015a. Different crystal-forms of one-dimensional MnO2 nanomaterials for the catalytic oxidation and adsorption of elemental mercury. J. Hazard. Mater. 299, 86–93. https://doi.org/10.1016/j.jhazmat.2015.06.012

Xu, Y., Zeng, X., Luo, G., Zhang, B., Xu, P., Xu, M., Yao, H., 2016. Chlorine-Char composite synthesized by co-pyrolysis of biomass wastes and polyvinyl chloride for elemental mercury removal. Fuel 183, 73–79. https://doi.org/10.1016/j.fuel.2016.06.024

Xu, Yang, Luo, G., He, S., Deng, F., Pang, Q., Xu, Yongqing, Yao, H., 2019. Efficient removal of elemental mercury by magnetic chlorinated biochars derived from co-pyrolysis of Fe(NO3)3-laden wood and polyvinyl chloride waste. Fuel 239, 982–990. https://doi.org/10.1016/j.fuel.2018.11.102

Yang, S., Guo, Y., Yan, N., Qu, Z., Xie, J., Yang, C., Jia, J., 2011. Capture of gaseous elemental mercury from flue gas using a magnetic and sulfur poisoning resistant sorbent Mn/γ-Fe2O3 at lower temperatures. J. Hazard. Mater. 186, 508–515. https://doi.org/10.1016/j.jhazmat.2010.11.034

Yuan, Y., Zhao, Y., Li, H., Li, Y., Gao, X., Zheng, C., Zhang, J., 2012. Electrospun metal oxide-TiO 2 nanofibers for elemental mercury removal from flue gas. J. Hazard. Mater. 227–228, 427–435. https://doi.org/10.1016/j.jhazmat.2012.05.003

Zhang, H., Lindberg, S.E., 1999. Processes influencing the emission of mercury from soils: A

conceptual model. J. Geophys. Res. Atmos. 104, 21889–21896. https://doi.org/10.1029/1999JD900194

Zhang, Y., Kang, W., Han, H., Wang, H., Chen, Y., Gong, X., Zhai, C., Song, H., 2019. In-situ synthesis of NaP zeolite doped with transition metals using fly ash. J. Am. Ceram. Soc. 102, 7665–7677. https://doi.org/10.1111/jace.16623

Zhang, X., H. Wang, L. He, K. Lu, A. Sarmah, J. Li, N.S. Bolan, J. Pei, Huang, H., 2013. Using biochar for remediation of soils contaminated with heavy metals and organic pollutants. Environ. Sci. Pollut. Res. 20, 8472–8483, https://doi.org/10.1007/s11356-013-1659-0.

Zhao, L., Huang, Y., Chen, H., Zhao, Y., Xiao, T., 2017. Study on the preparation of bimetallic oxide sorbent for mercury removal. Fuel 197, 20–27. https://doi.org/10.1016/j.fuel.2017.01.122

Supplementary Material

Volatilization of elemental Hg from soils: synthesis and characterization of adsorbent materials from industrial waste

J.R.Oliveira[a]; I.C.F. Vasques[b]; F.R.D. Lima[a]; M.T.P. Job[b]; G.S. Carvalho[a]; T.S. Oliveira[b]; J.J. Marques[a*]

[a] Department of Soil Science, Federal University of Lavras, Lavras, MG, CEP 37200-000, Brazil
[b] Departament of Soil Science, Federal University of Viçosa, Viçosa, MG, CEP 36570-000, Brazil

Contact: João José Marques; Federal University of Lavras, 1001, Dr Sylvio Menecucci Avenue, Minas Gerais, Brazil. Postal Code: 37200-000; E-mail: jmarques@ufla.br

Table S.1- Oxide composition of coal fly ash selected for synthesis (%)

SiO_2	TiO_2	Al_2O_3	MgO	CaO	Na_2O	K_2O	FeO_3	P_2O_5	MnO	SO_3	LOI*
58.42	0.57	19.21	0.80	3.03	1.00	1.43	5.03	0.03	0.05	0.31	10.12

*Loss on ignition.

Table S.2 - Characteristics physical and chemical of waste construction wood (W) and plastic PVC (P) selected for biochar production

Waste	pH	CEC	Da	WRC	FC	Ash	Tv	C	H	N	O
	H_2O	cmolc kg^{-1}	g cm^{-3}	---------- % ----------				-------- % (w/w) --------			
W	6.9	5.5	0.2	64.0	46.8	1.6	43.7	48.7	6.5	0.2	43.0
P	8.1	28.5	0.9	4.3	22.2	20.2	57.2	41.1	6.6	0.1	32.0

Waste	Mg	P	S	Ca	K	Mn	Zn	Cu	Fe	Al	Na
	----------g kg^{-1}----------										
W	0.0	0.7	0.3	57.9	0.3	0.0	0.0	0.0	0.1	0.2	0.3
P	5.6	0.4	0.9	60.6	0.1	0.0	1.8	1.1	1.2	3.6	0.1

* Adapted from Rodriguez et al. (2020). Da: density, WRC: water retention capacity, FC: fixed carbon content, Ash: ash proportions; Tv: volatile matter; pH em água: 1:2.5; CEC: cation exchange capacity. C, H, N e O determined in elementary analyzer.

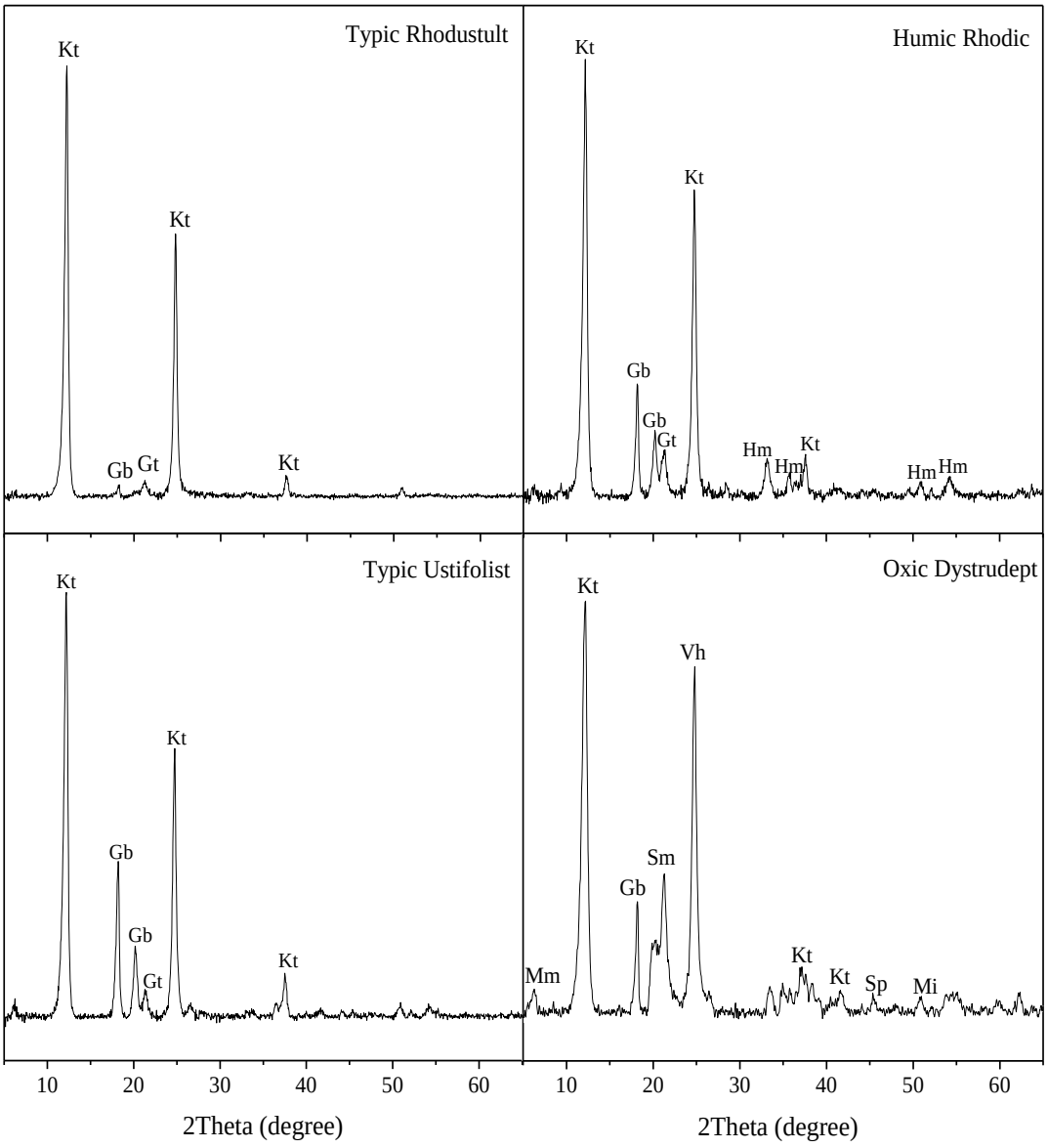

Figure S.1. X-ray diffractograms of soils. Kt = kaolinite; Gt =goethite; Gb =gibbsite; Hm =hematite; Qz = quartz, Mi = mica; Sm = smectite; Vh = vermiculite; Sp = serpentine.

CONCLUDING REMARKS

The Hg concentrations used in the adsorption study did not provide the maximum Hg adsorption, and future studies with concentrations above the value of 2.4 mg L^{-1} of Hg are necessary. Another investigation in future studies is to carry out adsorption studies in soils without the presence of O.M, in this way, it would be possible to state that the inorganic matrix of tropical soils are solely responsible for the high Hg adsorption capacity.

The application of liming in soils with the presence of Hg favors the retention of Hg, since the dominant species in solution at pH 6 are $HgOH_2$ in soils with low organic matter content. The $HgOH_2$ is strongly adsorbed by soil colloids and little mobile in the soil profile. However, in soils with a high O.M content, the dominant species at pH 6 are $HgOH_2$ and FA2-Hg. The FA2-Hg is a chemical species of Hg little adsorbed by the soil, but its formation occurs only in environments with a high concentration of DOC, which does not occur in tropical arable soils that receive liming. Thus, liming favors the retention of Hg in the soil.

Of the adsorbent materials produced to assess the Hg retention capacity, hopcalite and zeolite NaP showed desirable characteristics to be applied as elemental Hg adsorbents. Of these two materials, the zeolite NaP produced from a waste from thermoelectric plants (CFA) proves to be an economically viable option, and further studies are needed in situ conditions to verify the influence of all environmental variables on the Hg adsorption process volatilized contaminated soils.

This did not occur with biochars originating from waste wood and PVC, because they showed low capacity to adsorb Hg volatilized by soils, a fact that occurred due to the temperature of pyrolysis applied to the formation of biochars (500 ° C), since, high temperatures reduces the oxygenated functional groups, which are the main sites of Hg retention. A solution for the use of biochar as a Hg adsorbent volatilized by contaminated soils would be to reduce the temperature of pyrolysis and thus avoid, the reduction of oxygenated functional groups and activation with metallic elements that increase the Hg retention capacity.